Reducing conflicts in Haptic Shared Control during curve negotiation

MSc. Thesis

W.M. Scholtens

Technische Universiteit Delft

TU Delft

Reducing conflicts in Haptic Shared Control during curve negotiation

MSc. Thesis

by

W. M. Scholtens

to obtain the degree of Master of Science
at the Delft University of Technology,
to be defended publicly on Thursday January 18, 2018 at 13:15 AM.

Student number:	4141164	
Project duration:	Jan, 2017 – Jan, 2018	
Thesis committee:	Dr. Ir. D. A. Abbink	TU Delft, supervisor
	Ir. S. Barendswaard	TU Delft, supervisor
	Dr. Ir. M. M. van Paassen	TU Delft, external member
	Dr. Ir. D. M. Pool	TU Delft, external member

An electronic version of this thesis is available at `http://repository.tudelft.nl/`.

TU Delft

Preface

Technology is getting more and more integrated into our daily lives, as well as car driving is a becoming more and more a daily activity. To increase safety and comfort for the increasing amount of cars and hours spent on the road, driver assistance systems are developed. These assistance systems intend to support the drivers needs. However, every human is different and therefore desires different guidance from the automation. The current state of the art lacks of support systems which adjust to individual drivers, leading to conflicts between human and automation. Therefore I explored the possibilities to reduce conflicts when driving with haptic guidance systems, where I focused on conflicts in curved road segments.

The result of my study is presented in this master thesis, which discusses the method and outcome in the form of a scientific paper. The appendixes will provide more details and argumentation about the design choices.

W. M. Scholtens
Delft, January 2018

Acknowledgments

First of all I would like to thank my two supervisors David Abbink and Sarah Barendswaard. Long before I started my thesis David made me interested in human-machine interaction during the symposium and studytrip of Gezelschap Leeghwater. His positive energy and enthusiasm never failed to motivated me, combined with his critical feedback this made my work the quality that it is now. Without Sarah I would still be working with DUECA and programming the simulator in the HMI lab. Thank you for the many hours spend on helping me out and for the good balance between work and private conversations during our meetings.

I would also like to thank all other members of the Haptics Lab and in particular Timo, Bastiaan and Sarvesh. You never hesitated to answer my questions within no time and were always open to discuss the issues I faced during my work. Besides the practical help, I want to thank you for the endless supply of coffee and tea, the lunch breaks at the Haptics Hill, bitcoin discussions, climbing sessions, indispensable bad jokes and the great atmosphere in the lab.

Last, I would like to thank my parents for the unlimited support and encouragements. Without your believe and trust in me I would not have been able to achieve this result.

W. M. Scholtens
Delft, January 2018

Contents

List of Symbols

Abbreviations

BSD	Begin Steering Distance
ESD	End Steering Distance
FB	Feedback
FFW	Feed-Forward
HCR	Human Compatible Reference
LoHA	Level of Haptic Authority
LoHS	Level of Haptic Support
NMS	Neuromuscular System
OSFA	One Size Fits All
SoHF	Strength of Haptic Feedback
SW	Steering Wheel

Greek Letters

Δ	Difference
δ	Steering Wheel Angle
ψ	Heading
Γ	Torque
τ_p	Processing time delay
θ	Angle

Roman Letters

F	Force
I	Moment of Inertia
K	Gain
K_{sw}	Steering Wheel Stiffness
t_{far}	gaze-ahead time
T_N	Neuromuscular time constant
V	Velocity
y	Lateral position

Control system

iHCR	Individual Human Compatible Reference
mHCR	Average (mean) Human Compatible Reference
D	Driver without Control System: Manual Control
iFDCA	Four-Design-Choice-Architecture Controller with iHCR
mFDCA	Four-Design-Choice-Architecture Controller with mHCR
TwL	Conventional Two-Level Controller

I

Journal Paper

Reducing conflicts in Haptic Shared Control during curve negotiation

Wietske M. Scholtens, Sarah Barendswaard, and David A. Abbink, *Senior Member, IEEE*

***Abstract*—Haptic shared control enables continuous interaction between driver and automatic controller by means of torques on the steering wheel that guide towards a reference trajectory. Current haptic shared control systems induce conflicts when the reference trajectory of the automation differs from the drivers own desired trajectory, which can lead to rejection of the automation. This study investigated whether conflicts can be reduced by individualizing the automation. The approach of the study is twofold. First, a Four Design Choices Architecture (FDCA) is implemented that allows for separate tuning of the reference in a haptic shared controller that determines the total torques by separating feedback and feed-forward torques. Second, a driver-model was used to identify the individual steering parameters and determine the corresponding individualized reference in the curved road-sections. The combination of the FDCA controller and individualized reference was evaluated in an experiment using a fixed-based driving simulator. Sixteen subjects participated in a two-day experiment, where the first day was used to collect manual driving data to identify the individual and average steering parameters to construct the references. On the second day participants drove with four conditions: manual control, a conventional shared controller architecture using feedback torques towards a center-line reference, an individual tuned reference with FDCA controller, and an average tuned reference with FDCA controller. The results showed that the driver-model was able to identify differences in individual curve negotiation styles. Both FDCA controllers resulted in higher objective acceptance and lower workload; conflicts in torques and driver torques decreased significantly compared to manual control and the conventional controller. The usefulness and satisfaction scores were only marginally higher for the individualized FDCA compared to the average FDCA. Interestingly, only the individualized FDCA was perceived more satisfactory and useful than the conventional controller and manual control. Thus, the individualized FDCA can reduce conflicts and increase acceptance compared to the conventional shared controller.**

***Index Terms*—Haptic Shared Control, Conflicts, Individualization, Human-Machine interaction, driving simulator.**

I. Introduction

Haptic Shared Control (HSC) can support car drivers in the steering task by providing assisting torques on an actuated steering wheel. The driver and automation continuously share the control and can negotiate on the final steering wheel angle. The driver is in the loop and assisted by the HSC system, but can always overrule the guiding torques and thereby remains in direct control of the vehicle. Studies showed that HSC can improve the performance [12][13][28][33][32][39][40] and decrease workload [13][32][27] compared to manual control. Furthermore, the negative side effects that arise from autonomous driving, such as loss of awareness [31] and skill degradation [41] are limited for HSC [11][27].

However, this continuous interaction can result in annoyance and conflicts between the driver and the system when the intentions of the driver and automation are not aligned [2][7][14][26]. In some studies participants have complained that they were 'fighting' the system [2][27]. Drivers may turn of the guidance system if it is considered intrusive or annoying [24][26], thereby losing all the benefits of HSC. The current state of the art in HSC systems is not accepted by all drivers, therefore it is important to reduce conflicts to increase the acceptance.

The direct cause of conflicts is not clear, however, other studies seem to indicate that the largest conflicts occur in curves [7]. Drivers show variability in their trajectories in curves [37], especially in the amount of curve-cutting behaviour [7][21][22]. The approach of this study is based on the hypothesis that one of the underlying causes of conflicts in curved road profiles is a mismatch in desired trajectories [7][23] and the system needs to be adapted to the drivers own driving strategy [33]. Experiments in other fields showed reduced conflicts when the reference trajectory was individualized [16]. However, no studies were found that implemented and evaluated an individualized trajectory in a HSC driving system.

An attempt to individualize the haptic shared controller was made by Boink [7], who adjusted the control parameters for look-ahead time and the feedback gain over the lateral error with the lane-center at the look-ahead time. This effectively lead to different trajectories, but no curve-cutting trajectories could be generated. Since individualization was obtained by changing the feedback gain, the amount of feedback that was given became a major confounding factor, pointing to an inherent issue in the HSC control architecture. In order to address this issue of the coupling between the reference and the feedback torques the approach in this study is twofold; first the haptic shared controller and reference trajectory are separated. The proposed shared controller is based on a architecture that uses four design choices (figure 1), proposed by van Paassen [23]. This control structure (Four-Design-Choice-Architecture, FDCA) allows for separate tuning of the feedback and feed-forward torques towards a individualized reference trajectory and showed promising results in the simulation study from Wyzen [43], but has not been yet implemented and evaluated in a human factors experiment.

Second, the reference trajectory is individualized. Recent studies investigated methods to identify different driver trajectories [4][8][10][35]. The driver model that generates the reference trajectory must be able to identify the driver style and predict individual human driving behaviour. A promising approach to model individual human-like behaviour for

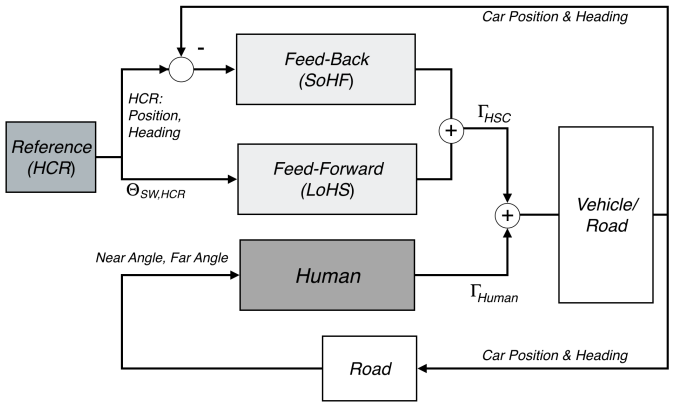

Fig. 1. The control algorithm is based on the Four-Design-Choice-Architecture (FDCA) as proposed by van Paassen [23], where in this study the Level of Haptic Authority (LoHA) is not implemented, resulting in the nominal steering wheel stiffness of 1.7 Nm. The human-compatible-reference (HCR) is the input for the SoHF (feed-back) and LoHS (feed-forward) component and can be selected to fit individual or average driver behaviour.

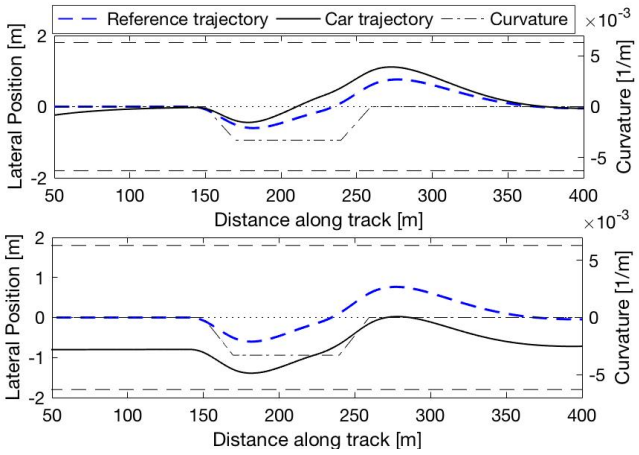

Fig. 2. Simulated response of the FDCA controller (black solid line) and the reference (blue dashed line). The top figure shows a tuning with only the feedback component active ($K_{FB} = 1$, $K_{\psi} = 50$, $K_y = 1.4$, $K_{FFW} = 0$). The bottom figure shows a tuning with only the feed-forward component active (K_{FB} = 0, K_{FFW} = 1).

curve negotiation include a compensation and anticipation component [3][20][34][35][36]. These models are based on the hypothesizes that drivers determine their steering input by anticipating for the upcoming curvature profile and compensating for the current position and heading of the vehicle relative to the road. The implemented reference trajectory in the FDCA structure is determined using individualized gains in a driver model inspired by the cybernetic model from Saleh [34].

The goal of this study is to quantify trajectory-based conflicts in curve negotiation between individual drivers and haptic shared controller and to investigate to what extent these conflicts can be reduced by means of a HSC architecture that allows individualized reference trajectories. It is hypothesized that the the separated control structure will reduce conflicts compared to a coupled shared controller and that individual tuning of the reference trajectory will further reduce conflicts and increase acceptance.

To distinguish between the benefits of individualization and the effects from the FDCA structure four conditions are evaluated. An individual and average reference trajectory, generated using a cybernetic driver-model, are compared with manual control and an earlier developed HSC algorithm that couples the reference and haptic shared controller. Section II will discuss the control models and the generation of the individual and average references by the driver-model. The methods that are used are discussed in section III, followed by the results in section IV, the discussion in section V and conclusion in section VI.

II. Haptic Shared Control Design

Three different HSC algorithms are compared; two versions of an adjusted FDCA [23] and one setting of a earlier developed HSC algorithm [32] that does not separate the reference trajectory and the haptic shared controller.

A. Four-Design-Choice-Architecture (FDCA)

The FDCA controller is based on four design choices for the Human-Compatible-Reference (HCR), Strength of Haptic Feedback (SoHF), Level of Haptic Support (LoHS) and Level of Haptic Authority (LoHA) [23]. In this study only the HCR, SoHF and LoHS will be implemented and tuned. The HCR can be interpreted as the behaviour from a virtual car driving automatically on the same road. The steering wheel angles of the HCR are used in the LoHS component and the position and heading are used for the SoHF.

1) Level of Haptic Support: The Level of Haptic Support (LoHS) acts as a feed-forward (FFW) controller and applies torques to the steering wheel based on the steering wheel angle from the HCR. These torques are applied even if there is no deviation from the HCR. Tuning the value for K_{LoHS} determines how much the controller contributes to the task. In the implementation in the driving simulator Γ_{HCR} is approximated using the dynamics of the steering wheel in the simulator and the steering wheel angle of the HCR. The final Γ_{FFW} is thereby determined as:

$$\begin{aligned} \Gamma_{LoHS} &= K_{LoHS} \cdot \Gamma_{HCR} && (1) \\ &\approx K_{LoHS} \cdot K_{SW} \cdot \Theta_{SW,HCR} && (2) \\ &= K_{FFW} \cdot \Theta_{SW,HCR} && (3) \end{aligned}$$

Here $\Theta_{SW,HCR}$ is the steering angle from the HCR and K_{SW} is the steering wheel stiffness. If K_{FFW} is tuned to result in equal steering wheel angles as the HCR this will lead to a car that behaves as an autonomous vehicle, visualized in figure 2. However, if a deviation from the nominal path occurs, this error will not be compensated for.

2) Strength of Haptic Feedback: The Strength of Haptic Feedback (SoHF) provides feedback torques to compensate for deviations from the HCR. The SoHF can be tuned with K_{ψ} and K_y for respectively the error in the current heading and current position between the HCR and real car.

$$\Gamma_{SoHF} = K_{FB} \cdot (K_{\psi} \cdot \Delta\psi + K_y \cdot \Delta y) \quad (4)$$

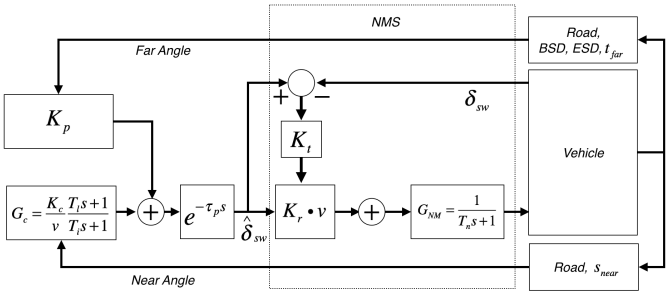

Fig. 3. The driver-model is used to generate the references and is based on the work from Saleh [34]. The near and far angles are the input in the driver-model and K_c and K_p determine their influence respectively. $T_I, T_L, \tau_p, K_r, K_t$ and T_N are indicated in II-B1 and based on the findings of Saleh [34]. The determination of the near and far angle is discussed in section II-B2.

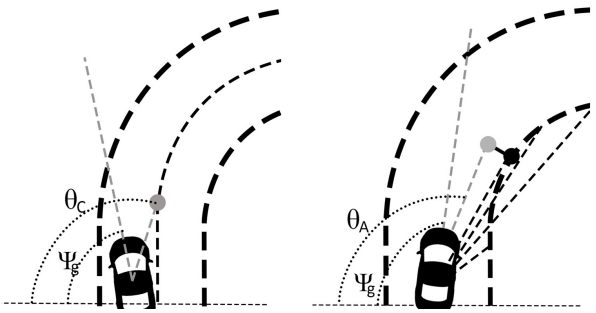

Fig. 4. The near angle (left) and far angle (right) are determined using the global heading and the angle to the corresponding point in the global reference frame.

Far Gain (K_p)	2:0.125:3.25 [-]
Near Gain (K_c)	0:1:5 [-]
Begin Steering Distance (BSD)	1, 2.5:2.5:25 [m]
End Steering Distance (ESD)	40:5:55 [m]
t_{far}	2:0.5:3.5 [sec]
T_I	1 [-]
T_L	3 [-]
τ_p	0.03 [sec]
K_r	0.3 [-]
K_t	0.5 [-]
T_N	0.1 [-]

TABLE I
PARAMETER VALUES USED FOR GENERATION OF THE HUMAN COMPATIBLE REFERENCES (HCR)

3) Level of Haptic Authority: The Level of Haptic Authority (LoHA) influences the weight of the controller in the final control torques. Van Paassen [23] defined the LoHA as the steering wheel stiffness around the desired steering wheel angle. Making the stiffness higher makes it harder for the driver to overrule the automation. Since the control torques are scaled with the LoHA, the desired steering wheel angle is not effected by changing the LoHA. How the LoHA should be tuned is investigated in multiple studies and it is argued that it should involve the personal settings of the neuromuscular stiffness [2][38]. However in this study the LoHA is not implemented, which results in the nominal steering wheel stiffness of 1.7 [Nm]. Thereby the drivers were always able to overrule the system.

B. Human Compatible Reference

In this study two FDCA controllers are designed which use a different human-compatible-reference (HCR). One that matches the individual steering behaviour, whereas the other resembles the average steering behavior (one-size-fits-all, OSFA). The HCR is generated using a two-level model inspired by the cybernetic model of Saleh [34], as shown in figure 3. The inputs are a near and far angle, which are derived from the geometric approximations of the near and far point respectively. A closed-loop model is generated by using the steering wheel torques as the input for the car-model, from which the new visual input can be determined for the human-model. The main difference with the work of Saleh is the geometric determination of the near and far angles and different vehicle dynamics. Section II-B1 of this paragraph will discuss the human model from Saleh, followed by the determination of the near and far angles in section II-B2 and II-B3. The car dynamics are discussed in II-B4, fitting procedure in II-B5 and last the implementation in II-B6.

1) Human Model: The human-model from Saleh [34] takes into account the human response to the visual environment inputs with respect to neuromuscular system (NMS), sensorimotor and cognitive control. The components in the model include the visual compensation (K_c, T_i, T_L) and anticipation (K_p), processing delay (τ_p), angle to torque coefficient (K_r), gain of the stretch reflex (K_t) and neuromuscular time constant (T_N). In this study $T_I, T_L, \tau_p, K_r, K_t$ and T_N are kept identical to the nominal values determined by Saleh [34]. However, the variation interval for the values of the visual compensation (K_c) and anticipation (K_p) do not match the range indicated by Saleh. This is due to the difference in determination of the near and far angles and different vehicle dynamics of the car, which will be discussed in the next section. The new range of parameters and resolutions is shown in table II-B1.

2) Near and far Angle: Using a near and far point, the near and far angles are determined. The near point is selected as the point in the middle of the road at a look-a-head distance (s_{near}) ahead. This distance is set to a constant of 5 meters, according to the work of Saleh [34]. The near angle is determined as in equation 5, where Θ_C is the angle in the global reference frame to the near point and Ψ_g is the global heading. A visual representation is shown in figure 4.

$$\Theta_{near} = \Theta_C - \Psi_{GlobalHeading} \tag{5}$$

The far point is selected by first determining the tangent point. The gradients of the lines from the car to future lane-boundary points are determined and the road-point corresponding to the line with the optimum in gradient is selected as tangent point. Boer [6] proposed to use an alternative far point instead of the tangent point, since 'the tangent point could never be reached'. The target point is a point shifted towards the road-center with respect to the tangent point, illustrated in figure 4 by the inner grey dot. The far angle is computed as in eq. 6, where Θ_A is the angle in the global reference frame to the tangent point.

$$\Theta_{far} = \Theta_A - \Psi_{GlobalHeading} \tag{6}$$

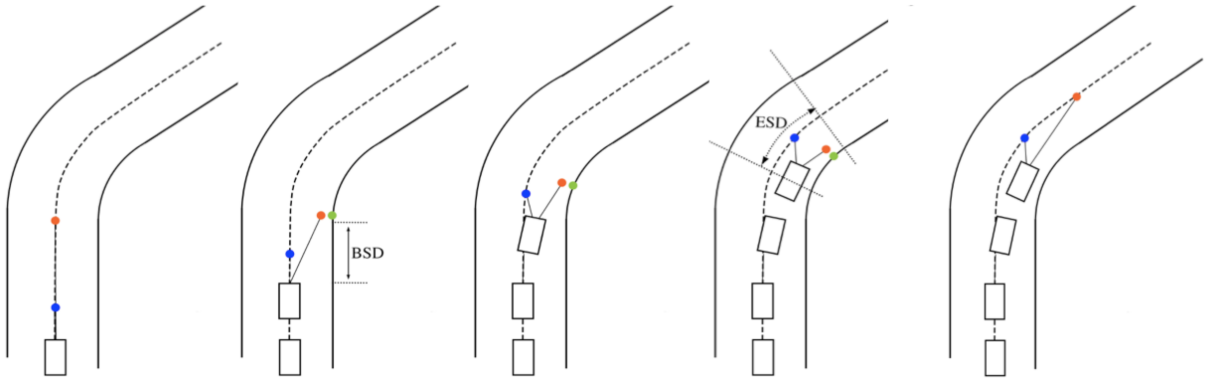

Fig. 5. Visual representation of the near point (blue dot) and far point (orange dot) over the length of the curve, the tangent point is indicated with the green dot. The steering initiation distances before the begin and end of the curve are indicated with respectively BSD and ESD. In the most right plot t_{far} determines how far in the future the far point is located.

3) Steering Initiation Distances: Curve negotiation behaviour is not only characterized by the lateral deviation from the center line. It is hypothesized that an important characteristic is the point where the driver initiates the steering behaviour. The model is extended with two threshold distances, one before the start and one at the end of the curve. The first parameter (Begin Steering Distance, BSD) determines where the model switches to the target point and thereby when the model starts anticipating on the upcoming curvature profile. If the threshold distance is less than the cars distance to the curve, the far point is located in the middle of the road at the gaze-ahead time t_{far}. The second parameter (End Steering Distance, ESD) determines when the far point switches back to the center of the road when steering out of the curve. A visual representation is shown in figure 5.

4) Vehicle Dynamics: The vehicle dynamics in the car-model are a linear approximation of the non-linear Nissan Dynamics in the HMI-lab located at the faculty of aerospace engineering at the Technical University of Delft, which are identical to those in earlier studies [32]. The equations of motions for the vehicle dynamics are:

$$x(t+T_s) = Ax(t) + Bu(t) \tag{7}$$

$$y(t) = Cx(t) + Du(t) \tag{8}$$

$$A = \begin{bmatrix} 0.8665 & -.03849 \\ 0.1313 & 0.9824 \end{bmatrix} B = \begin{bmatrix} -14.24 \\ 23.64 \end{bmatrix} \tag{9}$$

$$C = \begin{bmatrix} -0.292 & -0.1938 \\ -0.000577 & 0.02834 \end{bmatrix} D = \begin{bmatrix} 0 \\ 0 \end{bmatrix} \tag{10}$$

Here T_s is 0.01 [s]. The input is the front tyre angle, the outputs are the lateral acceleration and the yaw rate of the car. The equation of motion for the simulated steering wheel is:

$$I_{sw} \cdot \ddot{\delta} = \Gamma - K_{sw} \cdot \delta - B_{sw} \cdot \dot{\delta} \tag{11}$$

The stiffness K_{sw}, damping B_{sw} and inertia I_{sw} of the steering wheel are respectively 4.2 [Nm/rad], 2 [Nm·s/rad] and 0.3 [kg · m^2]. To convert the steering wheel angle to the front wheel angle it is multiplied with a ratio of 23.7. A validation study was made to show that this linear approximation is reasonable. The constant velocity in the simulation is 24 m/s.

5) Fitting procedure: To determine the individual and one-size-fits-all HCR, first all trajectories for the whole parameter range and resolutions of the five parameters as in table II-B1 are pre-generated. Next the RMS errors between the lateral positions from the trajectories driven with manual control and all pre-generated HCR's are determined. The RMS errors are determined separately for the beginning, middle and end of the curve, where each section has a length of 59 meter, starting at 325.2 [m] and 673.2 [m] for respectively the right and left curve (figure 11). The beginning and end section are weighed with a factor 2, the middle section is weighed with a factor 1.5; these factors are heuristically tuned. The HCR with the lowest sum of the weighed RMS values is selected as the HCR.

6) Implementation: The HCR is determined by simulating a human and linearized car-model in MATLAB as described earlier in this chapter. The position, heading and steering-wheel angles of the car are recorded and saved in a matrix that is used as input for the driving simulator. The index of the nearest trajectory point is determined using the position vectors in the matrix, the corresponding steering-wheel angle is used in the feed-forward components, whereas the global positions and heading are used in the feedback component.

C. Two-Level Controller (TwL)

The FDCA controllers are compared with an earlier developed feedback-controller [33]. This controller does not distinguish between reference and haptic shared controller and determines the continuous feedback torques using a two-level architecture. The first level uses the future lateral error with the lane center and the future lateral heading at a look-ahead-distance to determine the desired steering wheel angles. The second level determines the feedback torques using the variables from the first level as in equation 12, the parameters for D, P and K_f are indicated in table III-D2.

$$\Gamma_{FB} = (e_{lat\_future} \cdot D + e_{heading\_future} \cdot P) \cdot K_f \tag{12}$$

Fig. 6. Visual representation of the narrowing section located on the straight parts.

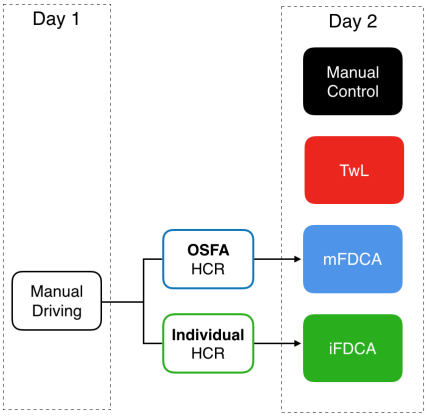

Fig. 7. The experiment is performed on two days, the first day is used to collect manual driving data on which the model is fitted to generate the individual and one-size-fits-all HCR for the second day. On the second day the participants drove with four different conditions.

III. Method

A within subjects human factors experiment is conducted to probe the benefits of individualization, as well as the influence of the new control structure. This chapter contains the experimental set-up, road design, subjects information, the experimental design, the four different conditions, used variables & metrics and the hypothesis.

A. Experimental set-up

The experiments were performed in a fixed-based driving simulator at the department of Control and Simulation at the Delft University of Technology. The visual representation was done with three projectors that covered a horizontal view of 180 degrees and a vertical view of 40 degrees. The actuation of the steering wheel was done with a MOOG FCS Ecol8000S Actuator. The steering wheel stiffness was set to 1.7 [Nm] and the vehicle dynamics are the default Nissan Dynamics in the simulator. These default dynamics are identical to earlier studies [7][30][32].

B. Road design

The road profile consists of a right and a left clothoidal curve of the same curvature, both repeated five times, thereby resulting in ten curves in total. The total length of the road was 3.7 km with a width of 3.6 m. The curvature profile was heuristically selected to evoke different driving behaviour, using data from experiments performed earlier in the same group. The curve radius was 300 meter and the total curve length was 108 meter with clothoidal sections of 18 meters at the begin and end. The driver-model is not able to capture biases in the straight section and it will always initiate the curve from the center. The HCR can therefore not replicate the drivers behaviour if participants initiate the curve with an offset. It was found that when curves follow up too soon, the effect of the previous curve is still visible in the initial start position of the following curve. To decrease the effect of the curves on each other the distances between the curves was 240 meter long. Furthermore, a narrowing section (figure 6) with a width of 2.5 meters was made on the straight sections between two alternating curves using cones. The narrowing section was 40 meters long and started at 125 meter after the previous curve end.

C. Subjects

Sixteen subjects voluntarily participated in the driving simulator experiment, without receiving financial compensation. All subjects were or had been students at Delft University of Technology. The average age was 26.6 years old, in the range of 23 and 28 years with a standard deviation of 1.3 years.

D. Experimental Design

The experiment was conducted on two separate days, with between 7 and 11 days in between. The first day was used to collect personal data for each driver to fit the HCR. On the second day the experiment to compare the four conditions was conducted.

1) Day 1: On the first day the subjects were asked to read and sign the informed consent and were explained about the purpose and procedures of this experiment. They were informed about the possibility to withdraw at any time. The participants were instructed to drive as they normally would and to hold their hands at ten to two position on the steering wheel. They were informed that the road was a one-lane road and they were sitting at the left side of the car. Furthermore, they were instructed to go through the narrowing sections by trying not to hit the cones, but no more specifications were given. Also, they were not instructed to specifically return to the lane center or enter the curve in a specific way. Before collecting the data of the behaviour of the driver, each participant had a training trial to familiarize themselves with the system. This would take 160 seconds which is considered enough to become familiar with the system. After the training session the real trial was conducted which was recorded and used to identify the individual and one-size-fits-all HCR.

2) Day 2: On the second day the four conditions were compared using a counterbalanced within-subjects design. The

Gain	FDCA	Gain	TwL
K_y	0.05	K_f	2.0
K_ψ	0.03	D	0.08
K_{FB}	1.5	P	0.9
K_{FFW}	0.45	t_{lh}	0.7

TABLE II
CONTROL GAINS FOR THE FDCA AND TWL CONTROLLERS

order of the conditions was determined by using a 4x4 latin-square design. Prior to the experiment itself the instructions were explained again, as well as their right to withdraw. Before each trial the participants had one familiarization run, which took on average 160 seconds. Each condition was performed once by each subject. After each trial the participants were asked to step out the simulator and fill in a questionnaire about their acceptance.

E. Conditions

Four conditions were compared, where for all conditions the road environment, vehicle dynamics and constant longitudinal velocity of 24 m/s were kept identical.

- *Manual (D)*
  The three controllers are compared with a manual control condition. No guidance torques were applied to the steering wheel in this condition.
- *One-size-fits-all TwL controller (TwL)*
  The FDCA controller is compared with an earlier developed feedback controller. One type of tuning is used for this controller, which is identical to the settings used in the work from Mulder et al. [32], shown in table III-D2.
- *One-size-fits-all FDCA controller (mFDCA)*
  The mFDCA controller contains the one-size-fits-all HCR (mHCR) tuned for the mean driver behaviour. This mHCR is determined using the fitting approach as mentioned in section II-B5, where the HCR is fitted separately for left and right curves. This resulted in 80 repetitions per curve direction, over which the mean is determined for the fitting procedure. The tuning of the control parameters (K_{FB}, K_y, K_ψ, K_{FFW}) is as in table III-D2.
- *Individualized FDCA controller (iFDCA)*
  The iFDCA contains the individualized HCR (iHCR). Again the model is fitted separately for left and right curves. This resulted in five repetitions per curve direction, over which the mean is determined for the fitting procedure. The tuning of the control parameters (K_{FB}, K_y, K_ψ, K_{FFW}) is identical to the tuning for the mFDCA.

F. Variables & Metrics

The first set of dependent variables evaluate the driver-models capabilities and how close the fit between the HCR and the manual behaviour on the second experiment day is. Part 2, 3 and 4 evaluate the different conditions on the second day using acceptance, performance and workload metrics, which is in accordance with earlier studies [30][**?**][27].

1) Human-Compatible-Reference:

- *Descriptiveness* To check whether the model is able to capture a broad range of human driver behaviour it is evaluated using the descriptiveness method as proposed by Barendswaard [5]. The descriptiveness is calculated as the percentage of total road surface that can be covered with the model. The road surface is selected as all positions on the road 1 second before and after the curve, which follow from the findings for the preview time of drivers from van der El [9]. To make sure only trajectories that are generated with realistic steering behaviour are evaluated, the maximum amount of steering reversals (explained later in this section) is set to three.
- *Error between Manual Trajectory and HCR [m]* The error is determined for the lateral position and the steering wheel angles. The lateral position error was defined as the distance from the middle of the car to the HCR at the same longitudinal distance along the road. The absolute lateral error is a measure of the ability of the model to capture the personal driving behaviour.
  The error in steering wheel angles is determined by taking the difference between the HCR steering wheel angle and steering wheel angle measured in the simulator.
- *Variance Accounted For* The Variance Accounted For (VAF) determines how similar two signals are and can be used to verify the correctness of a model; the higher the value the better the match between the signals is. The VAF is determined for each driver by taking the mean of the VAF's for each separate curve. Equation 13 shows the equation for the VAF, here u is the lateral position with respect to the center-line for either the HCR or the car.

$$VAF = \left(1 - \frac{\sum_{k=1}^{N} |u_{driver}[k] - u_{mod}[k]|^2}{\sum_{k=1}^{N} u_{driver}^2[k]}\right) \cdot 100\% \quad (13)$$

2) Acceptance:

- *Van der Laan* To asses the acceptance of the system the questionnaire from Van der Laan [19] is used, which uses two dimensions: a usefulness scale and a satisfaction scale. The questionnaire consists of nine likert items:
  1) Useful - Useless
  2) Pleasant - Unpleasant
  3) Bad - Good
  4) Nice - Annoying
  5) Effective - Superfluous
  6) Irritating - Likeable
  7) Assisting - Worthless
  8) Undesirable - Desirable
  9) Raising Alertness - Sleep-inducing

  Each item has to be graded with a score from -2 to + 2. The usefulness scale is determined with the sum of item 1, 3, 5 and 7, divided by 5. The satisfactory scale is the sum of 2, 4, 6 and 8, divided by 4.
- *Number of Conflicting Torques* Opposing torques from the driver and the controller can indicate conflicts in intentions. The conflict in torques is not determined in

magnitude, since the underlying control architecture of the different controllers makes it difficult to compare the magnitude of the conflicting torques. Therefore, only the occurrence of the conflicts in torques is evaluated. The occurrence of a conflict is determined by first selecting whether or not the directions of the driver torque and HSC torque are opposite in direction. In case the torques are opposed, the value is set to 1 or -1, depending on the direction of the driver torque. When the driver torque and HSC torque are in the same direction the conflicting value is zero; the HSC torque is supporting the intentions from the driver.

$$O_{conflict} = \begin{cases} 1 & \text{if } \Gamma_{Hum} \cdot \Gamma_{HSC} < 0 || \Gamma_{Hum} > 0 \\ -1 & \text{if } \Gamma_{Hum} \cdot \Gamma_{HSC} < 0 || \Gamma_{Hum} < 0 \\ 0, & \text{otherwise} \end{cases} \quad (14)$$

3) Performance:

- *Error to HCR* The lateral error and steering wheel error to the HCR as described for the HCR match is also used as independent metric for the FDCA conditions. For the two conditions with the FDCA controller it represents how accurate the driver follows the intentions from the controller.
- *Lateral Position* The lateral position is defined as the distance from the center of the car to the lane center, which measures the lane-keeping accuracy. It can not act to display performance, since a trajectory closer the lane center does not necessarily mean a better performance. However, it can give more insight in the personal driving behaviour and show how drivers changed their behaviour for the different conditions.
- *Time-to-Lane Crossing (TLC)* The TLC is used to measure the time before the car goes out of lane if the driver does not change the current heading and steering wheel angle. It represents the situational criticality and thereby the safety [44] and was computed using a trigonometric method [44].

4) Workload:

- *Steering Reversal Rate (SRR)* The steering reversal rate is used as an objective measure for the workload [15]. The steering reversal rate is determined by counting how many times the steering wheel is reversed with 2 degrees or more around a local minima and maxima [15].
- *Absolute Driver Torque* The Absolute Driver Torque is the torque applied by the driver on the steering wheel and is used as a measure for the driver's physical effort.

G. Hypothesis

The following hypothesis are drawn based on preliminary investigations and the earlier work from Wyzen [43], Melman[30], Boink [7] and van Paassen [23]. The first four hypothesis compare the mFDCA controller with the TwL controller and manual control:

- The acceptance in terms of objective and subjective measures will be higher for the mFDCA controller compared to the TwL controller.
- With the mFDCA controller the drivers will deviate more from the lane center than with the TwL controller.
- The driver torque will be lower with the mFDCA controller compared to both the TwL controller and manual control.
- The SRR for the mFDCA will be similar to the TwL controller, but both will be lower than with manual control.

The next four hypothesis compare the iFDCA and mFDCA controller.

- The individual HCR will have a lower error with the manual driving behaviour on the second day than the one-size-fits-all HCR. The VAF will be higher for the individual HCR than for the one-size-fits-all HCR.
- The subjective and objective acceptance will be higher with iFDCA than with mFDCA.
- The drivers will follow the systems intentions better with iFDCA than with mFDCA, resulting in a lower error with the HCR in terms of the lateral position and steering wheel angle.
- The workload in terms of driver torque will be lower with iFDCA than with mFDCA.

H. Data Analysis

To check the significance between the conditions a two-way repeated measures ANOVA comparison is done. The first factor has two levels which are the directions of the curve. The second factor has four levels, which are the conditions. To determine the mean over the variables the distance from 35 meter before to 35 meter after the curves is evaluated. For the curved sections each curve acted as a repetition, resulting in five repetitions per curve direction. The pairwise comparisons for the two factors were applied with Bonferroni corrections. Furthermore a one-way repeated measures ANOVA is done for the usefulness and satisfaction variables, since these were not evaluated for each separate curve but only after the whole trial.

IV. Results

The results are divided in three sections. Section IV-A shows the results of the implementation of the FDCA controller. Section IV-B evaluates to what extent the model could identify different driver behaviour. The sections IV-C, IV-D and IV-E show the results from the human-factors experiment for the four different conditions based on acceptance, performance and workload.

A. Haptic Shared Control Implementation

Figure 8 shows the functionality of the FDCA controller, by showing the lateral position, steering wheel angle and the combination of driver torque and total haptic shared control torque (decomposed into feed-forward and feedback torques) for subject 2. Two situations are shown: the situation where

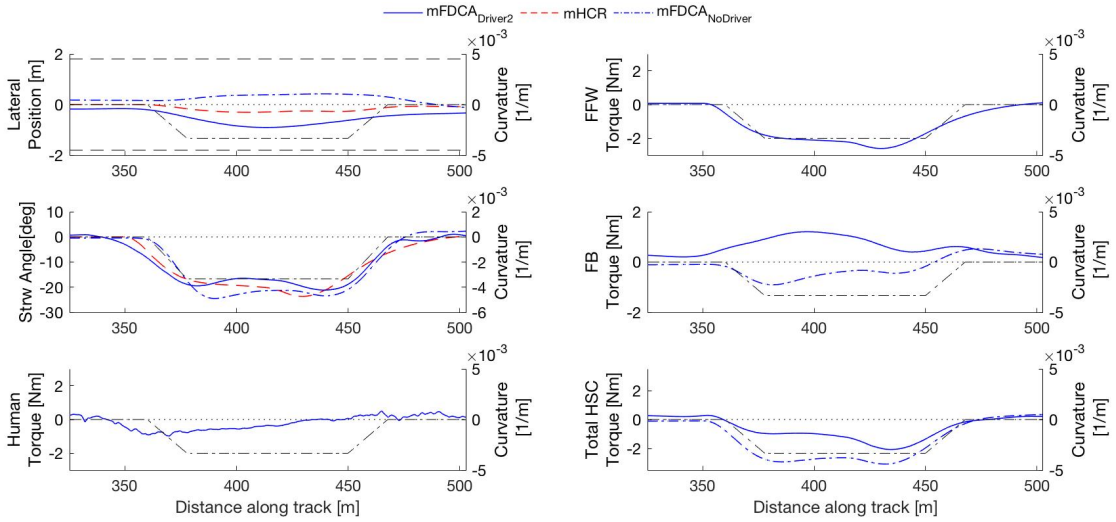

Fig. 8. Illustration of driving behaviour and torque contributions of subject 2 supported by the mFDCA controller (solid blue line), compared to the driving behaviour of only the controller without a driver present (dashed blue line). The red dashed lines illustrate the fitted average human-compatible reference (mHCR) trajectory and steering angle. The right column illustrated the feed-forward torque (top) and the feedback torque (middle) that together constitute the total haptic shared control torque (bottom).

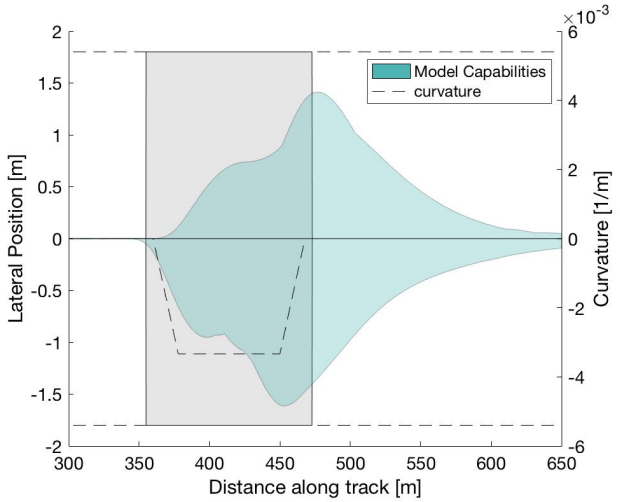

Fig. 9. Visualization of the FDCA model capabilities to represent different lateral positions, from an initial lateral position of zero. The green area shows the models capabilities for realistic driver behaviour. The gray area indicates all positions on the road 1 second before and after the curve.

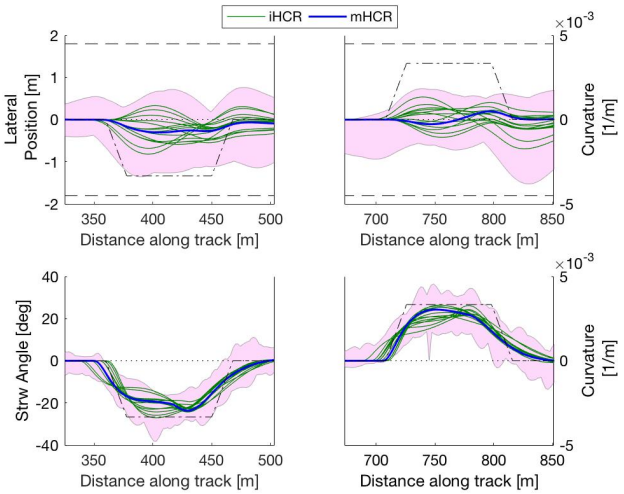

Fig. 10. The resulted individual fitted HCR's for all 16 participants are visualized (green lines) as well as the one-size-fits-all HCR (blue line). The pink area visualizes the range of driver behaviour on the first experiment day of all participants. The top figures show the lateral positions and the bottom figures the steering wheel angles.

subject 2 drives with the mFDCA controller and the mFDCA controller without driver input. The feed-forward component for the driver with mFDCA (blue) and for only the mFDCA controller (blue dashed) match each other almost perfectly. This is logical, since the feed-forward torque is designed to act independent from the lateral position, but links to the distance along track. The feedback component is dependent of the position and heading and is therefore different for the car driving with and without driver input. In the first plot the car driving without driver input (mFDCA) shows under-steer behaviour, since the controller is tuned to not follow the HCR autonomously. Therefore the driver still needs to provide torques to the steering wheel, which is seen in the bottom-left plot.

B. Human Compatible Reference

The capabilities of the FDCA model to represent different driver lines is illustrated in figure 9. The gray area represents all possible lateral positions a driver could possibly take, selected as the road surface from 1 second before, to 1 second after the curve. The green area illustrates all possible lateral positions the FDCA model could reach from an initial lateral position of zero. The descriptiveness [5] is the grey area covered by the green area and is 45.89 %.

Figure 10 shows the identified individual HCR's (iHCR) and one-size-fits-all HCR (mHCR), as well as the range of the trajectories driven by all 16 participants in pink. The individual HCR's do not cover the whole pink area since the

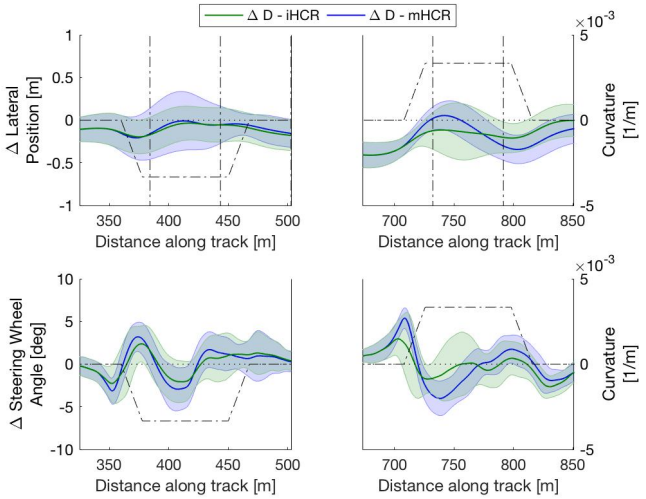

Fig. 11. The error between the manual driving behaviour on the second experiment day and the individual HCR (mean and STD in green) and one-size-fits-all HCR (mean and STD in blue) for right curves (left column) and left curves (right column) of all subjects. The top figures visualize the error in lateral positions and the bottom figures the error in steering wheel angles.

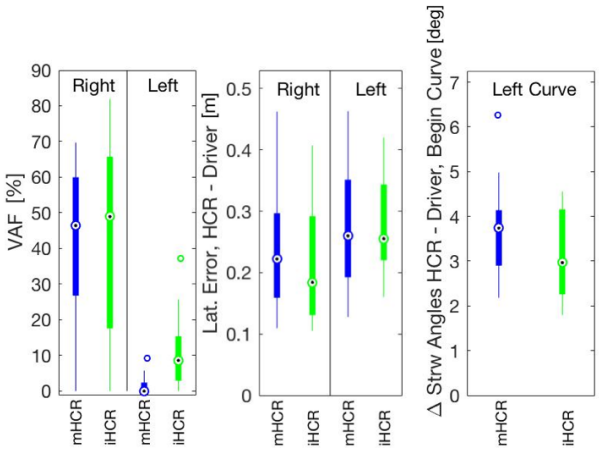

Fig. 12. *Left:* Mean VAF (over the whole curve) between the lateral positions of the HCR and manual driven trajectory on the second experiment day, *Middle:* Mean lateral error (over the whole curve) between HCR and manual driven trajectory on the second experiment day, *Right:* Mean error in steering wheel angle between HCR and manual driven trajectory, between 700 and 725 [m]. *All:* Dependent variables are visualized for individual HCR (green) and one-size-fits-all HCR (blue) and for left and right curves.

pink area visualizes also separate curves, where the model is fitted on the average of five curves. The between-driver variability in individual HCR's can be characterized with a standard deviation 0.18 [m], indicating that driver-model can capture different behaviour in the curves.

The lateral error between the trajectory driven with manual control and both individual HCR and one-size-fits-all HCR are shown in figure 11. The mean absolute lateral errors is shown in figure 12; the pairwise comparisons showed that the results are not significantly different for the individual HCR and one-size-fits-all HCR, but are significantly lower for the right curves ($p = 0.044$).

The absolute error in steering wheel angles is not found to be significantly different. However, figure 11 and figure 12 show that the peaks in the errors are higher for the one-

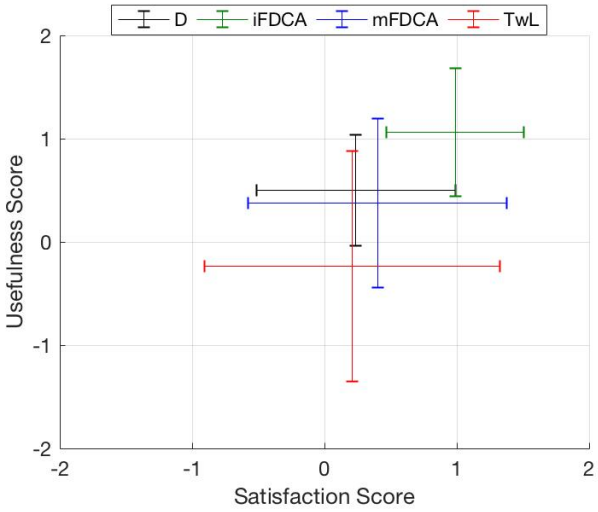

Fig. 13. Mean and STD of the Usefulness and Satisfaction score from the 'Vanderlaan' questionnaire for all subjects. In green for the FDCA with individual HCR, in blue for the FDCA with one-size-fits-all HCR, in red for the TwL condition and in black with manual control.

	Controller (4)		
	df	F	p
Acceptance			
Usefulness Score [-]	3, 1.74*	5.35	x
Satisfaction Score [-]	3	5.68	xx

TABLE III
RESULTS FOR ONE-WAY ANOVA FOR SUBJECTIVE ACCEPTANCE BETWEEN THE FOUR CONDITIONS. X = $p < 0.05$, XX = $p < 0.01$, *=CORRECTION FOR NON-SPHERITY

size-fits-all HCR, especially in the beginning of the left curve ($p = 0.0156$).

Figure 12 shows the VAF between the lateral positions of the manual driven trajectory on the second experiment day and both individual HCR and one-size-fits-all HCR for left and right curves. The pairwise comparison showed that the VAF for the individual HCR is slightly but not significantly higher than the VAF for the one-size-fits-all HCR ($p = 0.06$). The pairwise comparison between the curve directions showed that the VAF for right curves is significantly higher than for the left curves ($p < 0.01$).

C. Acceptance

The acceptance of drivers for each system was analyzed by the self-reported Van der Laan questionnaire. An additional objective indication of acceptance was proposed by the conflict in torque metric.

Figure 13 shows the results for the Van Der Laan questionnaire for all four conditions. The iFDCA is located at the most top-right position and TwL in the most bottom-left position. The ANOVA results show that the satisfaction and usefulness scores were significantly different between the conditions ($p < 0.01, p < 0.01$). The pairwise comparison for the satisfaction score showed that the results for mFDCA condition is not significantly different from the TwL condition. The iFDCA satisfaction score is significantly higher than manual and TwL ($p < 0.01, p = 0.03$), but not higher than

	Controller (2)			**Curve Direction** (2)			**Contr. * Curve Direction**		
Metric	df	F	p	df	F	p	df	F	p
Driver-model performance									
Mean Abs. Lat. Error (D - HCR) [m]	1	0.85	o”	1	4.86	x”	1	2.40	o”
Mean Abs. Strw Error (D - HCR) [deg]	1	0.13	o”	1	0.65	o”	1	0.63	o”
VAF [-]	1	4.02	o”	1	38.11	xx”	1	5.02	x”

TABLE IV

RESULTS FOR TWO-WAY ANOVA'S FOR THE DEPENDENT VARIABLES RELATED TO THE HCR FIT. X = $p < 0.05$, XX = $p < 0.01$, O = NOT SIGNIFICANT, *=CORRECTION FOR NON-SPHERITY, ” = ONE OF THE DEPENDENT VARIABLES IS NOT NORMALLY DISTRIBUTED.

	Controller (4)			**Curve Direction** (2)			**Contr. * Curve Direction**		
Metric	df	F	p	df	F	p	df	F	p
Acceptance									
Mean Conflict in Torques [-]	3, 1.55*	193.50	xx”	1	184.53	xx”	3, 1.42*	17.59	xx”
Performance									
Mean Abs. Lat. Position [m]	3	11.20	xx	1	13.68	xx	3	8.35	xx
Mean Time-to-lane Crossing [sec]	3	3.79	x”	1	4.25	o”	3, 1.78*	0.16	o”
Workload									
Steering Reversal Rate [-]	3	0.47	o	1	2.45	o	3 0.191	0.101	o
Mean Abs. Driver Torque [Nm]	3, 1.58*	548.88	xx	1	140.93	xx	3, 1.36*	16.73	xx

TABLE V

RESULTS TWO-WAY ANOVA FOR DEPENDENT VARIABLES OVER THE FOUR CONDITIONS. X = $p < 0.05$, XX = $p < 0.01$, O = NOT SIGNIFICANT, *=CORRECTION FOR NON-SPHERITY, ” = ONE OF THE DEPENDENT VARIABLES IS NOT NORMALLY DISTRIBUTED.

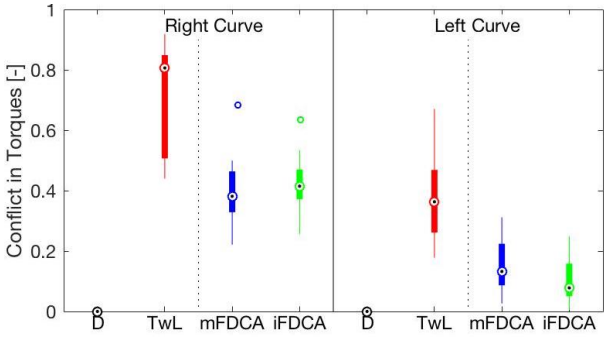

Fig. 14. Mean conflict occurrence over the distance from 35 meter before to 35 after the curve, indicated separately for right and left curves for all four conditions for all subjects.

mFDCA ($p = 0.3$). The usefulness score for mFDCA is not significantly different from any condition. For iFDCA the usefulness is significantly higher compared to the TwL ($p = 0.01$) and manual ($p = 0.018$).

Figure 14 shows the significant higher TwL conflict torques compared to both the iFDCA and mFDCA condition ($p < 0.01, p < 0.01$). Between iFDCA and mFDCA no significant difference was found. Figure 15 also shows that the conflicts with TwL consisted over the whole curve, where for iFDCA and mFDCA conflicts mainly show when steering in and steering out. In the right curves the torques conflict significantly more than in the left curves ($p < 0.01$). Furthermore, figure 15 shows that just before the curve entry for both curve directions peaks are seen in the amount of conflicts that occurred, where the peak is higher for mFDCA than for iFDCA.

D. Performance

The performance for the FDCA systems was analyzed by comparing the behaviour in terms of lateral positions and steering wheel angles to the HCR. To analyze the behaviour for all conditions the lateral positions and time-to-lane crossing (TLC) are evaluated, where the lateral position only indicates non-qualitative performance.

The error in steering wheel angle and lateral position to the HCR is similar for the iFDCA ($\mu_{err,lat} = 0.25, \mu_{err,strw} = 2.78$) and mFDCA ($\mu_{err,lat} = 0.26, \mu_{err,strw} = 2.81$), indicating that drivers did follow the suggestions of the system for both conditions.

The mean lateral position for all conditions is shown in figure 15. Figure 16 shows the absolute lateral position in the curved sections, which was significantly different ($p < 0.01$). The pairwise comparison showed it differs significantly between TwL and all other conditions ($p < 0.01$ for all comparisons); drivers drove closer to the lane center with TwL compared to the other conditions. For both FDCA conditions no significant difference was found compared to manual control, but figure 15 indicates that the curves were cut more with both iFDCA and mFDCA, especially in the end of the curves. Between iFDCA and mFDCA no significant differences are found. The pairwise comparison for the different curve directions showed that the lateral distance to the lane center was larger in the right curves ($p < 0.01$). Analyses for the manual condition showed a significant difference in lateral position at 35 m before the curves ($\mu_{Right} = -0.11$, $\mu_{Left} = -0.41$, $p < 0.01$).

The mean time-to-lane crossing (TLC) is significantly different between the conditions ($\mu_D = 5.81, \mu_{iFDCA} = 6.03, \mu_{mFDCA} = 6.57, \mu_{TwL} = 6.62, p = 0.017$). The pairwise comparison showed significant differences between manual and TwL ($p = 0.014$) and between mFDCA and TwL ($p = 0.019$). However, the pairwise comparisons showed the TLC does not increase significantly for both FDCA conditions compared to manual control.

E. Workload

The drivers workload is analyzed by the steering reversal rate (SRR) and the driver torque applied on the steering wheel. The steering reversal rate (SRR) over the whole trajectory

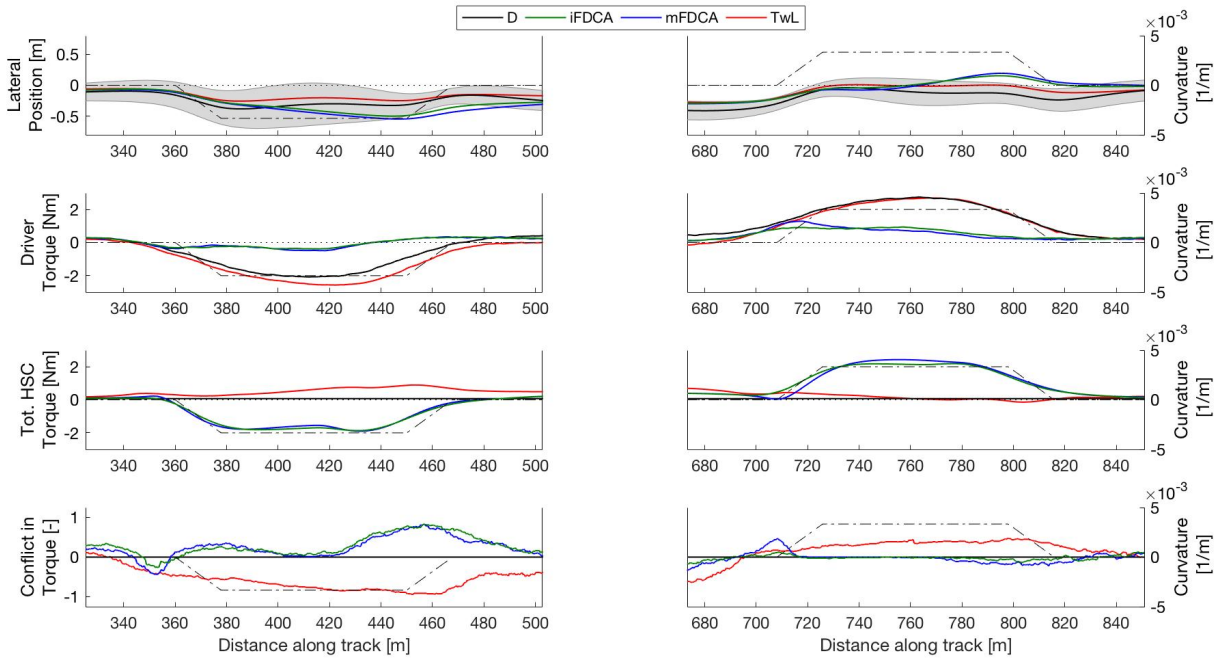

Fig. 15. Driving behaviour averaged over all participants, for each of the four conditions separated for left curves (left panels) and right curves (right panels). The driving behaviour is characterized by lateral position (top row), driver torque (second row), total torque generated by the shared controller (third row), and the conflict torque (bottow row). The black line (D) shows behaviour of unsupported drivers, the red line of drivers guided by TwL, the blue line of drivers guided by the new control architecture mFDCA, and the green line by the individualized new control architecture iFDCA.

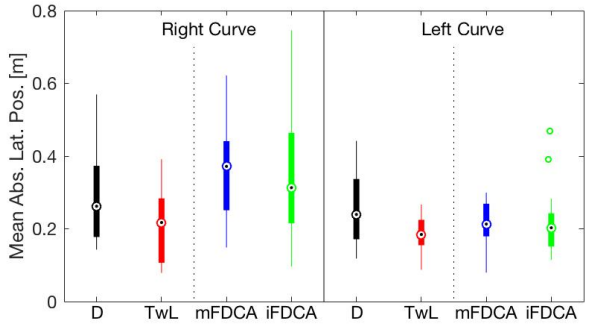

Fig. 16. Mean absolute lateral position over the distance from 35 meter before to 35 meter after the curve. The results for left and right curves are visualized for the four conditions for all subjects. With TwL (red) the drivers drove closer to the center-line.

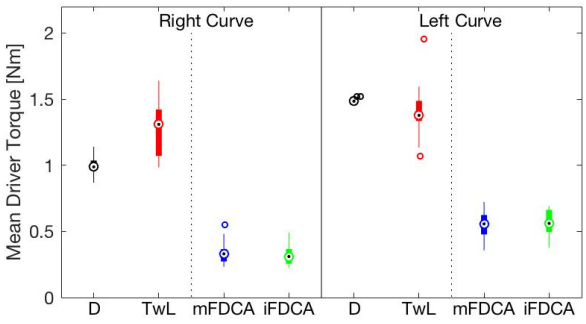

Fig. 17. Mean driver torque averaged over the distance from 35 meter before to 35 meter after the curve. The results for left and right curves are visualized for the four conditions for all subjects and show higher torques for TwL (red) for both curve directions.

showed no significant decrease for iFDCA ($\mu = 3.26$) and mFDCA ($\mu = 3.34$) compared to TwL ($\mu = 3.15$) and manual ($\mu = 3.31$). Also between left and right curves no significant differences were found.

The mean driver torque in figure 15 and the mean absolute driver torque in figure 17 show significant differences ($p < 0.01$). The mean absolute driver torque is significantly higher with TwL compared to both FDCA conditions (both $p < 0.01$), but between iFDCA and mFDCA no difference was found. With TwL the mean absolute driver torque in the right curves is also significantly higher than with manual control. The right plot of figure 15 shows that in the beginning of the left curves the driver torque with mFDCA is higher than with iFDCA.

V. Discussion

The goal of this study was to quantify trajectory-based conflicts in curve negotiation between individual drivers and a conventional two-level haptic shared control architecture (TwL) and to investigate to what extent these conflicts could be reduced by means of a HSC architecture that allows individualized reference trajectories. Two main comparison are relevant to make: first the comparison between the TwL controller and the FDCA algorithm with a reference (HCR) tuned on the average driver behaviour (mFDCA). Second,

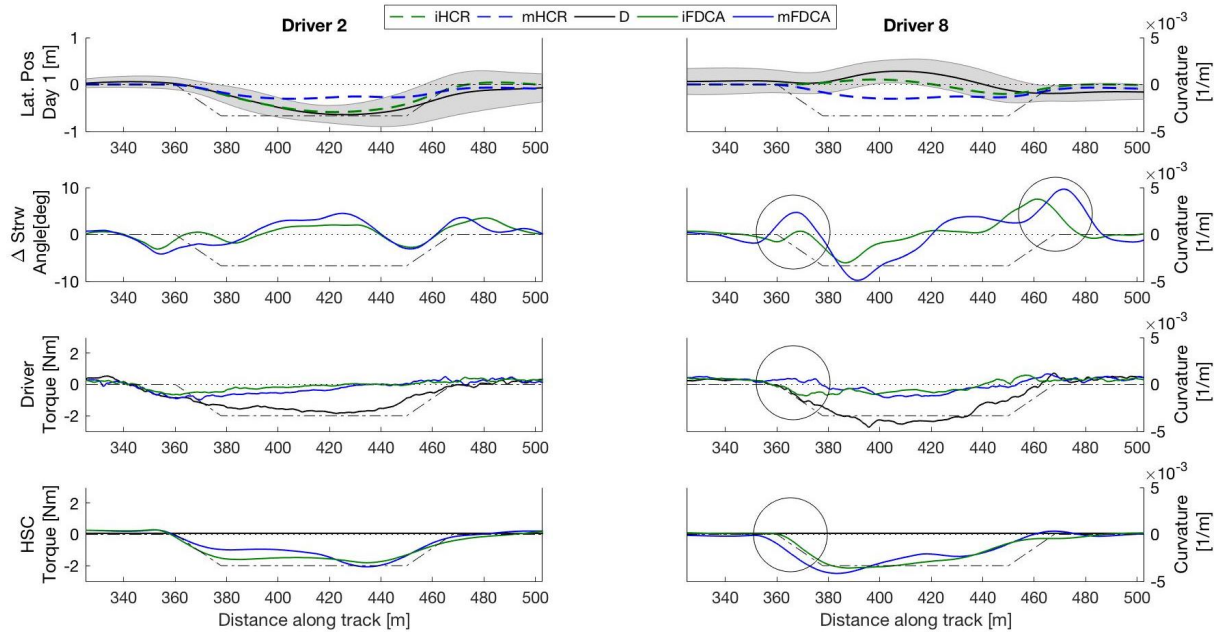

Fig. 18. The top plot shows two different manual driver styles (in black) with the identified individual reference (dashed green line) and average reference (dashed blue). In the other plots the solid green and blue line indicate the drivers and systems behaviour for the condition with the individual and average FDCA controller respectively on day 2 for subject 2 and 8. The circled areas show the differences which are hypothesized to result in the difference in subjective acceptance.

the comparison between the two FDCA algorithms with either average reference (mFDCA) and individualized reference (iFDCA). Additionally, the iFDCA is compared with TwL and both FDCA controllers are compared with Manual control (D).

1) Step 1: Main Results of mFDCA vs. TwL: As hypothesized the acceptance in terms of objective measures increased for mFDCA compared to TwL; the conflict in torques was significantly lower. Furthermore, with mFDCA the absolute driver torque was lower than with TwL and manual. Moreover, for TwL the driver torque increases in the right curve compared to manual control. Drivers did cut the curve more with mFDCA compared to TwL and manual control, especially in the last part of the curve. The direction of the conflict in torques indicate that drivers pushed against the system to return to the lane center. This is opposite to the TwL condition, where conflicts arise because the drivers persists on cutting the curve. Although clear differences in objective conflicts were found between mFDCA and TwL, these significant differences were not found for the subjective acceptance results.

2) Step 2: Main Results of mFDCA vs. iFDCA: The second step in this study individualized the HCR in the FDCA algorithm. No significant difference was found between the FDCA controllers for the conflict in torques and lateral positions. Also the error between the drivers behaviour and the HCR is not significantly lower for iFDCA. Likewise, the workload in terms of driver torque and steering reversal rate is not significantly lower for iFDCA compared to mFDCA. The results indicate a higher satisfaction and usefulness for iFDCA compared to mFDCA, however no significant differences were found. Interestingly, the subjective and objective acceptance was improved for the iFDCA compared to TwL. This suggests that iFDCA is promising to reduce conflicts.

	Satisfaction iFDCA	Usefulness iFDCA	Satisfaction mFDCA	Usefulness mFDCA
Subject 2	1.2	1	0.8	1
Subject 8	2	2	0.2	0.75

TABLE VI
RESULTS FROM 'VANDERLAAN' QUESTIONNAIRE FOR SUBJECT 2 AND 8

A. Influence of the HCR

1) Errors with the HCR: Small local differences in objective measures might have resulted in the difference in subjective acceptance for iFDCA. The errors in steering wheel angles with the HCR's are not significant different over the whole curve, but differences are seen in the peaks (figure 11). It could be argued that the height of the error with the HCR is related to the acceptance. Two cases for individual drivers in figure 18 show different curve-negotiation behaviour, where for both situations the iHCR is closer match than the mHCR. The error in the steering wheel angles is seen in the third plot, which shows a larger error in the begin and end of the curve for the mFDCA for driver 8. The subjective results in table VI show that subject 2 had similar ratings for the iFDCA and mFDCA controllers. Subject 8 however has large differences in the ratings, which can be related to the fact that the error in steering wheel angles differ more for driver 8. Driver 8 stated for the mFDCA that it felt like it was intervening in peaks, where the iFDCA controller that it felt really nice. Figure 18 also shows that driver 8 applies torques to the left in the beginning of the curve, thereby conflicting the HSC torque. Similar results are found over all subjects; the error in steering wheel angles at the start of the curve is higher for the mHCR (figure 11).

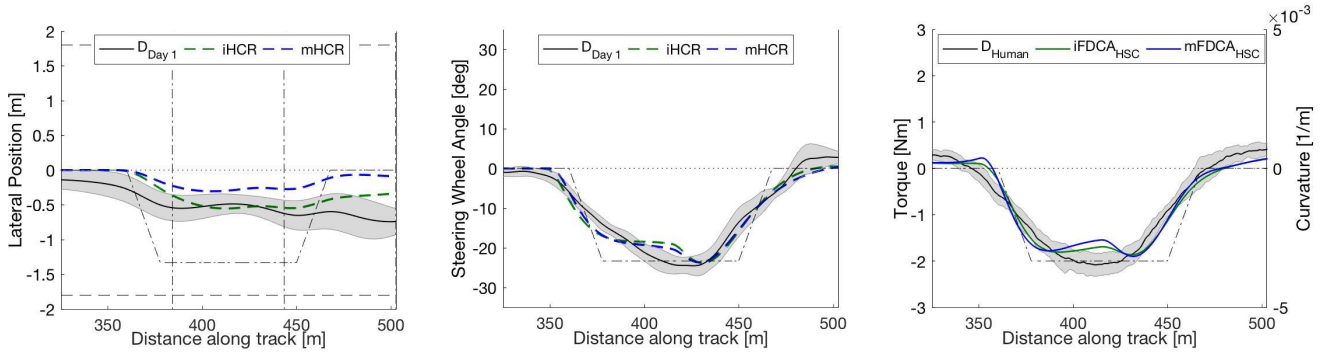

Fig. 19. *Left:* Results for the lateral positions of the individual reference fit of subject 3 (green line), the one-size-fits all reference (blue line), and the manual driver behaviour (black). The driver approaches the curve with a bias that the model can not capture. *Middle:* The resulting steering wheel angles of the references fits for subject 3. *Right:* The mean driver torque over all subjects in manual driving behaviour (black), the mean HSC torque of the mFDCA controller (blue line) and mean HSC torque of the iFDCA controller (green line).

2) Driver-Model: It can be argued that the capabilities of the driver-model are too limited, despite the descriptiveness results that show that the driver-model was able to capture different kind of driving behaviour. Particularly in the transition phases of the curve the driver-model is lacking in matching the drivers behaviour. One of the causes is that the driver-model can not capture biases in the straight sections and curve-entry (figure 19). This also results in the low VAF values, especially in the left curves. Furthermore, the HCR is the selected based on the lowest RMS value to the pre-generated trajectories. The pre-generated HCR's are only determined for the indicated parameters range and resolutions. Additionally, the HCR is determined by taking the lowest overall error, which increases the difficulty to determine a good HCR fit. If the fit is very close in the middle and end of the curve, a trajectory with an high error in the beginning can still be selected as HCR. In this study the weighing factors for the begin, middle and end section of the curve are selected heuristically. It is interesting to further investigate in what sections drivers are likely to perceive more conflicts and therefore weigh that section higher. Another method to fit the HCR could involve the variability. A lower variability could indicate that the driver is more strict on the desired trajectory at that location [29]. All the mentioned methods focus on the lateral position, where possibly the steering wheel angles should be incorporated in the fitting as well.

3) Other Factors and Personal Preferences: It is deduced that a possible factor for a lack of significance between mFDCA and iFDCA could be caused by the accuracy of the iHCR fit. However, to conclude that limitations of the iHCR fit are the cause for the small differences between the FDCA controllers further research is required. Some drivers had a close fit for the left curve, but large errors in the fit for the right curve, or vice versa. This makes it difficult to draw conclusions on the relationship of the HCR match and the acceptance. The small sample size and the difference in personal preferences enhances this difficulty. Furthermore, even when the iHCR is a perfect fit some driver might prefer the mHCR. During the experiment some drivers liked the mFDCA controller even when the mHCR did not fit on their manual driving style. Also, some drivers with a good iHCR fit still preferred the mFDCA. However, in general no drivers disliked the iFDCA, where some driver did not like the mFDCA. This promotes for further research to develop the driver model to better individualize the HCR.

4) Driver Adaptation: The only small differences between the iFDCA and mFDCA could be the result of the drivers adaptation to the controllers. Drivers may have adapted another driving style after driving with a guidance system or could drive different with a controller than their personal manual driver style would be. Resulting in a iHCR that does reflect the drivers adapted intentions. Some participants thought the manual condition on the second day was different from the manual condition on the first day if they received this condition after the iFDCA or mFDCA condition. Furthermore, once drivers get familiar with a system they might adapt to the shared controller and change their driving behavior as is shown by Melman [30], therefore desiring another trajectory over time. It can be argued that the iHCR should not only be determined once [16]. However, adjusting to a extreme curve-cutting HCR might decrease the safety, since drivers also show to take more risk when driving with guidance systems [30]. Setting a limit to what extent the model should be personalized should prevent this. The drivers acceptance can also increase if they adapt towards the guidance intentions. How acceptation for all systems differ in the long term should be investigated in further research.

B. Design choices for FDCA

1) Incorrect Tuning of Control Gains : The tuning of the gains for the feedback (SoHF) and feed-forward (LoHS) components might have provoked conflicts and thereby influenced the acceptance of the participants. The conflict in torques in figure 15 and lateral positions in figure 16 indicate that the drivers were actually cutting the curve more aggressively than desired and drivers applied small torques that were opposing the direction of the curve.

Different initial lateral positions at the curve-entry can have resulted that the controller is not correctly tuned as it assumes the entering of the curve from the lane center. Since drivers

started from another initial position, this resulted in different desired angles later in the curve. The tuning of the feed-forward (FFW) gain might have been too high compared to the feedback (FB) gain. The higher torques later in the curve thereby act upon the discrepancy further in time, which resulted in higher HSC torques than in manual control (figure 19). A large lateral error from the HCR should trigger the FB torques. However, despite the fact that the drivers were more curve-cutting than the HCR, still the total HSC torque was directed towards the inner boundary of the curve (figure 15). Thereby the system imposed the steering wheel angles from the HCR to the drivers and thus worked as as a reinforcing factor in the existing mismatches with the HCR. This can also be seen in the error in steering wheel angles in figure 11, which shows peaks at the same longitudinal distances as the conflicts in torque in figure 15, where the error in lateral position seems to have less influence.

Figure 15 shows that conflicts occur more in the right curves, which also follow from this argumentation. The HCR cuts the right curves more, resulting in higher FFW torques. On top of that, on average drivers already had a bias towards the right side of the road, requiring lower steering wheel angles in the right curve compared to the HCR. In the left curves the drivers approached the curve from the right side. As a result the drivers desired steering wheel angle was higher than the HCR steering wheel angle, which approaches the curve from the center. The high FFW torques are thereby not directly noticed or contradicted by the drivers, resulting in lower conflicts. The bias to the right side of the road indicates that drivers were driving as they would sit in the middle of the car, if this is a result of the simulator setup could be investigated in further research.

The high FFW torques also resulted in low required torques from the driver compared to the HSC torques (figure 18), reducing the benefits of HSC [41]. Furthermore, the relative low tuning of the FB torques might have influenced the total perception of the FDCA controller. In the straight sections no FFW torques are applied and only the FB component was providing guidance. When participants were driving with the FDCA controller they stated that the were more free in the straight sections compared to the TwL controller.

However, it can also be hypothesized that the slight increase in subjective acceptance for the mFDCA controller over the TwL controller resulted from the high FFW gain. The decrease in conflict in torques is in line with the results from Wyzen [43], who found a decrease in conflicts when FFW torques were applied by the controller. The difference of the direction of the conflicts between TwL and FDCA could be perceived different by the drivers, since it might increase the transparity of the system when drivers understand the intentions of the system. In this study only one parameter tuning of the FDCA controller is evaluated, further research should evaluate the effect for another distribution of FFW and FB torques.

2) Stiffness & Authority: In this study the LoHA is not varied, which is argued to be important in the acceptance of drivers [2][23]. For each driver one individualized HCR was generated, where this study as well as earlier studies found that drivers show variability in their behaviour [7][22][37][21]. Due to the variability, errors between the HCR and the drivers intentions will always exist. Future research could investigate the effect of determining an individual HCR and lower the LoHA around this reference line, such that the drivers are still able to drive freely around this reference.

3) Haptic Shared Control performance: Approximations made on the steering wheel dynamics and vehicle dynamics in the driving simulator could have resulted in a discrepancy between simulated HCR and implemented HCR. Although the offline simulation allowed for perfect trajectory following with only FFW torques (figure 2), this was not the case when implemented in the driving simulator. The first cause is that the HCR steering wheel angles are determined with a linearized model in MATLAB. The non-linear car in the driving simulator will respond different to the steering wheel inputs. The second cause is that the dynamics of the steering wheel are not taken into account in the FFW torques. The FFW torques are determined by only multiplying the HCR steering wheel angles with a gain, where the dynamic response of the steering wheel in the simulator is different due to the damping and inertia. Without driver-input the car is able to follow the HCR relatively close due to the FB torques. However, these effects cause a confound and controversy in determining whether the controller was accurately individualized. It is unknown what the effect of these approximations are on the perception and thereby acceptation of the drivers.

C. Experiment Design

1) Subjective Acceptance: Although the 'Vanderlaan' questionnaire is an often used questionnaire to asses acceptance [30][27], it can be argued that is difficult to measure acceptance only using nine questions. Using more questionnaires could help to give a better representation of the drivers acceptance. Furthermore, participants were asked to fill in the questionnaire after the whole trial, thereby not indicating how drivers perceived the guidance specifically in the curves. Nevertheless, the results from the 'Vanderlaan' questionnaire were in line with the participants comments during the experiment. Drivers often made negative comments for TwL, mentioning it was uncomfortable and correcting in a unpleasant manner. For iFDCA the comments were primarily positive, however for some participants it worked sleep-inducing. Participants were more conscious of the self-steering intentions of the guidance and noted they did not have to do much. Furthermore, some participants mentioned the system sometimes felt untrustworthy because the timing of the steering did not match or it steered too aggressive. These comments increased for mFDCA, were participants mentioned to prefer mFDCA over TwL, but did not agree on when the system started to steer in and out of the curve. Further research should evaluate the acceptance for different parts of the curve, and could specifically ask what their opinion was for the steering in and out behaviour to get a

better understanding where the controller is interfering with the drivers intentions.

2) Road Design: The curve was designed to evoke different curve-cutting behaviour and the same curve was repeated over the trajectory, inducing precognitive feed-forward control. The repetition of identical curves might lead to more curve-cutting behaviour than drivers normally would. This could have resulted in the lower acceptance for TwL compared to earlier studies [32][30]. However, earlier studies found that drivers were most annoyed in curved road sections [7] [33]. Consequently, drivers can turn of the system [24] [27], even if they are not annoyed all the time. Therefore the evaluation for one type of curve might be a sufficient indication for the total acceptance of system. Further investigations for different road designs should be done to evaluate the driver-model and HSC performance in different curves.

3) Additional Effects of HSC Systems: The experiment only measured 160 seconds of driving, which did not give drivers the opportunity to get bored and tired. Furthermore, no other traffic or objects that needed to be avoided were included. A Haptic Shared Control system could help to alarm drivers for potential hazardous situations and support drivers to avoid these [17], however these situations are not evaluated in this study. Therefore, the potential benefits of an haptic shared control system are not fully evaluated in this study. However, also the opposite might be true: De winter et al [41] concluded that supplementary information should not be provided continuously since this can work sleep-inducing and reduce situation-awareness. The FDCA controller does not only provide feedback torques, but also feed-forward torques, which can increase the sleep-inducingness even more. Longer experiments in less simplified environments should show the the advantages and drawbacks of continuous guidance systems with feed-forward support.

4) Transfer of simulator results to real-world driving: During the experiment the speed was fixed at 24 m/s, which facilitated comparisons in steering behaviour. Some drivers stated that in real life they would reduce their speed when entering a curve. With different speeds the taken trajectory might also differ, as well as the shared control torques provided by the different controllers [30]. Furthermore, the simplified simulated environment with a single-lane road and no other traffic might lead to more curve-cutting than in real life, since driver might not perceive real danger and risk [42]. Nevertheless, simulator studies show advantages compared to real car studies on ethical and technical implementation aspects. Furthermore, the results from simulator test can still be valid in terms of relative comparison between the conditions [18]. However, the validity of this study for real life situations should be further investigated.

D. Future Work

Although FDCA is a promising architecture to reduce conflicts, there are still many questions remaining that should be investigated by future research. First, a better understanding of the tuning of the control gains for the feed-forward (LoHS) and feedback (SoHF) gains in the FDCA is needed, before investigating the effects of individualizing the reference. Secondly, the driver-model needs to be improved to generate closer matching HCR's. In order to reduce the errors in the beginning of the curve, the driver-model should be able capture different lateral positions at the curve entry. The model proposed by Schnelle [35] includes a factor for the bias and is therefore promising to investigate.

After these first two essential improvements several other factors are interesting for future research. The influence of different curves and road environments should be evaluated, as well as the driver-models capabilities to paramaterize that. Since drivers show variability in curve-negotiation the authority (LoHA) might also need to be considered in the tuning. Small differences in intentions between the driver and HCR will always exist, changing the authority around the HCR gives drivers more freedom around the HCR. Also, how drivers adapt to the individualized support in short and long term, and if the controller should adapt [16], potentially online, to conflicts [29] is not yet investigated for this field.

VI. Conclusion

The goal of this study was to objectively and subjectively evaluate a novel haptic shared control architecture (FDCA) that allowed for individualized support, by comparing it to manual control and a conventional haptic shared control algorithm (TwL). The novel haptic shared control architecture was taken from literature and is characterized by its ability to separate torque contributions from a feed-forward controller (to anticipate on a human-compatible reference trajectory) and a feedback controller (on the difference in lateral position and heading with respect to that trajectory). To construct the references manual control data from 16 participants was gathered to parameterize the driven trajectories using a driver model fitted on the measured lateral positions. A single controller (mFDCA) was constructed by implementing a reference based on the average driver behaviour, as well as 16 individualized controllers (iFDCA) with personalized reference. From the experimental results the following conclusions can be drawn:

- Compared to TwL, the mFDCA resulted in significantly reduced driver torques and conflicts in torques, but not in significantly improved subjective acceptance. Compared to manual control the driver torques also significantly reduced for mFDCA.
- Compared to mFDCA, the iFDCA did not result in further improvement in objective and subjective terms. It had the same objective benefits compared to both TwL and manual control as the mFDCA.
- Interestingly, the iFDCA did show significant improvement in subjective rating compared to manual control and TwL.

These results show that the individualized FDCA can reduce conflicts and increase acceptance compared to the conventional shared controller. Further research should focus on tuning the control gains and developing the driver-model for better matching references.

REFERENCES

[1] D. A. Abbink, E. R. Boer, and M. Mulder, Motivation for Continuous Haptic Gas Pedal Feedback to Support Car Following, pp. 283-290, 2008.

[2] D. A. Abbink, D. Cleij, M. Mulder, and M. M. Van Paassen, The importance of including knowledge of neuromuscular behaviour in haptic shared control, in Conf. Proc. - IEEE Int. Conf. Syst. Man, Cybern., 2012, pp. 3350-3355.

[3] A. Ameyoe, P. Chevrel, E. Le-Carpentier, F. Mars, and H. Illy, Identification of a Linear Parameter Varying Driver Model for the Detection of Distraction, IFAC-PapersOnLine, vol. 48, no. 26, pp. 37-42, 2015.

[4] P. Angkititrakul, C. Miyajima, and K. Takeda, An improved driver-behavior model with combined individual and general driving characteristics, IEEE Intell. Veh. Symp. Proc., pp. 426-431, 2012.

[5] S. Barendswaard, D. M. Pool, and D. A. Abbink, A Method to Assess Individualized Driver Models: Descriptiveness , Identifiability and Realism, pp. 6-8, 2017.

[6] E. R. Boer and N. Cambridge, Tangent Point Oriented Curve Negotiation, in proc. of conf. on Intelligent Vehicles, 1996, no. 617.

[7] R. Boink, M. M. Van Paassen, M. Mulder, and D. A. Abbink, Understanding and reducing conflicts between driver and haptic shared control, in Conf. Proc. - IEEE Int. Conf. Syst. Man, Cybern. 2014, vol. 2014-January, no. January, pp. 1510-1515.

[8] G. Diehm, S. Maier, M. Flad, and S. Hohmann, Online identification of individual driver steering behaviour and experimental results, Proc. - 2013 IEEE Int. Conf. Syst. Man, Cybern. SMC 2013, pp. 221-227, 2013.

[9] K. van der El, D. M. Pool, M. M. van Paassen and M. Mulder, Effects of Preview on Human Control Behavior in Tracking Tasks With Various Controlled Elements, IEEE Trans. on Cybern., 2017.

[10] M. Flad, C. Trautmann, G. Diehm, and S. Hohmann, Individual driver modeling via optimal selection of steering primitives, vol. 19, no. 3. IFAC, 2014.

[11] F. Flemisch, J. Kelsch, C. Loper, A. Schieben, J. Schindler, and M. Heesen, Cooperative Control and Active Interfaces for Vehicle Assistance and Automation, in FISITA World Automotive Congress, 2008.

[12] B. Forsyth and K. MacLean, Predictive haptic guidance: intelligent user assistance for the control of dynamic tasks., IEEE Trans. Vis. Comput. Graph., vol. 12, no. 1, pp. 103-113, 2006.

[13] P. G. Griffiths and R. B. Gillespie, Sharing Control Between Humans and Automation Using Haptic Interface: Primary and Secondary Task Performance Benefits, Hum. Factors J. Hum. Factors Ergon. Soc., vol. 47, no. 3, pp. 574-590, 2005.

[14] M. Itoh, F. Flemisch, and D. Abbink, A hierarchical framework to analyze shared control conflicts between human and machine, IFAC-PapersOnLine, vol. 49, no. 19, pp. 96-101, 2016.

[15] Johansson, E., Engstrm, J., Cherri, C., Nodari, E., Toffetti, A., Schindhelm, R., Gelau, C. (2004). Review of existing techniques and metrics for IVIS and ADAS assessment (AIDE IST-1-507674-IP).

[16] A. W. De Jonge, J. G. W. Wildenbeest, H. Boessenkool, and D. A. Abbink, The Effect of Trial-by-Trial Adaptation on Conflicts in Haptic Shared Control for Free-Air Teleoperation Tasks, IEEE Trans. Haptics, vol. 9, no. 1, pp. 111 - 120, 2016.

[17] D. I. Katzourakis, J. C. F. de Winter, M. Alirezaei, M. Corno and R. Happee, "Road-Departure Prevention in an Emergency Obstacle Avoidance Situation," in IEEE Int. Conf. Syst. Man, Cybern.: Systems, vol. 44, no. 5, pp. 621 - 629, May 2014.

[18] Klüver, M., Herrigel, C., Heinrich, C., Schner, H.-P., Hecht, H. (2016). The behavioral validity of dual- task driving performance in fixed and moving base driving simulators. Transportation Research Part F: Traffic Psychology and Behaviour, 37, 7896.

[19] Van der Laan, J. D., Heino, A., De Waard, D. (1997). A simple procedure for the assessment of acceptance of advanced transport telematics. Transportation Research Part C: Emerging Technologies, 5(1), 1-10.

[20] M. Land and D. Lee, Where we look when we steer, Nature, no. July 1994, pp. 7 - 10, 1994.

[21] Levison, W. H., Simsek, O., Bittner, A. C., Hunn, S. J. (2007). Computational techniques used in the driver performance model of the interactive highway safety design model. Transportation Research Record: Journal of the Transportation Research Board, 1779/2001, 17 - 25.

[22] M. M. van Paassen, D. Abbink, M. Mulder, and M. Mulder, Haptic Guidance, Interaction between the Guidance Model and Tuning, in 18th Intern. Symp. on Aviation Psychology (pp 410-415), Dayton OH.

[23] M. M. Van Paassen, R. Boink, D. A. Abbink, M. Mulder, and M. Mulder, Four design choices for haptic shared control, Adv. Aviat. Psychol., no. July, pp. 237 - 254, 2017.

[24] R. Parasuraman and V. Riley, Humans and Automation: Use, Misuse, Disuse, Abuse, Hum. Factors J. Hum. Factors Ergon. Soc., vol. 39, no. 2, pp. 230 - 253, 1997.

[25] C. Passenberg, A. Glaser, and A. Peer, Exploring the Design Space of Haptic Assistants : The Assistance Policy Module, IEEE Trans. Haptics, vol. 6, no. 4, pp. 440 - 452, 2013.

[26] S. M. Petermeijer, D. A. Abbink, M. Mulder, and J. C. F. De Winter, The Effect of Haptic Support Systems on Driver Performance : A Literature Survey, IEEE Trans. Haptics, vol. 8, no. 4, pp. 467 - 479, 2015.

[27] S. M. Petermeijer, D. a. Abbink, and J. C. F. de Winter, Should Drivers Be Operating Within an Automation-Free Bandwidth? Evaluating Haptic Steering Support Systems With Different Levels of Authority, Hum. Factors J. Hum. Factors Ergon. Soc., vol. 57, pp. 5 - 20, 2014.

[28] F. Mars, M. Deroo, and C. Charron, Driver adaptation to haptic shared control of the steering wheel in Conference Proceedings - IEEE Int. Conf. Syst. Man, Cybern., 2014, vol. 2014, no. January, pp. 1505 - 1509.

[29] J. R. Medina, T. Lorenz, D. Lee, and S. Hirche, Disagreement-aware physical assistance through risk-sensitive optimal feedback control, in IEEE Int. Conf. on Intel. Robots and Syst., 2012, pp. 36393645.

[30] Melman, T., Abbink, D. A., Van Paassen, M. M., Boer, E.R., De Winter, J.C.F., (2018) What determines drivers speed? A replication of three behavioural adaptation experiments in a single driving simulator study, in press

[31] N. Merat and a. H. Jamson, How do drivers behave in a highly automated car? Proc. Fifth Int. Driv. Symp. Hum. Factors Driv. Assessment, Train. Veh. Des. HOW, pp. 514 - 521, 2008.

[32] M. Mulder, D. A. Abbink, and E. R. Boer, The effect of haptic guidance on curve negotiation behavior of young, experienced drivers, in Conference Proceedings - IEEE Int. Conf. Syst. Man, Cybern., 2008, pp. 804 - 809.

[33] M. Mulder, D. A. Abbink, and E. R. Boer, Sharing Control With Haptics Seamless Driver Support From Manual to Automatic Control, Hum. Factors J. Hum. Factors Ergon. Soc., vol. 54, no. 5, pp. 786 - 798, 2012.

[34] L. Saleh, P. Chevrel, F. Claveau, J. F. Lafay, and F. Mars, Shared steering control between a driver and an automation: Stability in the presence of driver behavior uncertainty, IEEE Trans. Intell. Transp. Syst., vol. 14, no. 2, pp. 974 - 983, 2013.

[35] S. Schnelle, J. Wang, S. Member, H. Su, and R. Jagacinski, Desired Path Generation, vol. 47, no. 1, pp. 111 - 120, 2017.

[36] C. Sentouh, P. Chevrel, F. Mars, and F. Claveau, A sensorimotor driver model for steering control, Conf. Proc. - IEEE Int. Conf. Syst. Man Cybern., no. October, pp. 2462 - 2467, 2009.

[37] P. Spacek, Track Behavior in Curve Areas: Attempt at Typology, J. Transp. Eng., vol. 131, no. 9, pp. 669 - 676, 2005.

[38] J. Smisek et al., Neuromuscular-System-Based Tuning of a Haptic Shared Control Interface for UAV Teleoperation, IEEE Trans. Human-Machine Syst., vol. pp, no. 99, pp. 1 - 13, 2016.

[39] M. Steele and R. Brent Gillespie, Shared Control between human and machine: using a haptic steering wheel to aid in land vehicle guidance, in proc. of the human factors and ergonomics society 45th annual meeting, 2001, no. 1992, pp. 1671 - 1675.

[40] K. K. Tsoi, M. Mulder, and D. A. Abbink, Balancing Safety and Support: Changing Lanes with a Haptic Lane-keeping Support System, in 2010 IEEE Int. Conf. Syst. Man, Cybern., 2010, pp. 1236 - 1243.

[41] J. C. F. De Winter and D. Dodou, Preparing drivers for dangerous situations: A critical reflection on continuous shared control, in Conference Proceedings - IEEE Int. Conf. Syst. Man, Cybern., 2011, pp. 1050 - 1056.

[42] De Winter, J. C. F., van Leeuwen, P. M., Happee, R. (2012). Advantages and Disadvantages of Driving Simulators: A Discussion. In Proc. of Measuring Behavior 2012 (pp. 75-78).

[43] P. Wyzen, Separating Haptic Feedback and Support Signals: a Solution for Human-Machine Cooperation?, 2017.

[44] van Winsum, W., Brookhuis, K. ., de Waard, D. (2000). A comparison of different ways to approximate time-to-line crossing (TLC) during car driving. Accident Analysis Prevention, 32(1), 47 - 56.

A

Appendix A: HCR Generation

This appendix is intended as an additional explanation to the paper on how the reference trajectory (HCR) is constructed. To generate the HCR the driver-model from Saleh [8] is used as a starting point. The cybernetic driver-model is simulated in MATLAB and determines the human torque on the steering wheel using three inputs: the near angle, the far angle and the current steering wheel angle. The generated steering torques are the input for a simulated car as shown in figure A.1, where the human driver-model is represented in the green blocks. The orange subsystems contain the vehicle dynamics, which go into the pink subsystem together with the road profile to determine the position of the car relative to the road.

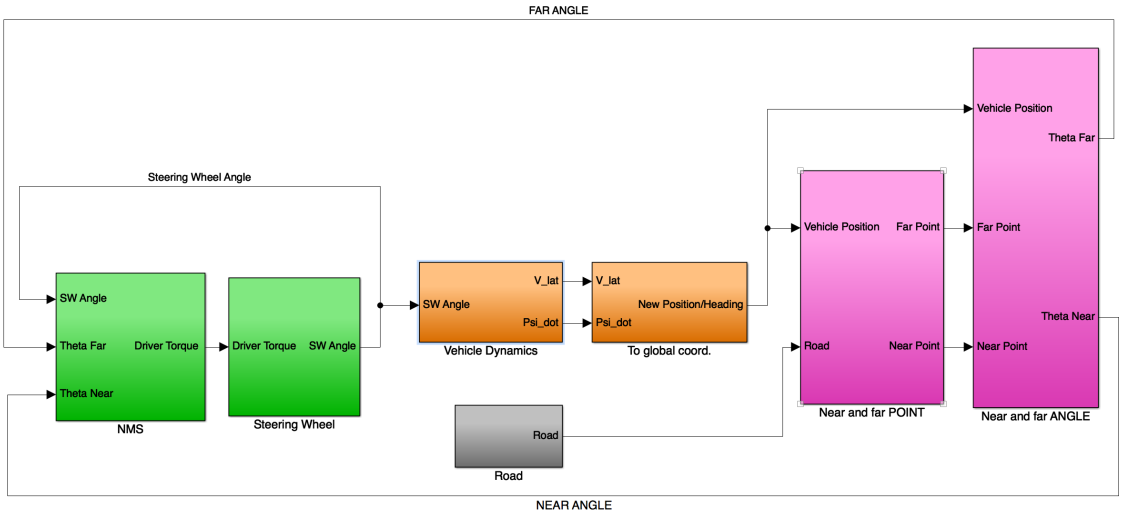

Figure A.1: Schematic overview of generating the trajectory of the Human-Compatible-Reference. In green the driver and steering wheel, in orange the car dynamics and the transformation to global coordinates, and in pink the determination of first the near and far point and second the near and far angle.

A.1. Human Behaviour

The near and far angle enter the cybernetic model of the human driver as in figure A.2. K_c determines the contribution of the near angle and K_p the contribution of the far angle. The near angle is visually compensated, using two constants for the lead- and lag-time. Constant values are chosen for the lead ($T_L = 3$) and lag ($T_i = 1$) parameters based on Saleh's [8] findings. Since the lead constant is bigger than the lag constant the human response to changes is the near angle is less for higher frequencies. By dividing the signal by the velocity the signal is less influenced by the near angle for higher velocities. Other values in the driver-model are the processing time delay ($\tau_p = 0.03$), angle to torque coefficient ($K_r = 0.3$), Neuromuscular reflex gain ($K_t = 0.5$) and Neuromuscular time constant ($T_N = 0.1$). All variables are chosen based on the findings of Saleh [8].

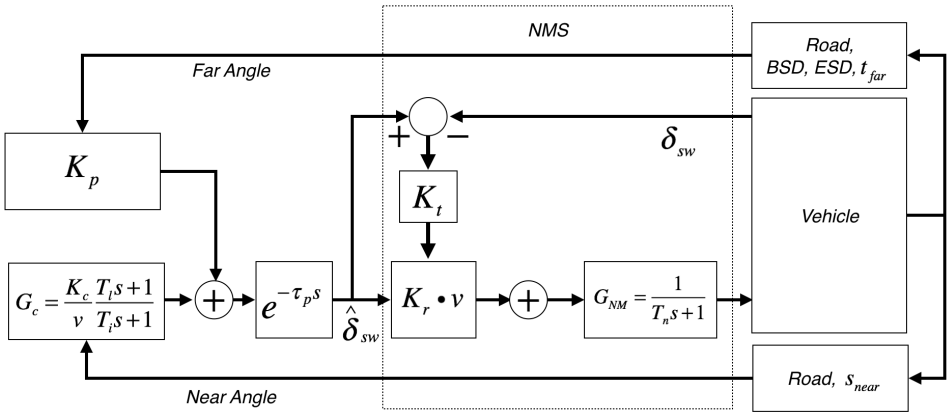

Figure A.2: Cybernetic driver model, based on the driver model from Saleh [8]. The near angle, far angle and current steering wheel angle are the input from the model, the output is a torque.

A.2. Two-point model

The driver-model from Saleh [8] uses two sources to generate the desired steering wheel angle: a far angle and a near angle. Saleh [8] states that 'The developed model is based on the hypothesis that drivers use visual information to identify the approaching road curvature and the position of the vehicle in relation to the edge lines.' The statement is based on studies [9] that found that drivers use near and far visual information to maintain their position on the road. In order to generate human-like trajectories it therefore seems promising to use these two distinct road points. Saleh [8] determines the near and far angle as:

$$\Theta_{near} = \frac{y_L}{l_p} + \psi_L \tag{A.1}$$

$$\Theta_{far} = \frac{D_{far}}{v} r \tag{A.2}$$

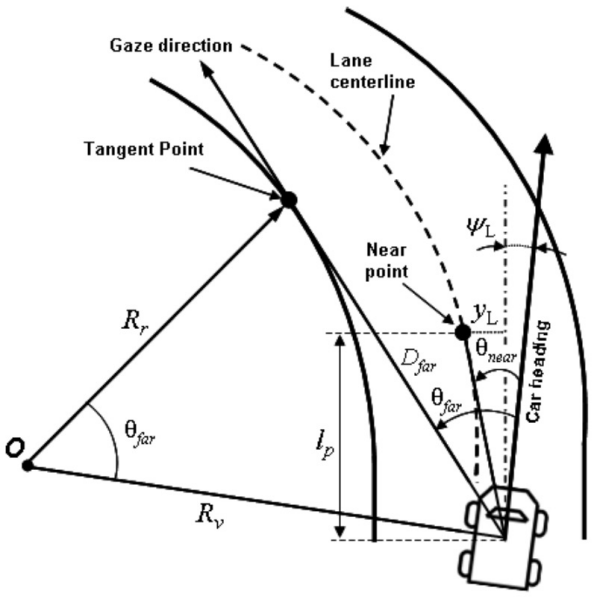

Figure A.3: Determination of far point in Saleh [8], figure replicated from [10]. The far angle is determined using the radius of the road, the distance to the tangent point and the vehicle speed.

A.2.1. Near Point & Near Angle

The near point is determined as the point in the middle of the road, at a set look-a-head distance ahead. This distance is set to a constant 5 meters, since this is close enough to observe the lateral position, but not too close, such that it is still visible for the driver [8]. The near point is used to determine the near angle, which is the angle between the heading of the car in global reference frame and the angle to the near point in global reference frame as in figure A.3. Thereby effectively this results in the angle between the heading and the vector from the car to the near point.

$$\Theta_{near} = \Theta_C - \Psi_{GlobalHeading} \tag{A.3}$$

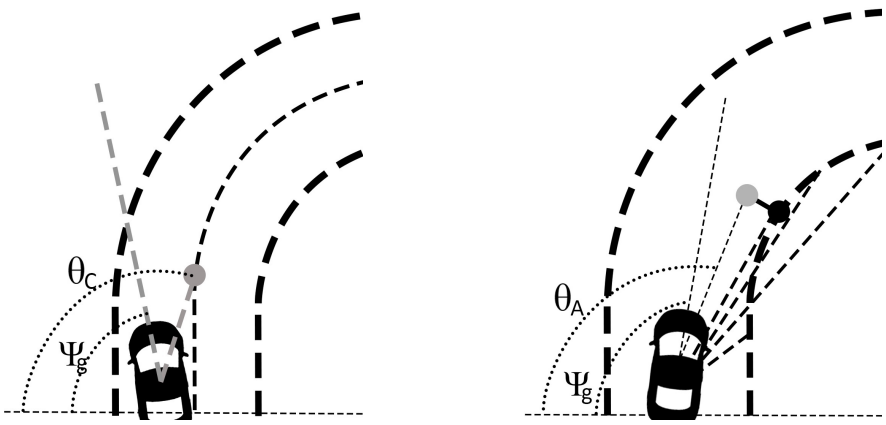

Figure A.4: *Left:* Determination of near point, Θ_c is the angle to the near point in the global reference frame. Ψ_g is the heading of the car in the global reference frame. *Right:* Determination of far point, Θ_A is the angle to the near point in the global reference frame.

A.2.2. Far point & Far angle

By using the far point drivers are able to anticipate on the the upcoming roadway curvature. In the work from Saleh [8] the tangent point is determined by using the road radius and distance from the vehicle to the rotation curvature center (R_v) as in figure A.3. In this study the tangent point is determined by taking the gradients to future road points till an optimum is found, see figure A.4.

Boer [4] proposed to use an alternative far point instead of the tangent point, since 'the tangent point could never be reached'. This far point (target point) is a point shifted towards the road-center with respect to the tangent point, illustrated in the right plot of figure A.4 by the gray dot. The target point is determined by shifting the tangent point 45 cm towards the lane center, which is equivalent to a quarter of the car width. The direction is of shift in location perpendicular to the gradient of the lane boundary. The far angle is than determined with the equation:

$$\Theta_{far} = \Theta_A - \Psi_{GlobalHeading} \tag{A.4}$$

In a first attempt to determine the far point all road points within a set time frame (gaze-ahead distance s_{far}) in front of the car are considered to be potential tangent points. If no tangent point can be found within the set distance, the center of the road at the maximum gaze-ahead distance is taken as far point. However, this method led to too early steering behaviour, causing the car to dive into the tangent point far before the beginning of the curve as in figure A.5. This resulted in different desired gains during the curve, where for this model the gains are fixed. This led to different and unrealistic lateral positions in the beginning and end of the curve, with respect to the middle of the curve. Note that in figure A.5 the tangent point was still used as far point, using the target point slightly reduced this behaviour, but could not solve the early steering problem.

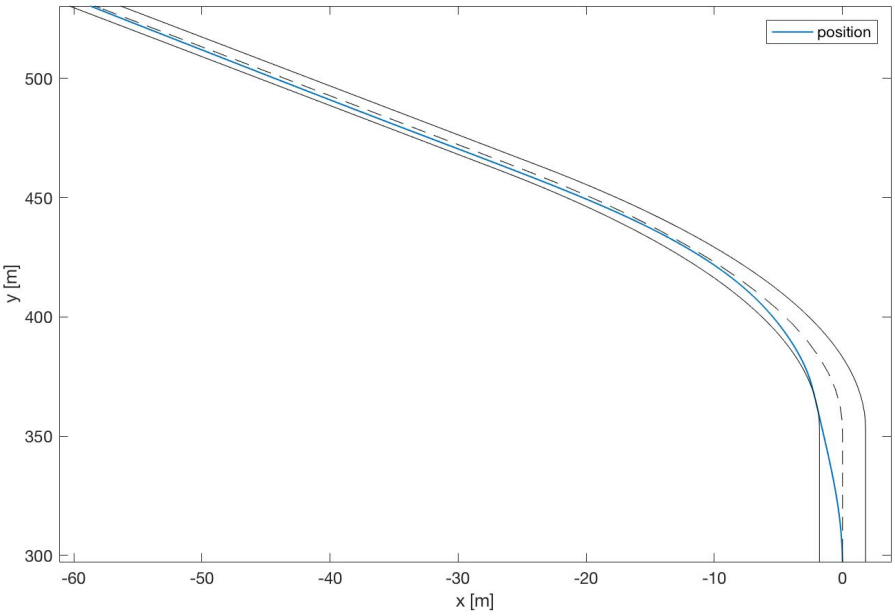

Figure A.5: The blue line represents the car position over the curve. If the tangent point is determined too early, the far angle increases too early and the car will dive into the tangent point too early. This results in different required gains for the far angles over the length of the curve, where for this model the gains are fixed.

The early steering behaviour could be solved by lowering the gaze-ahead distance (s_{far}), or equivalent gaze-ahead-time (t_{far}) for the tangent point. This way the tangent point is only determined when the car is closer to the curve, since only then an optimum in the gradients to the road points can be found. When it is desired to model late steering behaviour, the tangent point should only be determined when the car is close to curve. This requires a low value for t_{far}, however for smoother curves the tangent point can not be determined anymore, as shown in figure A.6. Note that in this figure the value for the corresponding distance (s_{far}) for t_{far} and the used speed is indicated. As can be seen for this particular road, the tangent point can only be found when s_{far} is 40 meters (equivalent to t_{far} = 2 s) or higher. For roads with smaller curvatures the required s_{far} is lower, but for all realistic curvatures a minimum s_{far} is required to find the Tangent Point.

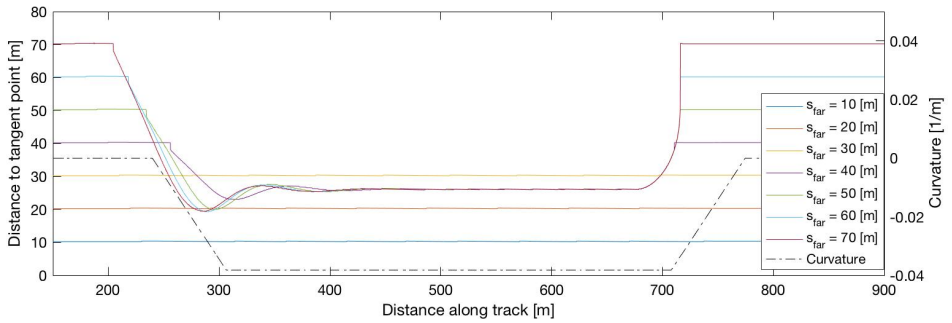

Figure A.6: Distance to the tangent point for varying values of s_{far}, with a fixed speed op 20 m/s. The tangent point can not be generated when the gaze-ahead distance s_{far} is too low. The far point will therefore remain in the middle of the road.

So, implementing t_{far} as described above influences the point where the driver starts steering. When the tangent point is found, the driver will start anticipation on the generated far angle as can be seen in figure A.8. Thus, the point where the driver starts steering can not be changed independently from t_{far}. When the tangent point is not found due to a too low t_{far}, curve cutting behaviour can not be produced by the model. This is due to the fact that the tangent point will always lie close to the car in the road centre, such that the far angle will never get big enough to generate curve cutting behaviour. Thus, late steering behaviour could in this case never be combined with curve-cutting behaviour.

To support the statement that the tangent point needs to be determined to generate curve cutting behaviour the effect of changing t_{far} is shown in figure A.8. It can be seen that changing t_{far} influences the place where the model starts steering into the curve, but also that when t_{far} is low the model does not produce curve cutting behaviour.

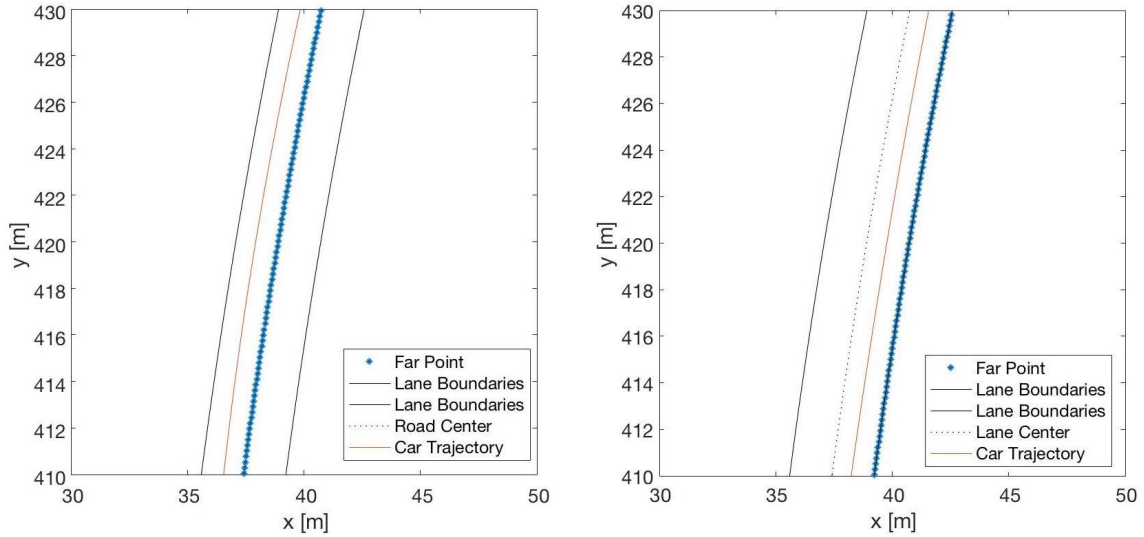

Figure A.7: Top view on the road, the tangent point is indicated in blue and the car trajectory in red. *Left:* The tangent point can not be found when the gaze-ahead distance is too low, the far point will therefore remain in the middle of the road. Resulting in under-steer trajectories. *Right:* For larger search distance the tangent point can be found, resulting in curve cutting trajectories.

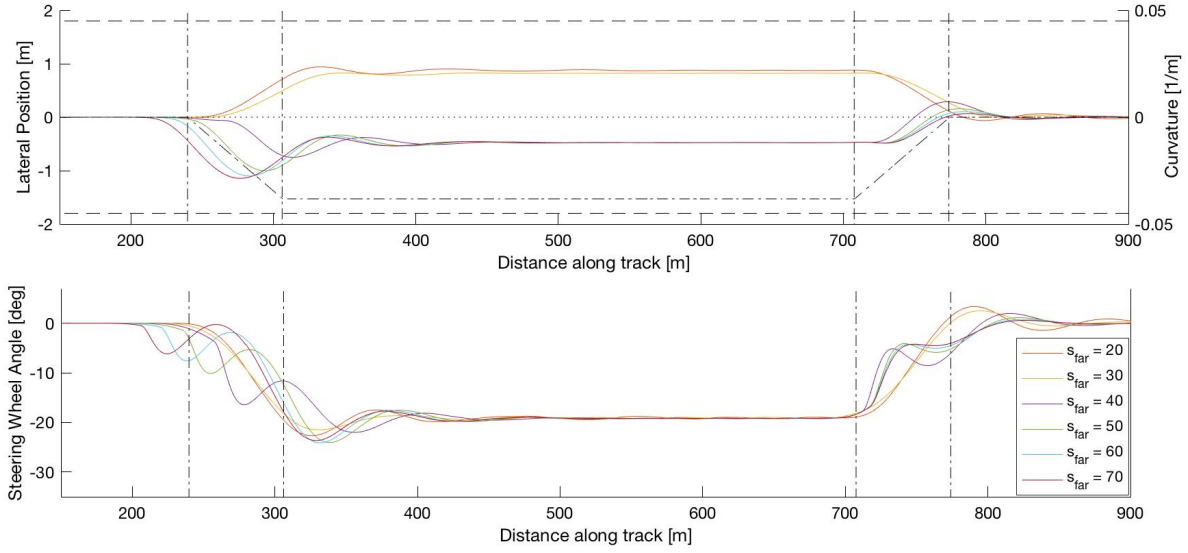

Figure A.8: Birds eye view over the road. The behaviour for different gaze-ahead distances (s_{far}) in meters are visualized for the lateral positions (top) and steering wheel angles (bottom). If s_{far} is too low, the far point can not be determined, resulting in different trajectories.

A.2.3. Behaviour in transition phases

Analysis of experimental data (Appendix F.1.3) suggests that a characteristic parameter for different drivers styles is the position where the driver starts to initiate the steering in and out movement. The analyses also showed that the transition phases are the regions where most conflicts occur and where drivers that dislike the guidance change their behaviour. Therefore the model is extended with two parameters.

Begin steering distance

The first extension is the begin steering distance (BSD), which defines the distance before the beginning of the curve where the driver-model starts taking the far point into account. This way t_{far} and the BSD are decoupled. Only when the car is closer to the curve than the BSD the far point switches from the centre of the road to the target point. By implementing the BSD it could be argued that t_{far} does not have to vary anymore, as long as it is large enough to find the tangent point. However, the next section explains why it is still important to also vary t_{far}.

End steering distance

At the end of the curve the tangent point can not be determined anymore when there is no more optimum in the gradient to the future road points. The far point then switches to the center of the road at the corresponding distance from t_{far}, which causes a sudden decrease in the far angle as seen in figure A.9. To reduce this sudden decrease, the second parameter that is added is the end steering distance (ESD), which defines the distance before the end of the curve when the driver will start to anticipate on the upcoming straight section instead of the target point. At this position in the curve the far point switches from the target point to the middle of the road at the corresponding distance from t_{far}.

Without varying the value for t_{far} and implementing the ESD parameters, the trajectory will often show overshoot behaviour in the end of the curve as in figure A.9. The far point would switch from the red '+' located in the inner part of the lane to the blue '+'. This causes a sudden decreased in the far angle. By selecting a higher t_{far} the new far point is located further away, which reduces the overshoot as in figure A.10.

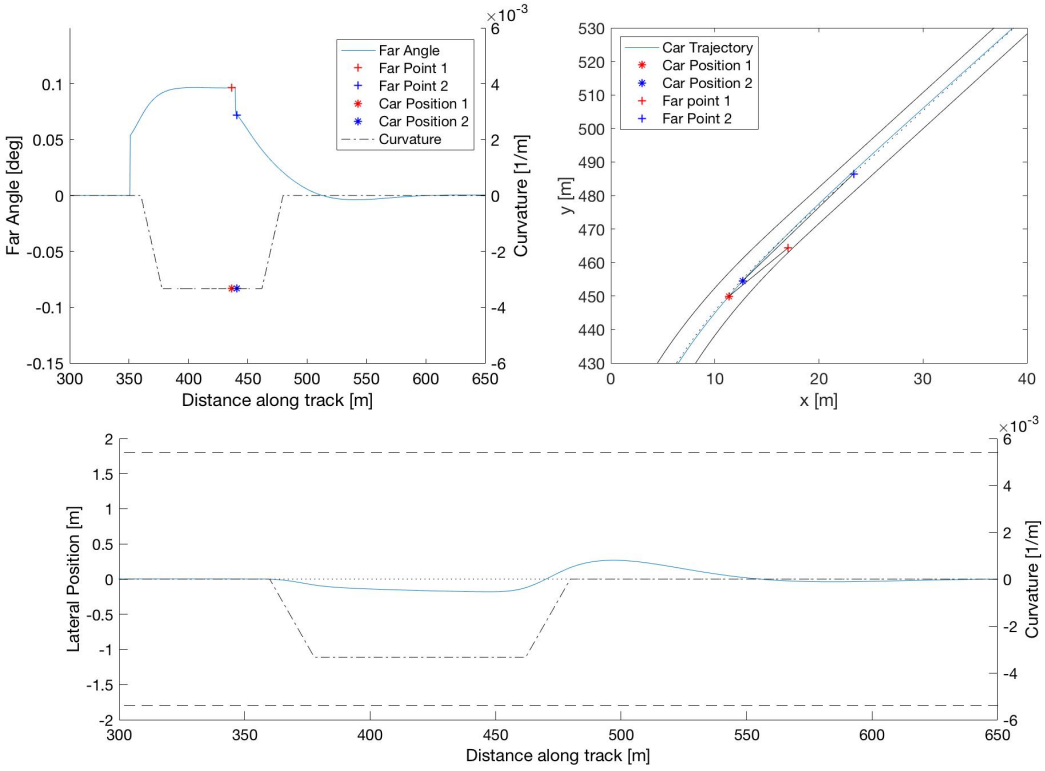

Figure A.9: *Top:* The '+' indicates the longitudinal distance of the far point when the car is located at the '*' longitudinal distance. The corresponding far angle between the car and far point is indicated with the blue line in the left plot. In the right plot the trajectory of the car is indicated with the blue line. *Bottom:* The results for the lateral position of the car (blue line) shows overshoot in the end of the curve due to the sudden decrease in far angle in the top figure.

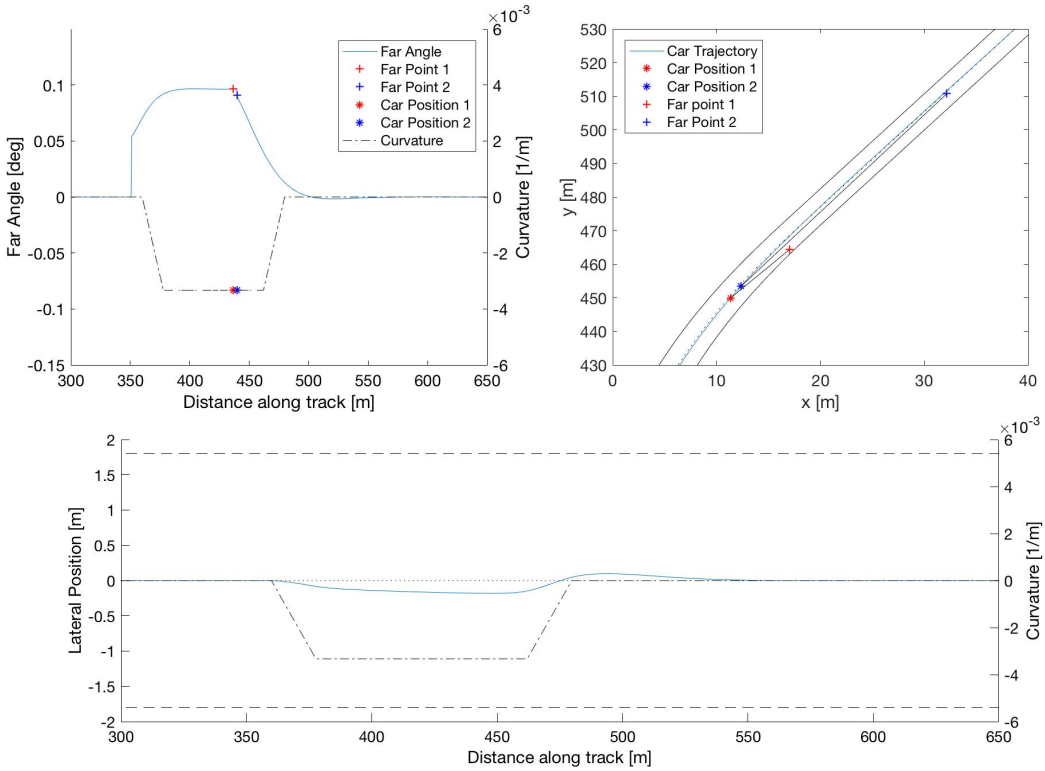

Figure A.10: *Top:* The '+' indicates the longitudinal distance of the far point when the car is located at the '*' longitudinal distance. The corresponding far angle between the car and far point is indicated with the blue line. Due to the change in t_{far} the sudden decrease in far angle is reduced. *Bottom:* The blue line in the bottom figure represents the lateral position of the car. The black dashed line represents the curvature profile. Due to the varied value of t_{far} the overshoot is reduced.

A.2.4. Summarized changes

In conclusion, the far point that is used in the driver-model to determine the far angle differs in the far point from Saleh on the following points:

- The tangent point is determined by evaluating the gradients to future road points within the gaze-ahead time t_{far}. The road point with the optimum in gradients is selected as tangent point. This also influences the steering behaviour and the end of the curve, since the far point will shift to the middle of the road at the gaze-a-head time t_{far}.
- The tangent point is used to determine the target point, which is used as far point.
- The model is extended with a parameter that influences the position of the steering-in initiation.
- The model is extended with a parameter that influences the position of the steering-out initiation.

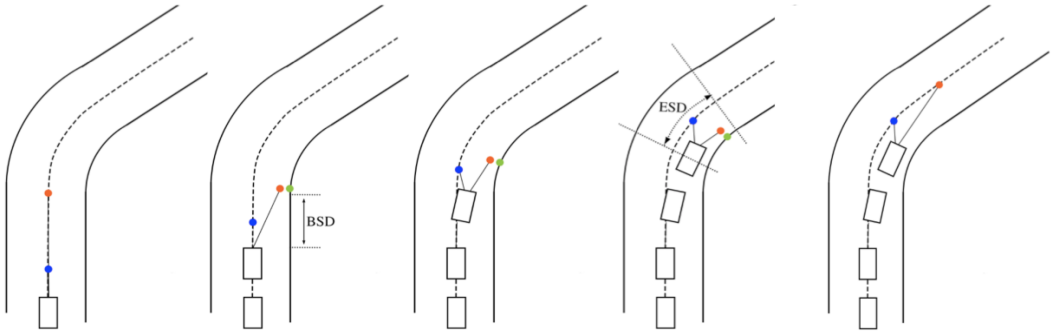

Figure A.11: Visual representation of the influence of BSD, ESD and t_{far}. The blue dot represents the near point, the green dot the tangent point and the orange dot the used target point. The distance when the target point switches to the inner lane and back to the lane center are indicated with BSD and ESD. Furthermore the outer right plots show the effect of t_{far} on the position of the far point when the far point switches back to the center line.

A.3. Parameter Sensitivity

To explore the effect of the parameters on the HCR, five parameters are changed separately and evaluated for the road used in the experiment. The first two parameters are the anticipation gain (K_p) and the compensation gain (K_c) which respectively represent the influence of the far angle and near angle. The parameters BSD and ESD influence the steering initiation distances. Finally the t_{far} determines at what distance ahead the far point is located when it is switched back to the center of the lane. The simulation is done with a constant velocity of 24 m/s and a road width of 3.6 meters.

A.3.1. Effect of changing K_p

The effect of changing K_p can be seen in figure A.12, here the lateral position and steering wheel angle are shown. It can be seen that increasing K_p increases the curve cutting behaviour. However, if K_p would increase too much the trajectory become oscillatory. The sudden increase in the far angle in the beginning of the curve results in overshoot in the steering wheel angle, as was also seen in the analyses in appendix F.1.3. Due to the short length of the curve the response does not reach the steady state value.

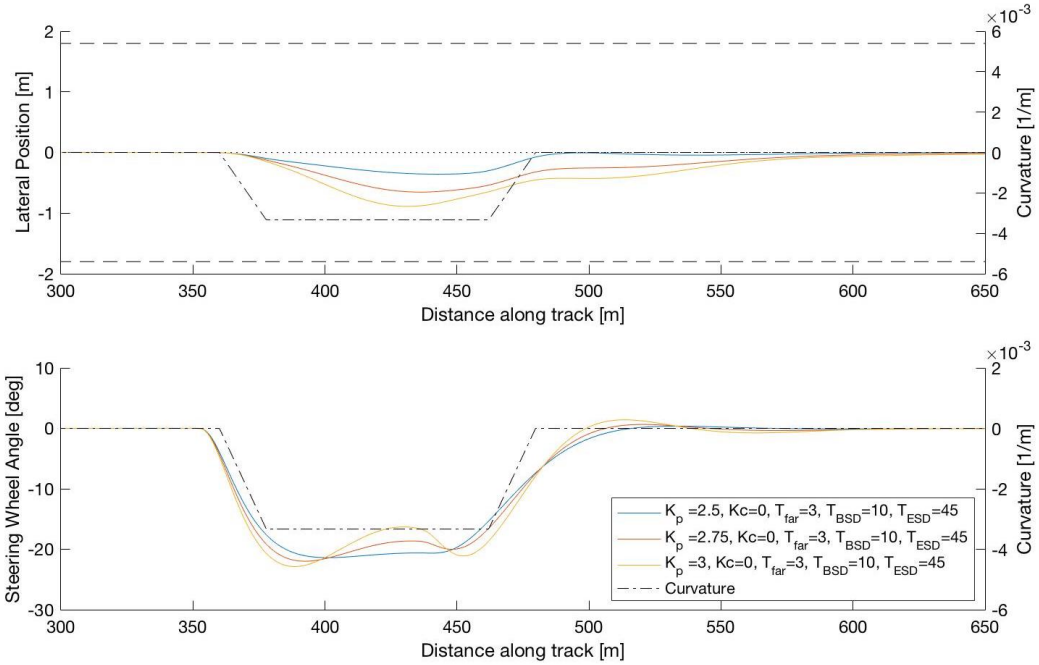

Figure A.12: Effect of changing the gain over the far angle (K_p) on the lateral positions (top) and steering wheel angles (bottom).

A.3.2. Effect of changing K_c

Figure A.13 shows the results of changing K_c, where the effect seems to be smaller than for changing K_p. The contribution from the near point is directed in the opposite direction from the contribution of K_p. It is indeed seen that for higher compensation gains the lateral position is closer to the lane center.

The peaks in steering wheel angle become higher for increasing values of K_c, increasing them further to the values given in the work from Saleh [8] lead to oscillating trajectories. This might be due to different vehicle dynamics of the car or the geometrical determination of the near and far point.

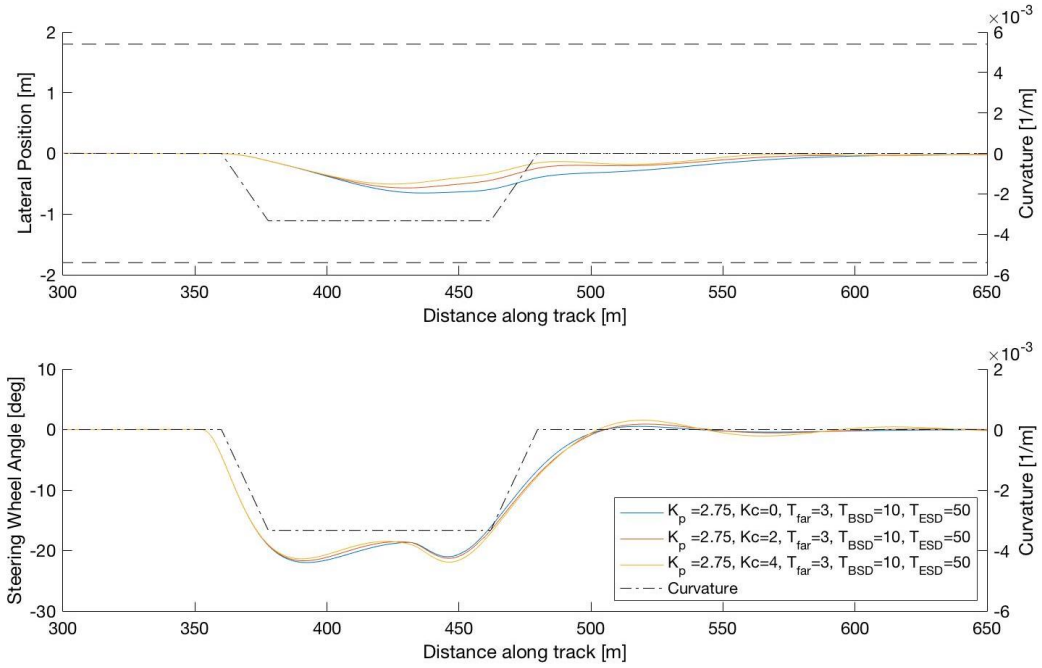

Figure A.13: Effect of changing the gain over the near angle (K_c) on the lateral positions (top) and steering wheel angles (bottom).

A.3.3. Effect of changing the BSD

The effect of changing the point where the driver starts steering into the curve (Begin Steering Distance) can be seen in figure A.14. With this approach is it possible to generate trajectories that steer late into the curve, but also cut the curve. This is not possible when t_{far} is coupled to the position where the drivers starts steering.

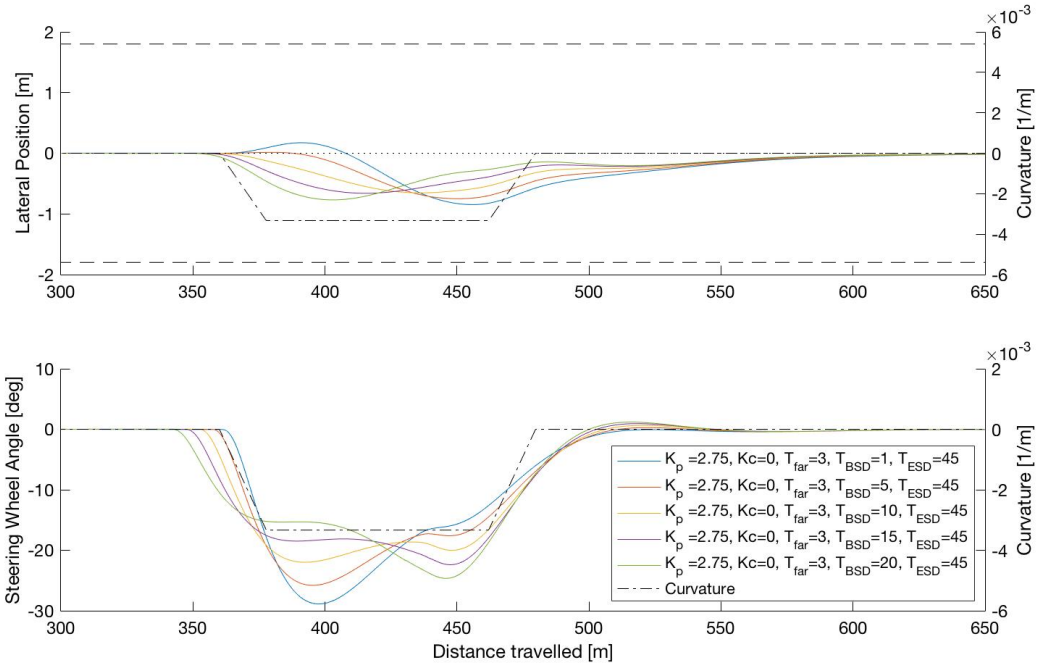

Figure A.14: Effect of changing the point where the driver starts steering into the curve (BSD) on the lateral positions (top) and steering wheel angles (bottom).

A.3.4. Effect of changing the ESD

The steering out behaviour of the model is effected by both the ESD and t_{far}. The effect of different values for the ESD is shown in figure A.15.

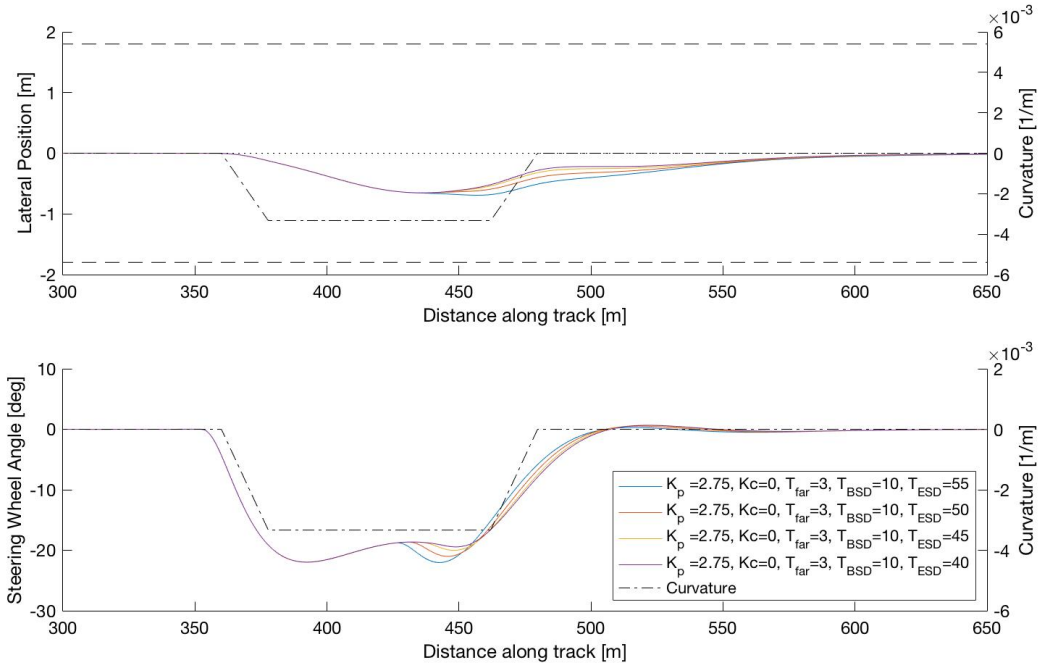

Figure A.15: The effect of different values for the ESD on the lateral positions (top) and steering wheel angles (bottom).

A.3.5. Effect of changing the t_{far}

The effect of changing t_{far} is shown in figure A.16, which indeed shows that the driver will steer back to the center sooner if t_{far} is lower. Because of the extra BSD parameter the behaviour in the beginning is not effected by changing t_{far} . However if t_{far} would be lower than 2 seconds, the tangent point could not be determined anymore, which would effect the behaviour over the total curve.

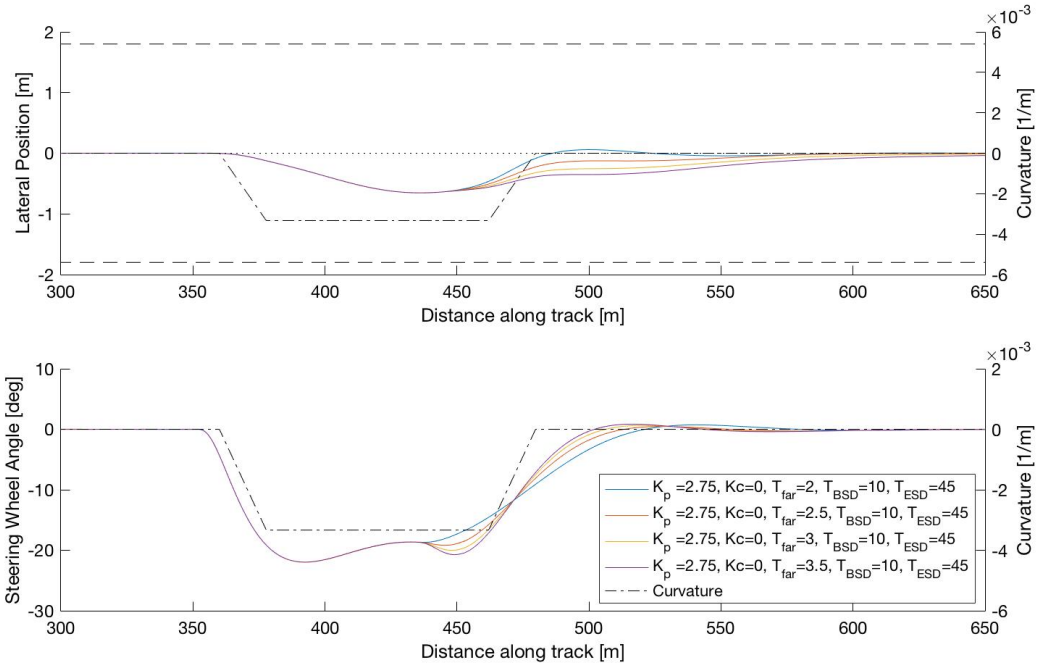

Figure A.16: Effect of changing t_{far} on the lateral positions (top) and steering wheel angles (bottom). Due to the decoupling of t_{far} and BSD in the beginning the different values show no effect, but in the end of the curve it does influence the response of the driver-model.

A.4. Evaluation driver-model capabilities on experiment road

To check the capabilities of the driver-model it is evaluated using the method proposed by Barendswaard [2], who uses descriptiveness, identifiability and realism metrics to assess individualized driver models. A road with a road-width of 3.6 meters and a constant velocity of 24 m/s is used. The parameters used for generating the trajectories are listed in table A.1.

Kp [-]	[2:0.125:3.5]
Kc [-]	[0:1:5]
t_{far} [sec]	[2:0.25:3.5]
BSD [m]	[1, 2.5:2.5:25]
ESD [m]	[40:5:55]

Table A.1: Parameter range and resolutions used as input for the MATLAB driver-model to produce all possible trajectories

The BSD is chosen based on the recorded data from earlier experiments in our group and on Boer [4] who found that drivers start steering into the curve between 20 and 30 meters before the start of the curve. Since this curve starts with a clothoidal section of 20 meters, lower distances are evaluated since drivers might not perceive the first part of the clothoidal road as beginning of the curve.

A.4.1. Descriptiveness

Using the definition from Barendswaard [2] the descriptiveness is defined as: 'the extent to which a driver-model is capable to capture different driver styles'. The possible solution range from the driver-model for the first curves is indicated as a green area in figure A.17, here only the trajectories with a lateral position that does not exceed an absolute value of 1.5 meters are used. The descriptiveness is thereafter calculated as a percentage of the grey area that is covered. In this case the descriptiveness is 61.6%.

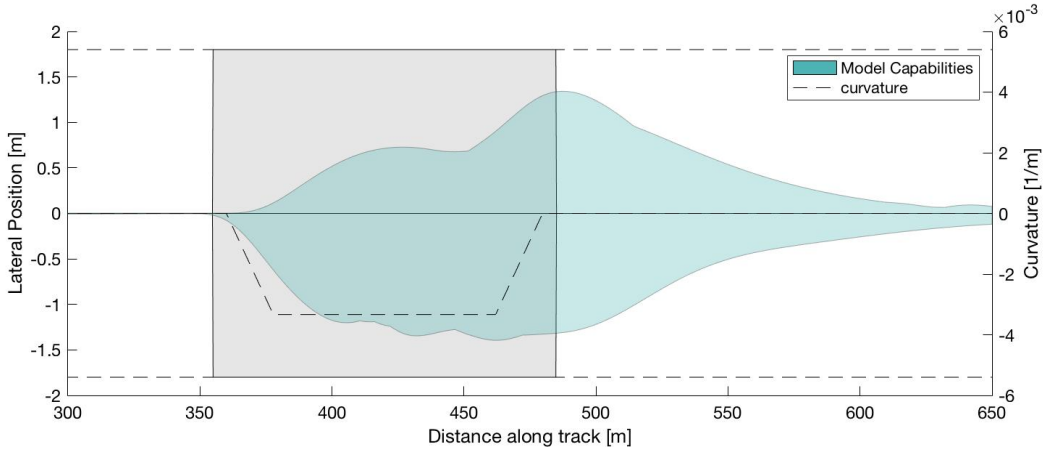

Figure A.17: Results for the descriptiveness area: the green area visualizes the model capabilities for the whole parameter range and resolution, starting from an initial position of zero. Only trajectories are visualized that does not exceed a absolute lateral position of 1.5 meter. The gray area represents all possible lateral positions in the curve that the driver can drive. The descriptiveness is the percentage of the gray area that is covered by the green area, which is 61.6%.

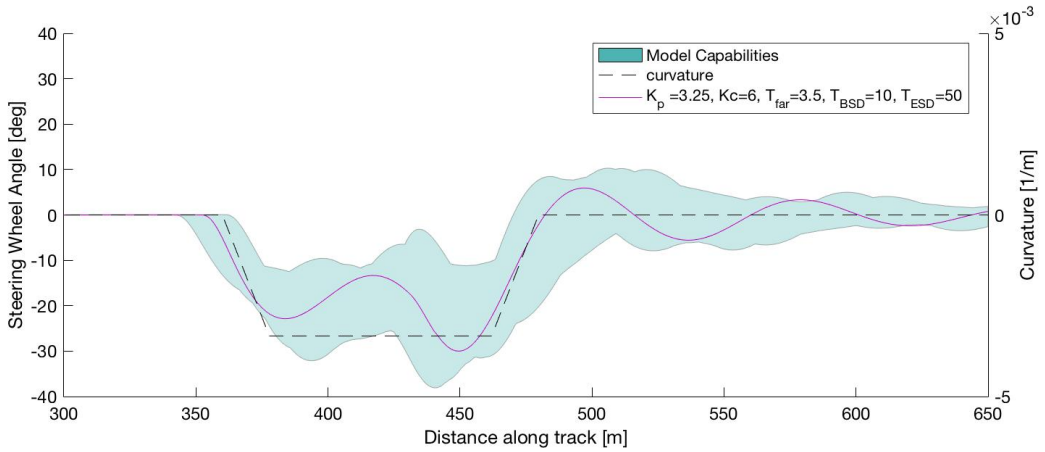

Figure A.18: Results for the steering wheel inputs that generate the range trajectories in green area in plot A.17. One example is given that shows that swinging steering wheel inputs.

A.4.2. Realism

The last metric Barendswaard [2] uses is realism, which is defined as 'the extent at which the modelled steering wheel deflections δ_s are realistic and acceptable for the application of advanced driver assistance systems'. The descriptiveness plot in figure A.17 showed a large area of captured trajectories. However, it is not determined yet if these trajectories are reached with realistic steering wheel angles. Therefore, the steering reversal rate is determined by counting how many times the steering wheel is reversed with 2 degrees or more around a local minima and maxima. If the maximum amount of reversals is set to 3 the plots show a different result, which is shown in figure A.19. Reducing the maximum steering reversals to 3 reduces the descriptiveness to 45.89%.

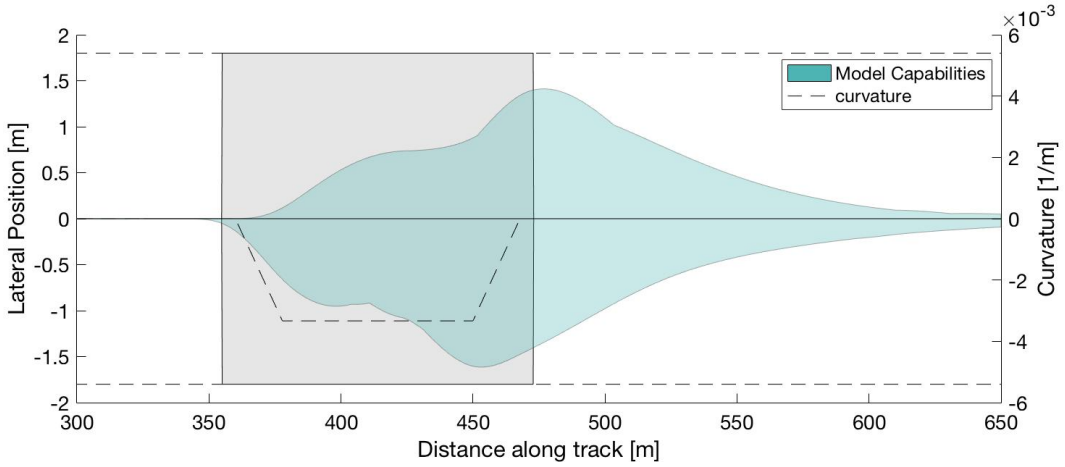

Figure A.19: Results for the descriptiveness area, generated with steering reversals < 3 per curve. The green area visualizes the model capabilities from an initial position of zero. The gray area represents all possible lateral positions in the curve that the driver can drive. The descriptiveness is the percentage of the gray area that is covered by the green area, which is 45.89%

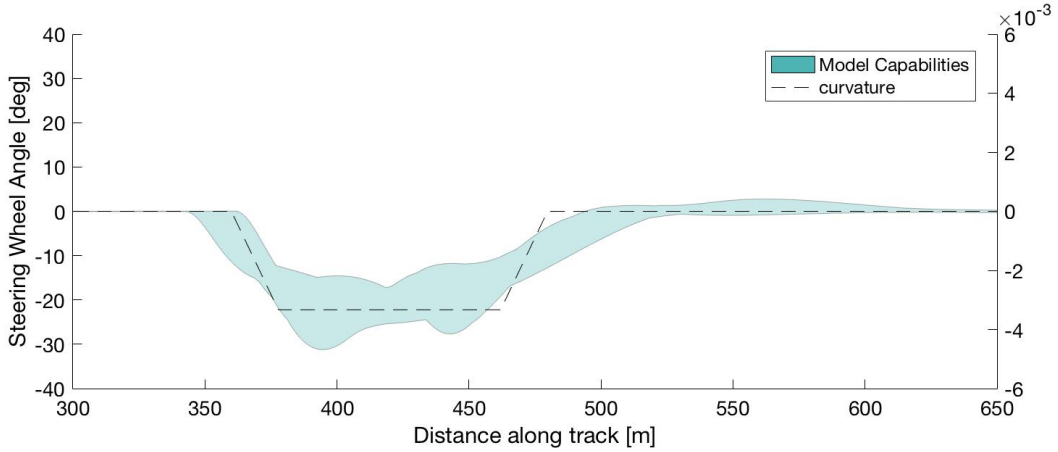

Figure A.20: Results for the measured steering angles during the experiment and the generated steering angles from the model, filtered for SRR < 3 per curve

The descriptiveness plots from Barendswaard [2] might not give a complete view on the captured driver behaviour. Looking deeper into the generated trajectories shows that not all possible combination of trajectories within the descriptiveness area are possible. The produced trajectories show a characteristic profile as seen in figure A.21.

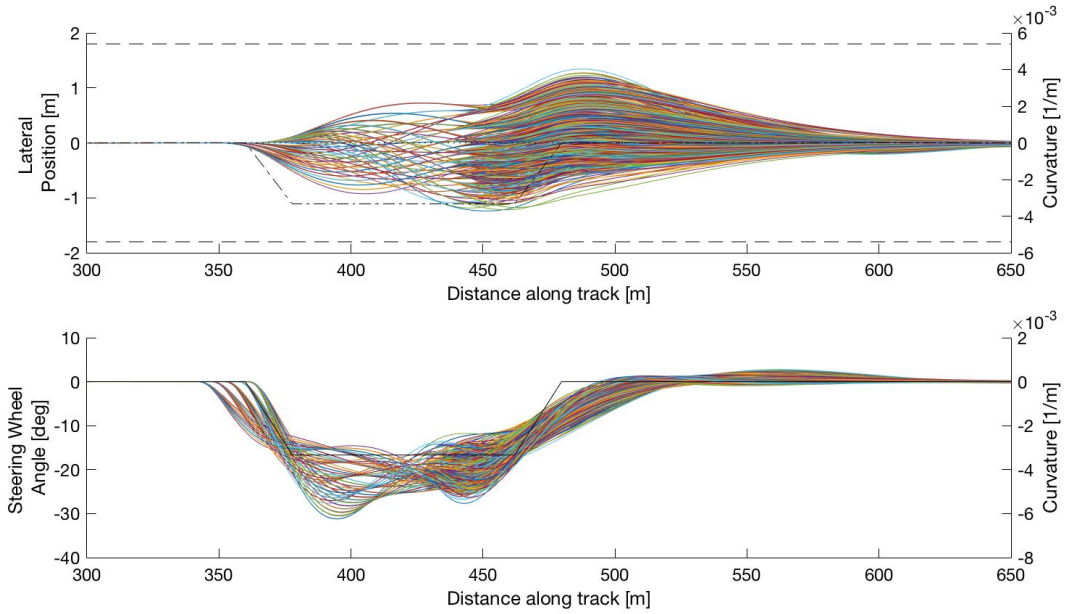

Figure A.21: The generated trajectories in the descriptiveness area show a characteristic pattern in the lateral positions (top) and steering wheel angles (bottom), therefore the capabilities within the area are finite and not all trajectories within the area can be generated.

A.4.3. Driver-Model Cases

The figures above do not give a full insight in the HCR's that the driver-model can produce. A couple of cases for possible HCR's are shown below the give a better insight on the capabilities of the driver-model.

Curve cut trajectories

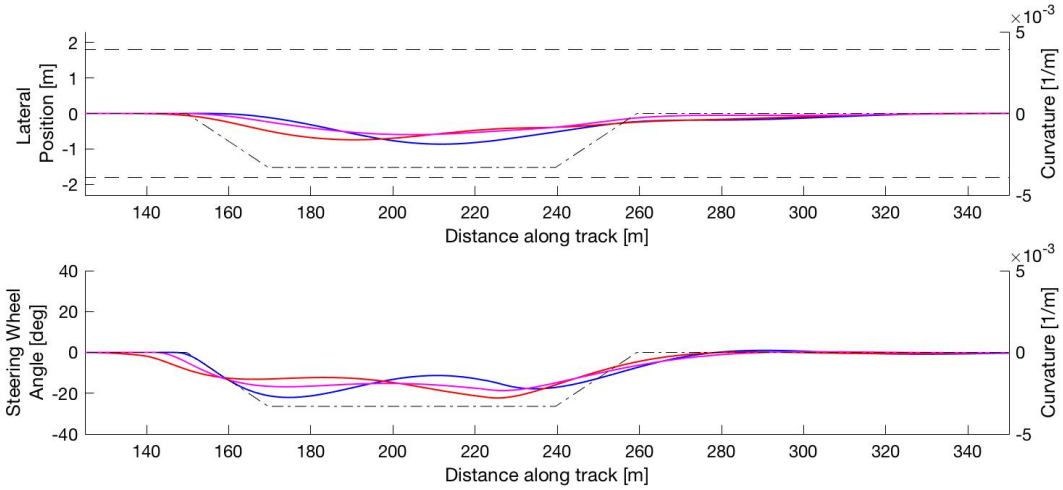

Figure A.22: Example of the lateral positions (top) and steering wheel angles (bottom) of curve cut trajectories. The driver-model can capture different initial steering positions as well as different degrees of curve cutting in the middle of the curve.

Understeer trajectories

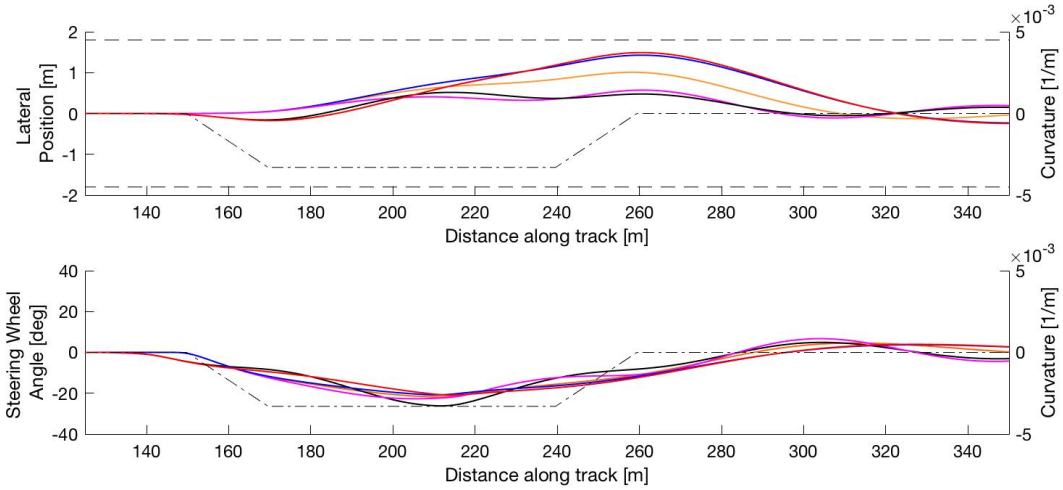

Figure A.23: Example of the lateral positions (top) and steering wheel angles (bottom) of under-steer trajectories. The driver-model will always approach the curve from the lane center and trajectories with a positive lateral error in the beginning of the curve can not be produced.

Center trajectories

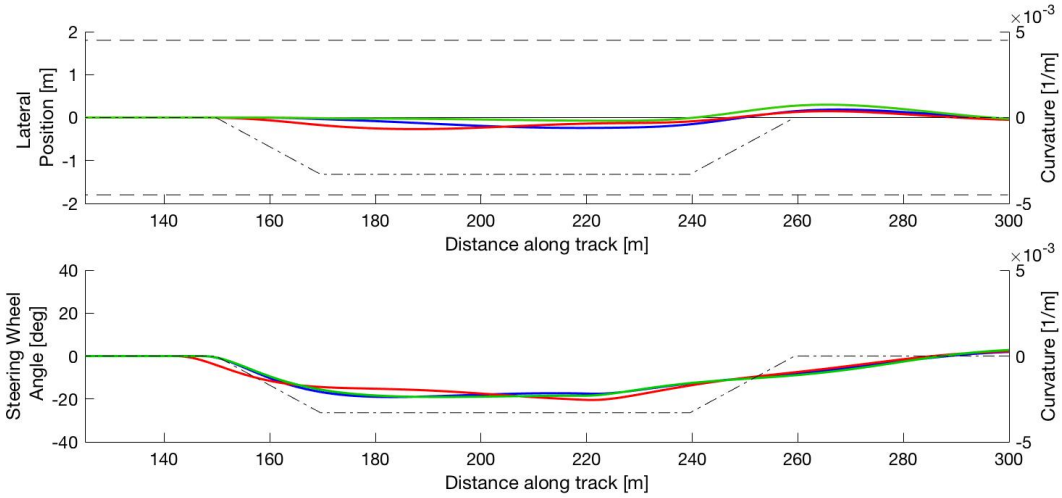

Figure A.24: Example of the lateral positions (top) and steering wheel angles (bottom) of center trajectories. A HCR that stays exactly in the middle of the road is not possible to generate for the current implementation and parameter range and resolution of the driver-model.

Diagonal trajectory

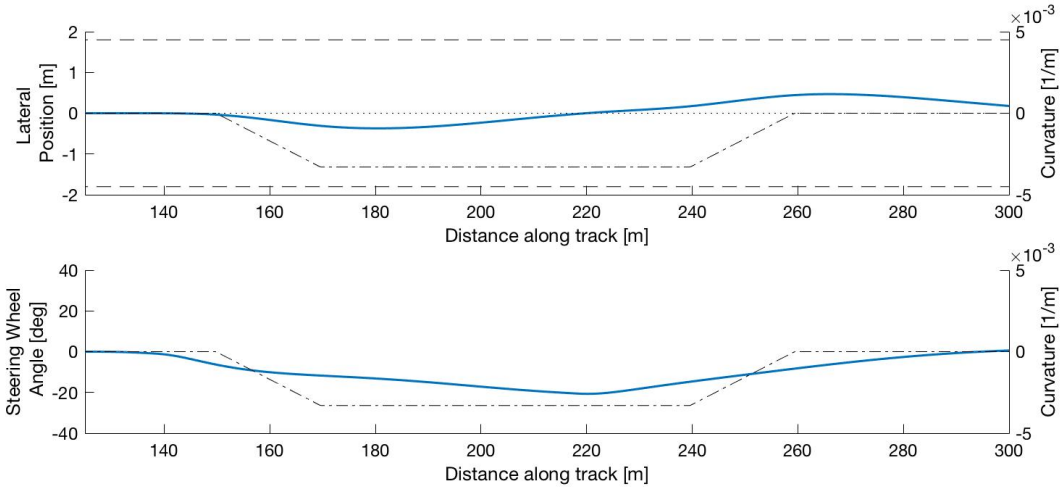

Figure A.25: Example of the lateral positions (top) and steering wheel angles (bottom) of diagonal trajectory which first shows curve-cut behaviour, followed with under-steer behaviour. A diagonal trajectory which under-steers first and ends with curve cutting can not be generated by the driver-model.

A.5. Personalizing Gains

In section A.4 the driver-model capabilities are explored. The select the individual and average HCR first all outputs for the whole parameter range and resolution are generated, on which the model is fitted.

A.5.1. Fitting method

The HCR is determined by optimizing the lateral error between the HCR's and the manual driving behaviour. To find the parameters which produce the closest fit, the error between the lateral position of the HCR and the real driver trajectory is determined using:

$$f_{Lateral\_Error} = \sum |(Driver\_lateral\_Error - Model\_lateral\_Error)^2| \tag{A.5}$$

The curve is separated in different parts to assign different weights to different locations in the curve. The error values are multiplied with the weighing values to determine the total error value:

$$f_{tot} = g_1 * f_{Lat.ErrorIn} + g_2 * f_{Lat.ErrorMid} + g_3 * f_{Lat.ErrorOut} \tag{A.6}$$

	Begin [m]	End [m]	Gain
Begin section	325.16	384.4	2
Middle section	384.4	433.6	1.5
Out section	433.6	503.8	2
Curve	359.8	467.8	
Curve excl. clothoidal section	377.9	450	

Table A.2: Definition of different road sections and the weighing factors.

Because the driver behaviour largely differs for left and right curves the driver-model is fitted separately for both directions. An example for a fitted trajectory is seen in figure A.26. The results of all fitted trajectories for each subject are shown in appendix C.3.

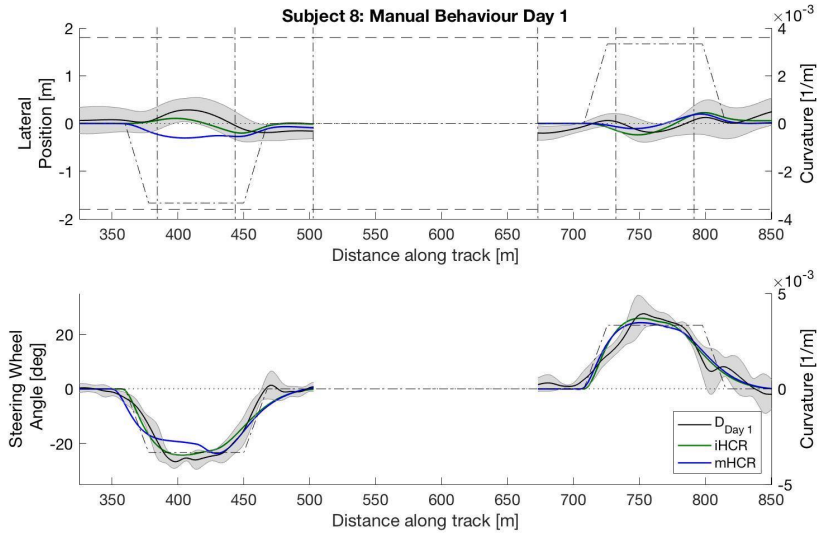

Figure A.26: Example of fitted references for subject 8. The blue lines represents the fitted trajectory for the mean of all drivers. The green line represents the individual fitted trajectory. The vertical dash-dotted lines in the top plot indicate the three fitting sections.

A.6. Discussion

The goal of the implementation of the driver-model was to generate human-like references. The evaluation showed that a range of different trajectories can be generated, as well for drivers that cut the curve as drivers that show under-steer trajectories.

A.6.1. Driver-model

An ideal driver-model would be able to capture all human-driving behaviour to make sure all drivers have a perfect fitted individual HCR. However, the human can not be modelled as an equation. Trying to approach the human with a simple driver-model particularly resulted in limitations in the beginning and end of the curve. Wyzen [12] also found limitations in the driver-models behaviour in the transition phases and proposed to use the target point. This indeed showed a reduction in overshoot, but could not fully eliminate the mismatch with the drivers.

The determination of the far angle cause a discontinuity in the input signals. The driver-model therefore produces high peaks in the torques on the steering wheel. The reason why these peaks are less visible in the output steering wheel angles is because these high frequency inputs are damped by the dynamics of the steering wheel. When the steering wheel for the car in the MATLAB simulation is replaced with a simple spring, the steering wheel angles become unrealistic. This indicates that the steering wheel acts as a fix to counteract high frequency torque inputs from the human.

Wyzen [12] used roads with a road-radius of 500m and 350m and road-length of 300 meters, where in this study the road-length is a lot shorter to evoke different driver behaviour. Because of the shorter curve length the trajectories will not reach the steady state output. In section A.5.1 the HCR is fit for one curvature profile. One of the biggest added values from a driver-model can be that it can predict individual trajectories for different curves. The trajectory in figure A.27 shows the generated trajectory for one set of parameters over different curvatures. The driver-model generates different behaviour for different curves, in this study therefore only one curvature profile is evaluated. To make sure the generated trajectories match the driver behaviour also in different curvatures, curve-lengths and road-widths the driver-model should be further developed.

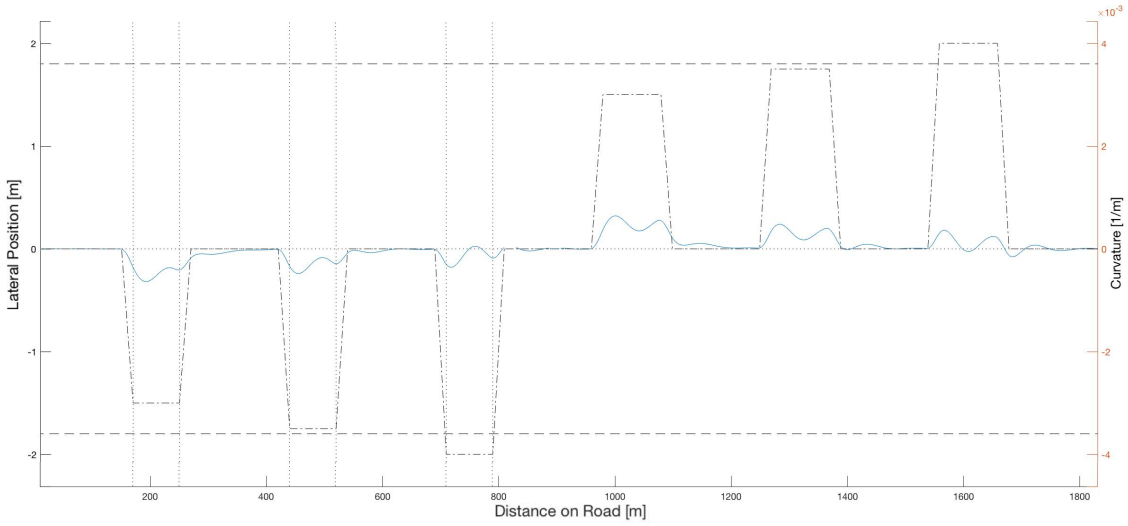

Figure A.27: The driver-model shows different behaviour for curves with different road widths and road lengths.

The near angle is filtered with a low-pass filter, such that these inputs are not leading to high frequency torques on the steering wheel. However, increasing the gain for the near angle to values mentioned in the work of [8] leads to oscillating reference trajectories. This is probably due to the fact that different determination of the input angles and different car dynamics are used. However, the exact cause for this behaviour was not further investigated due to time limits for this project.

The driver-model lacks in generating trajectories that have a bias on straight sections and the driver-model will always return to the middle of the road. Therefore the initial position at curve entrance is always

the middle of the road, where some drivers might start the curve with a lateral deviation from the center. Limitations are seen for curves shortly after each other where real human drivers do not fully return to the late center. In that case the drivers steering-out behaviour of a previous curve influences the steering in behaviour of the next curve. Since the driver-model will always approach curves from the center-line this will result in errors in the beginning of the curve.

A.6.2. Fitting method

In this study the weighing factors for the begin, middle and end section of the curve are selected heuristically. It future work it is interesting to investigate in what sections drivers are likely to perceive more conflicts and therefore weigh that section higher. Another method to fit the reference could involve the variability. A lower variability could indicate that the driver is more strict on the desired trajectory at that location. All the mentioned methods focus on the lateral position, where maybe the steering wheel angles or heading should be incorporated in the fitting as well.

A.6.3. Future work

For use in further studies the driver-model should be extended on four points:

- It should be able to produce the same output when the car-model changes, where currently the damping of the steering wheel ensures reasonable HCR's.
- It should be able to produce more human-like behaviour in the beginning and end of the curve. The input signals (near and far angle) should be determined differently or the human response to the inputs should compensate for the assumptions and approximations in the inputs.
- It should be able to capture biases in the straight sections and curve entry.
- It should be able to produce HCR's for multiple curves with one parameter set.

A.7. Conclusion

To generate human-like trajectories a drivel model from literature is used, where for this study the derivation of the input signals is changed. The capabilities of the adjusted driver-model to generate human-like trajectories is first evaluated using 2 metrics; the descriptiveness and realism. For the used curvature profile and a realistic amount steering reversals the versatility is 45.89%. However not all trajectories within the descriptiveness area can be generated. Particularly in the transition phases of the curve the driver-model has limitations and shows overshoot in the input torques and thereby in the HCR's. Another drawback of the driver-model is that it does not work optimal for all curve and road designs. The limitations in the HCR also led to conflicts with the drivers in the human-factors experiment. Future studies should develop the driver-model to evaluate the effect of a better matching HCR on the acceptance of the drivers.

B

Appendix C: Simulink Models

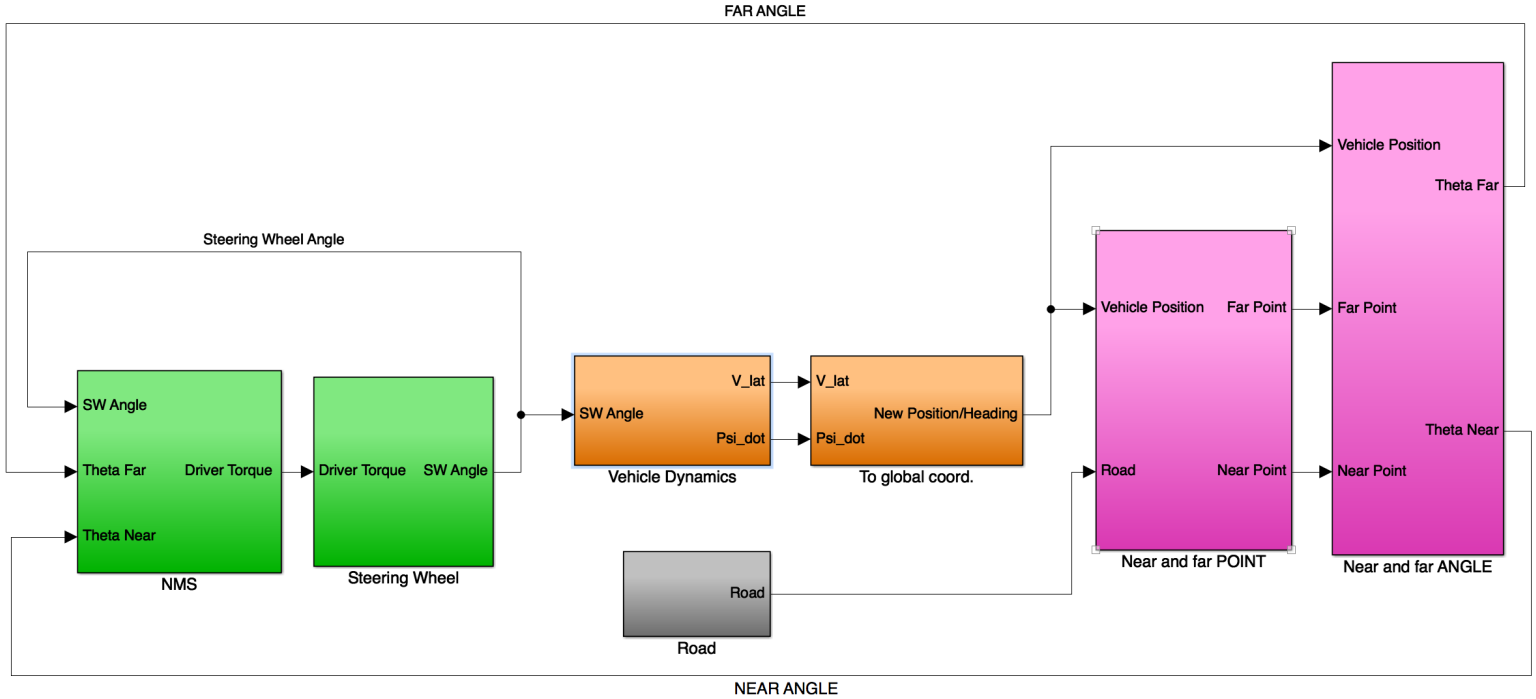

Figure B.1: Schematic overview of generating the trajectory of the ghost car

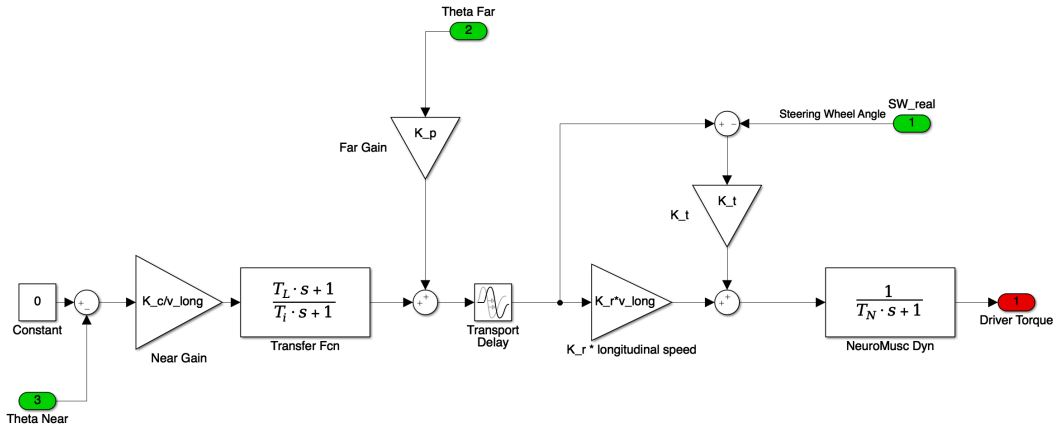

Figure B.2: Schematic overview the human simulated in Simulink.

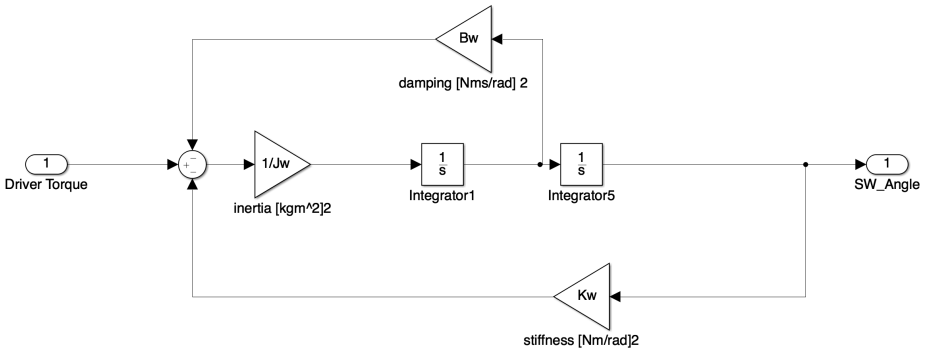

Figure B.3: Schematic overview of steering wheel. K_w, B_w and Jw are respectively the stiffness, damping and inertia of the steering wheel.

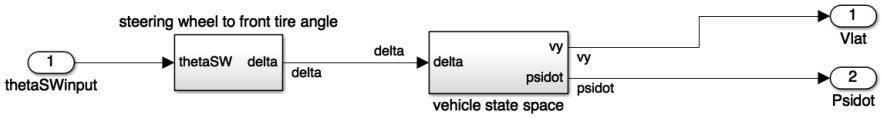

Figure B.4: Schematic overview of the determination from the state space output (lateral velocity and yaw rate), using the steering wheel angles.

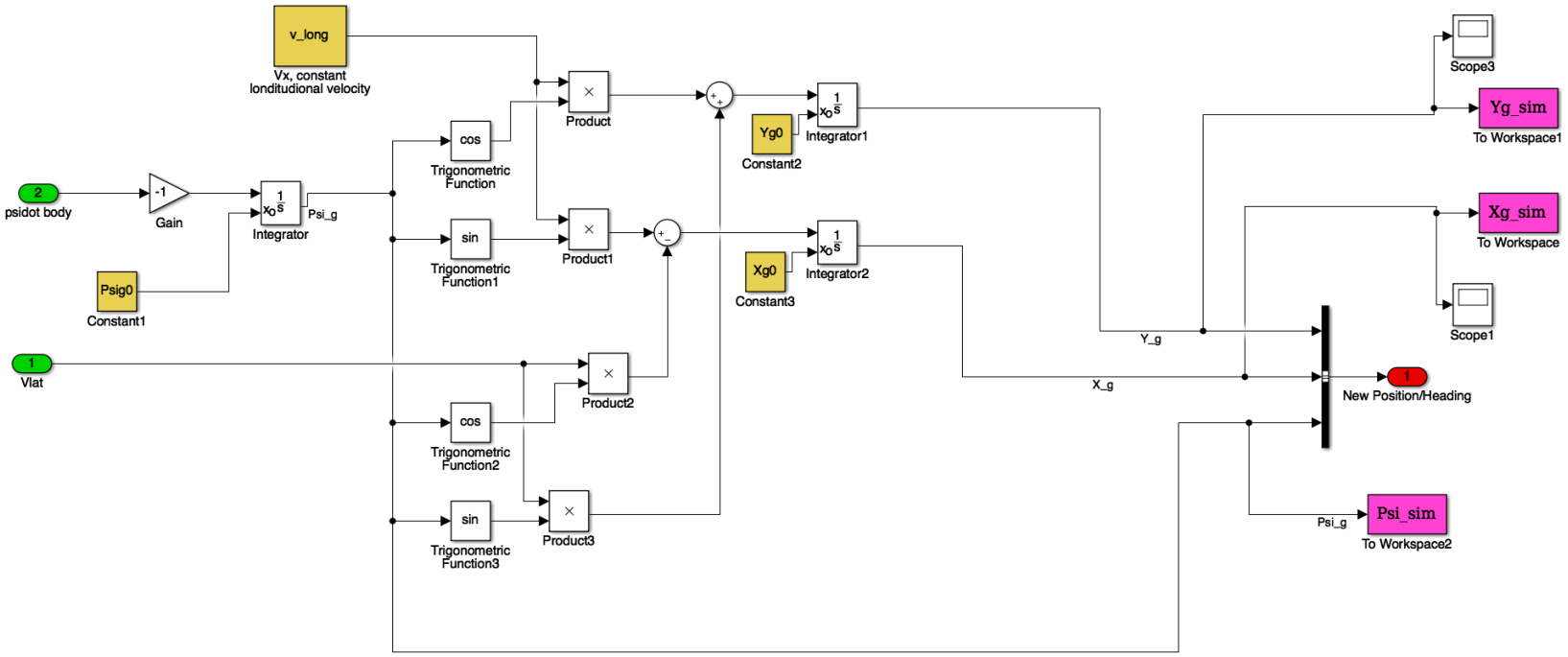

Figure B.5: Schematic overview of the determination of the updated car states using the outputs from the vehicle dynamics. The vehicle yaw rate is first integrated to obtain the yaw angle. The position is determined using the lateral and (constant) longitudinal velocity.

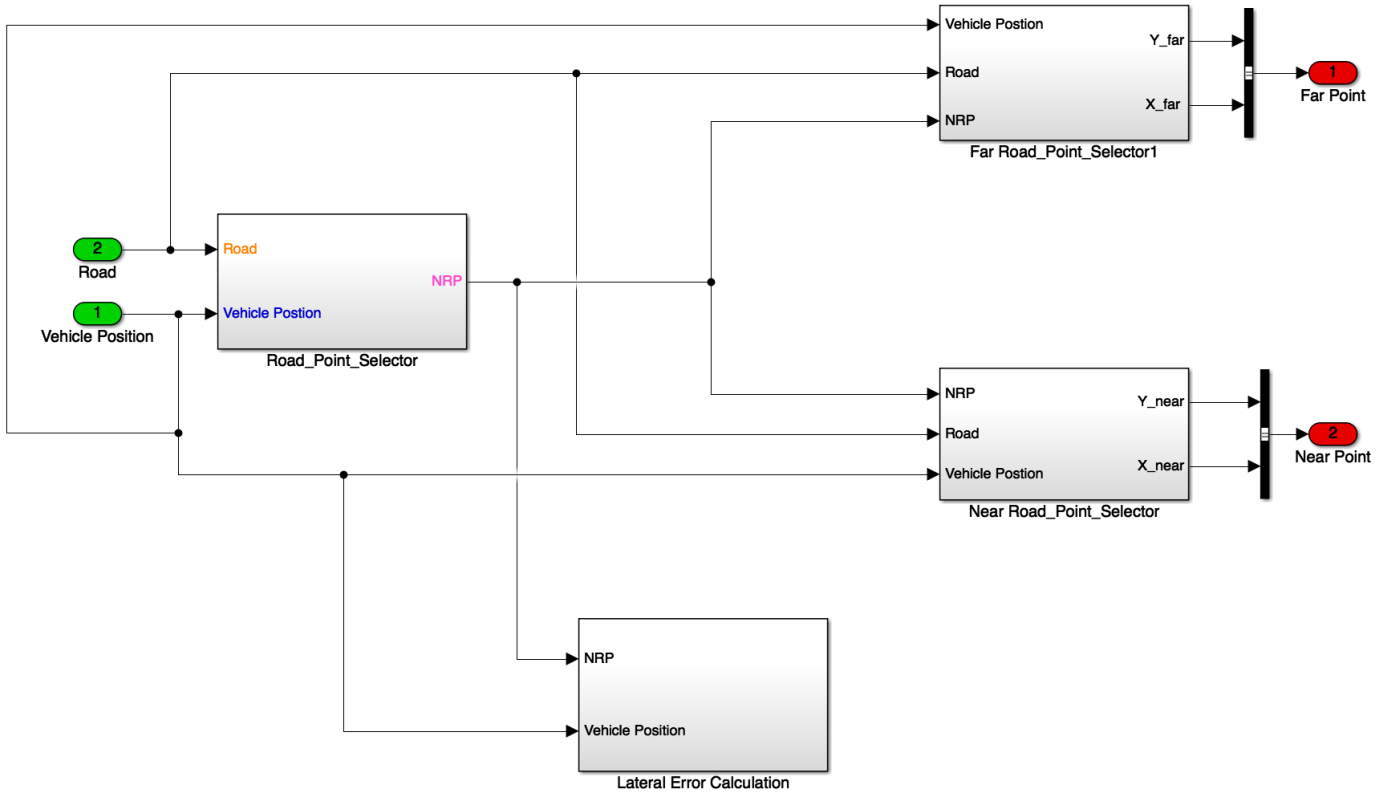

Figure B.6: Schematic overview of the determination of the near and far point. First the nearest road point is determined, together with the road and vehicle states these are used to determine the outputs.

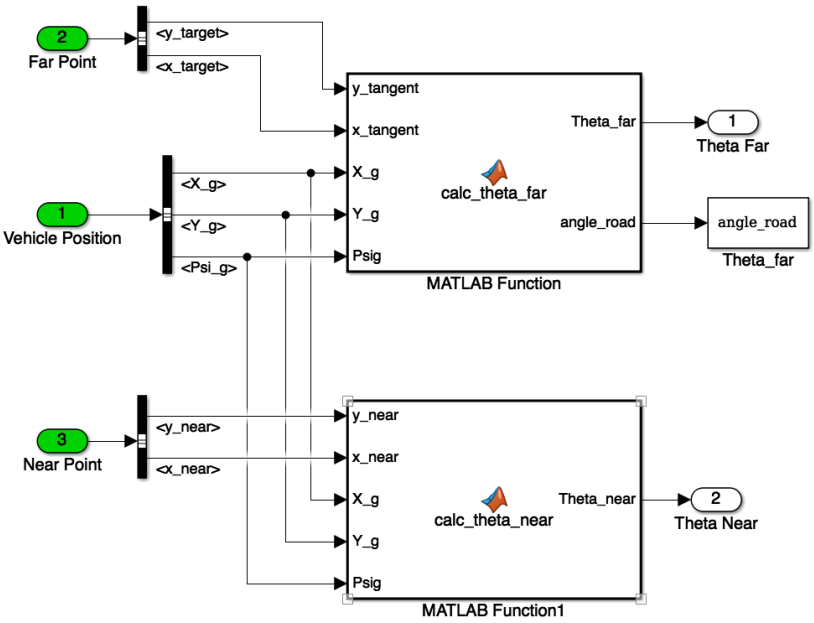

Figure B.7: Schematic overview of the determination of near and far angles, using the near and far point and the current vehicle state. The lateral error is determined using the nearest point on the lane center of the road and the current vehicle position.

C

Appendix C: Extensive Results

C.1. Matlab Simulation

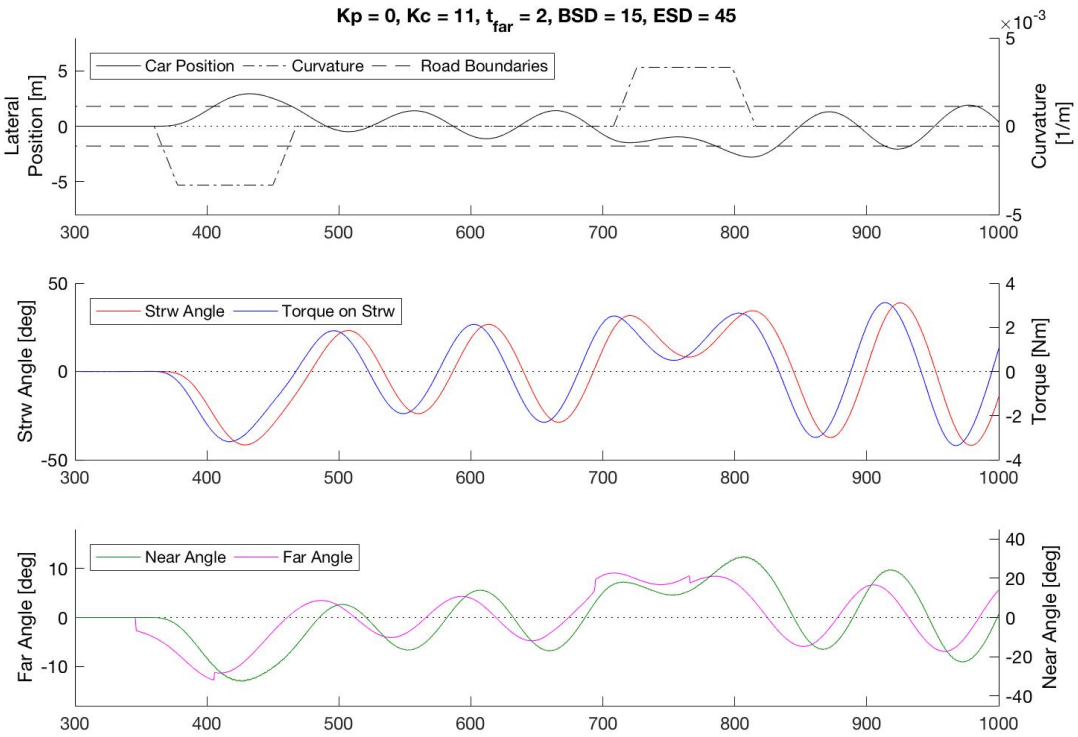

Figure C.1: Generation of the reference (HCR) in matlab with only the near angle active. The gain over the near angle (K_c) = 11, the gain over the far angle (K_p) = 0, the gaze-ahead-time (t_{far}) = 2, the Begin Steering Distance (BSD) = 15, End Steering Distance (ESD) = 45. The generated trajectory is not able to stay within the lane boundaries and can not return to the lane center.

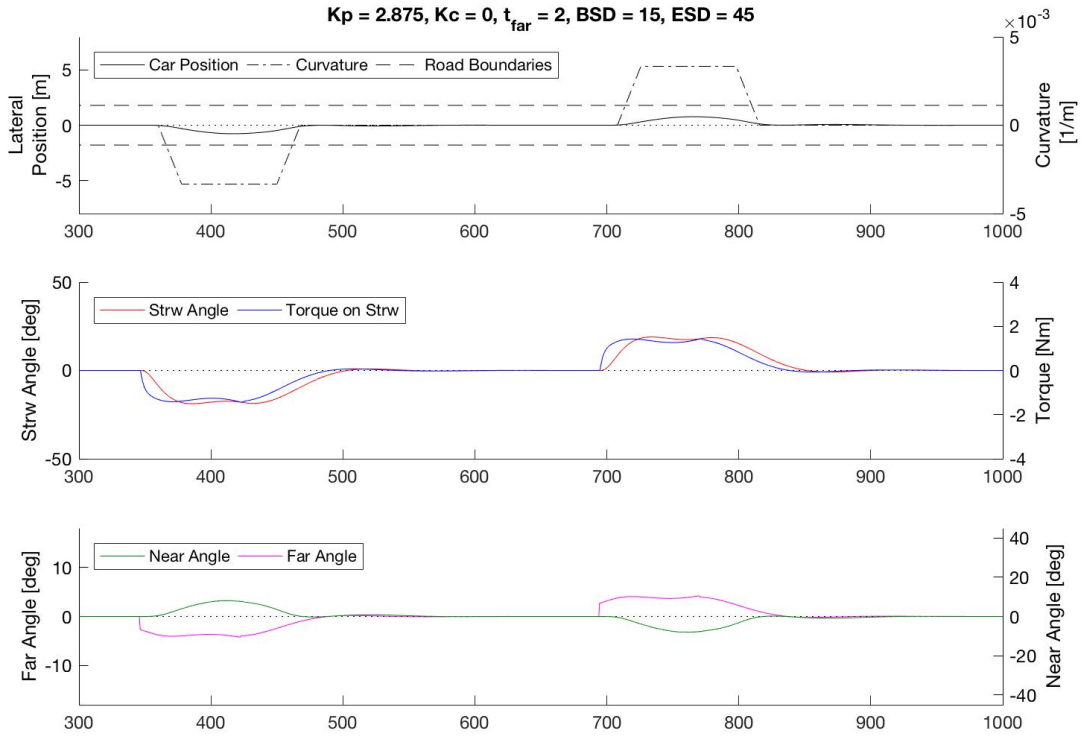

Figure C.2: Generation of the reference (HCR) in matlab with only the far angle active. The gain over the near angle (K_c) = 0, the gain over the far angle (K_p) = 2.875, the gaze-ahead-time (t_{far}) = 2, the Begin Steering Distance (BSD) = 15, End Steering Distance (ESD) = 45. The generated trajectory is able to cut the curve and return to the lane center.

C.2. FDCA Architecture

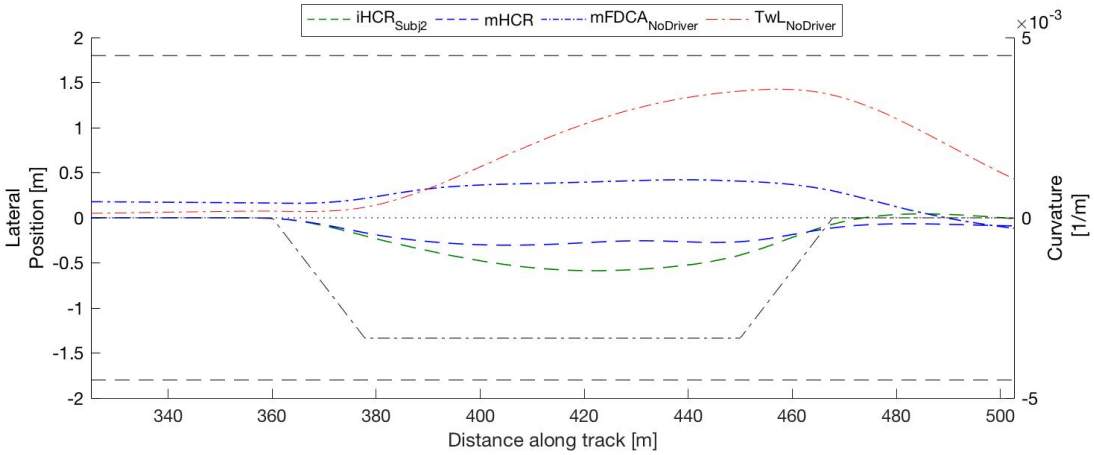

Figure C.3: Behaviour of the FDCA controller without human input (blue dotted-dashed line) and TwL controller without human input (red dotted-dashed lines), both visualized for a right curve. Also the references used in the FDCA controllers are visualized for both the reference tuned for the average behaviour (blue dashed line) and for the individual behaviour of subject 2 (green dashed line).

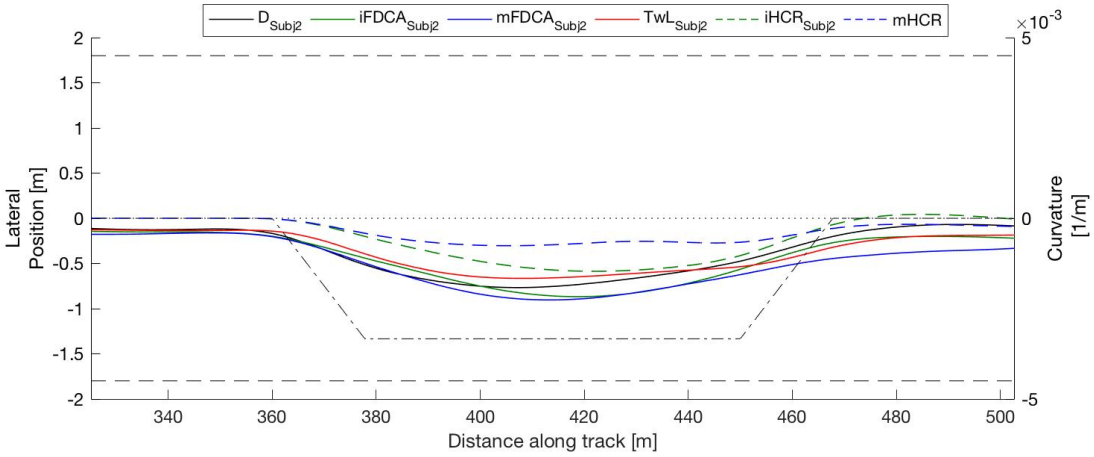

Figure C.4: Behaviour of subject 11 for a right curve. The reference for the iFDCA (dashed green line) and mFDCA (dashed blue line). The behaviour of subject 11 in manual control (solid black line) and the behaviour when supported with iFDCA (solid green line), with FDCA (solid blue line), and with TwL (solid red line)

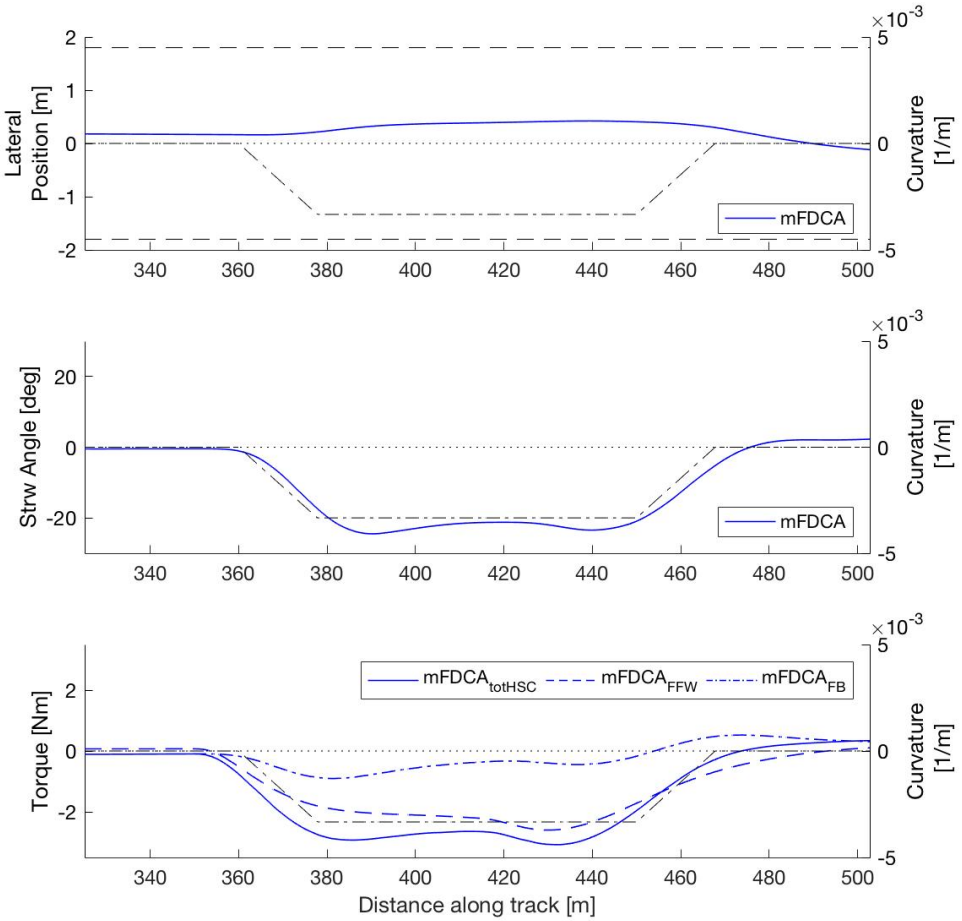

Figure C.5: The solid blue lines represent the position (top plot), steering wheel angle (middle plot) and total HSC torque (bottom plot) when only the mFDCA controller is active, without human input. The dashed line shows the torque generated by the feed-forward component and the dotted-dashed line the torque generated by the feedback component. The steering wheel angles (middle plot) show a time delay, which results in under-steer behaviour of the car. In the tuning of the feed-forward forces this delay was not taken into account, therefore it was assumed that the feed-forward torque was not tuned too high, however: when the driver already applies torques it was found that the HSC torques are often higher than the driver torques in manual control.

C.3. Model Fit

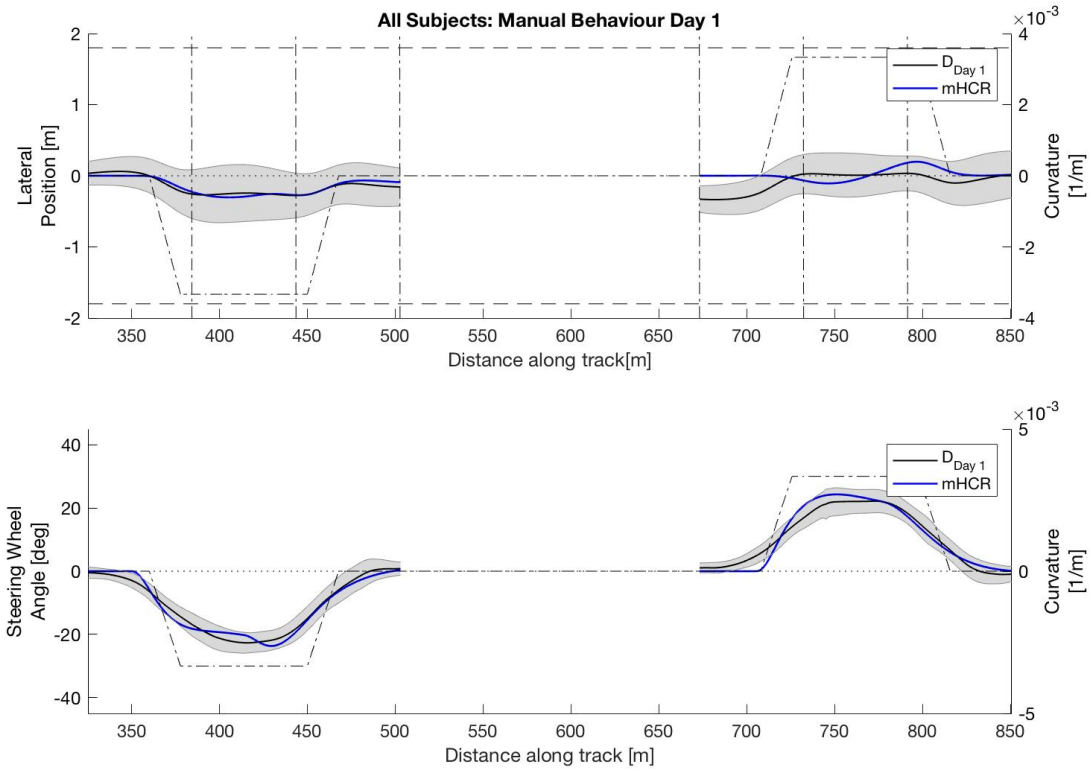

Figure C.6: The behaviour of all subjects (mean and STD between subjects) on the first experiment day (black) and the result for the fitted mHCR (blue). The top plot shows the lateral positions and the bottom plot the steering wheel angles.

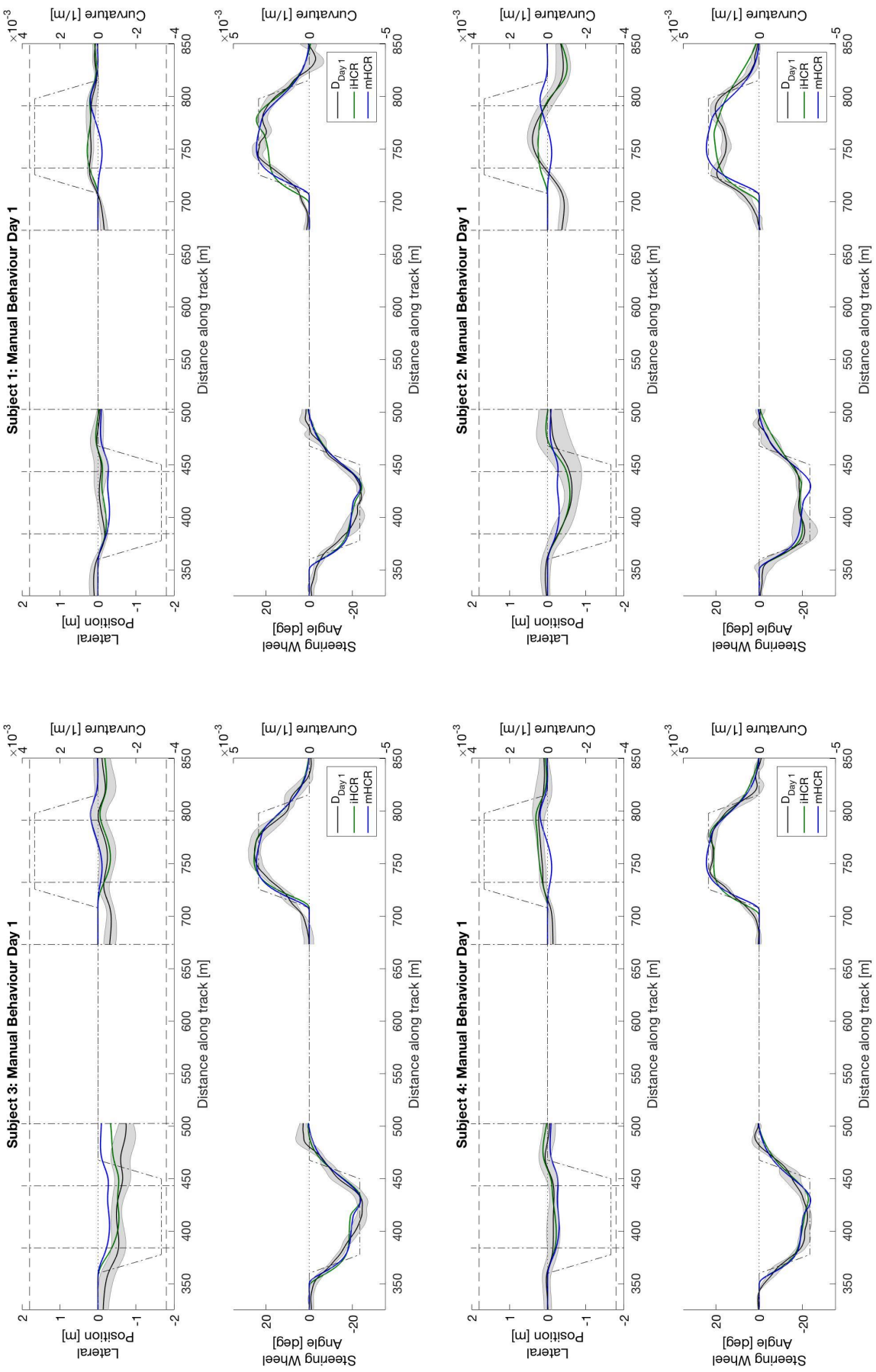
Subject 1: Manual Behaviour Day 1
Subject 2: Manual Behaviour Day 1
Subject 3: Manual Behaviour Day 1
Subject 4: Manual Behaviour Day 1
Lateral Position [m]
Steering Wheel Angle [deg]
Curvature [1/m]
Distance along track [m]
D_Day 1
iHCR
mHCR

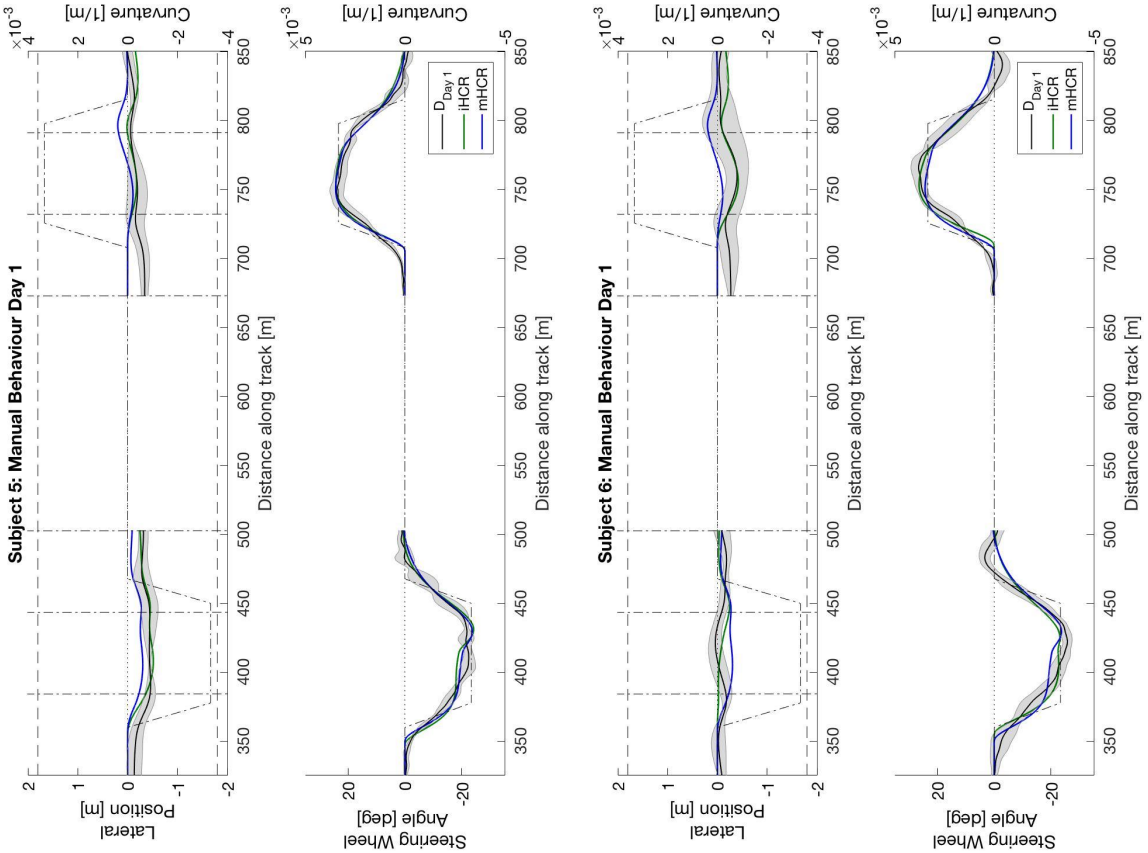
Subject 5: Manual Behaviour Day 1
Subject 6: Manual Behaviour Day 1
Lateral Position [m]
Curvature [1/m]
Steering Wheel Angle [deg]
Distance along track [m]
D Day 1
iHCR
mHCR

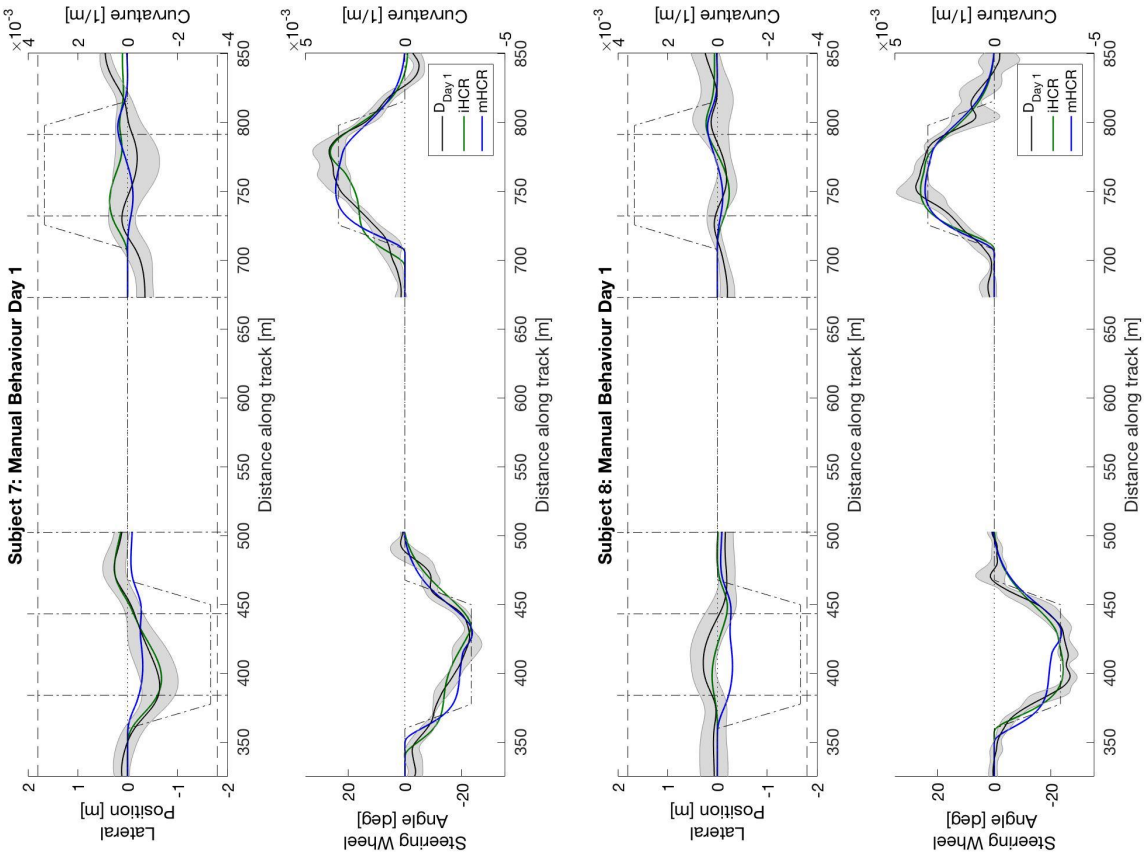
Subject 7: Manual Behaviour Day 1
Subject 8: Manual Behaviour Day 1
Lateral Position [m]
Curvature [1/m]
Steering Wheel Angle [deg]
Distance along track [m]
D Day 1
iHCR
mHCR

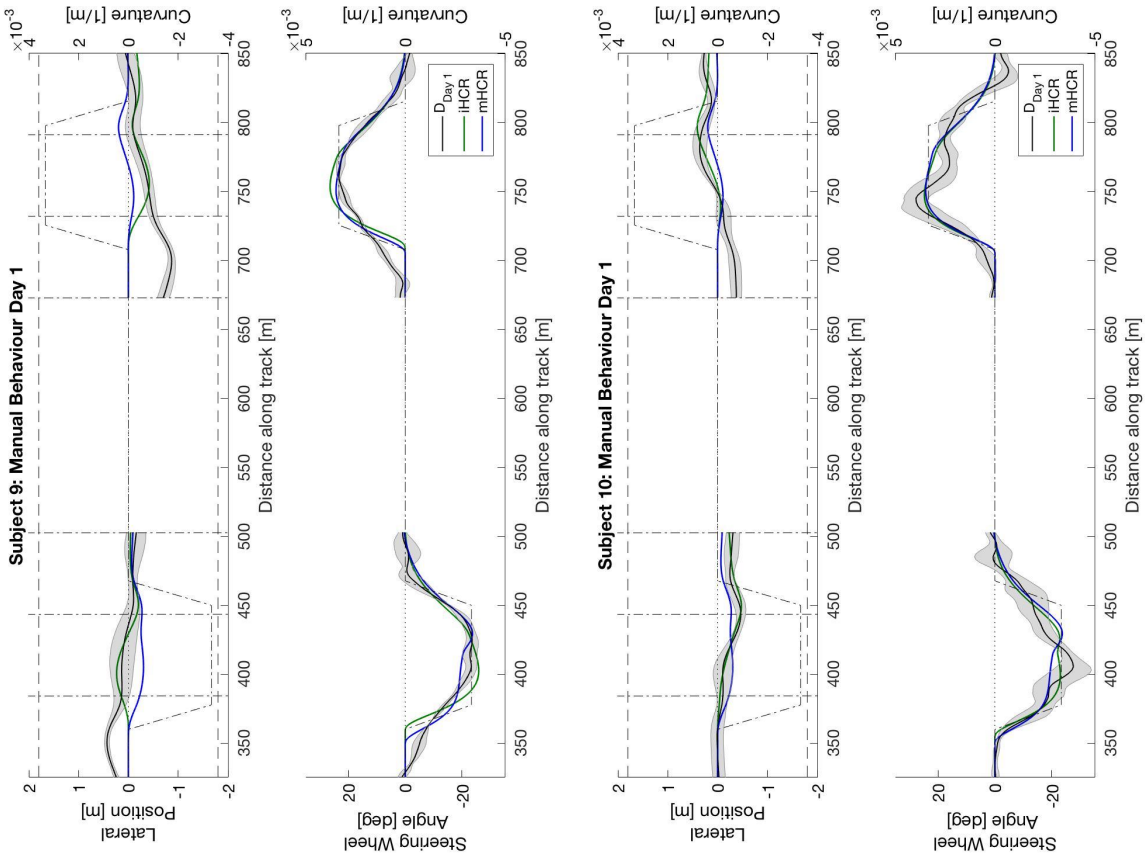
Subject 9: Manual Behaviour Day 1
Subject 10: Manual Behaviour Day 1
Lateral Position [m]
Steering Wheel Angle [deg]
Curvature [1/m]
Distance along track [m]
D_Day 1
iHCR
mHCR

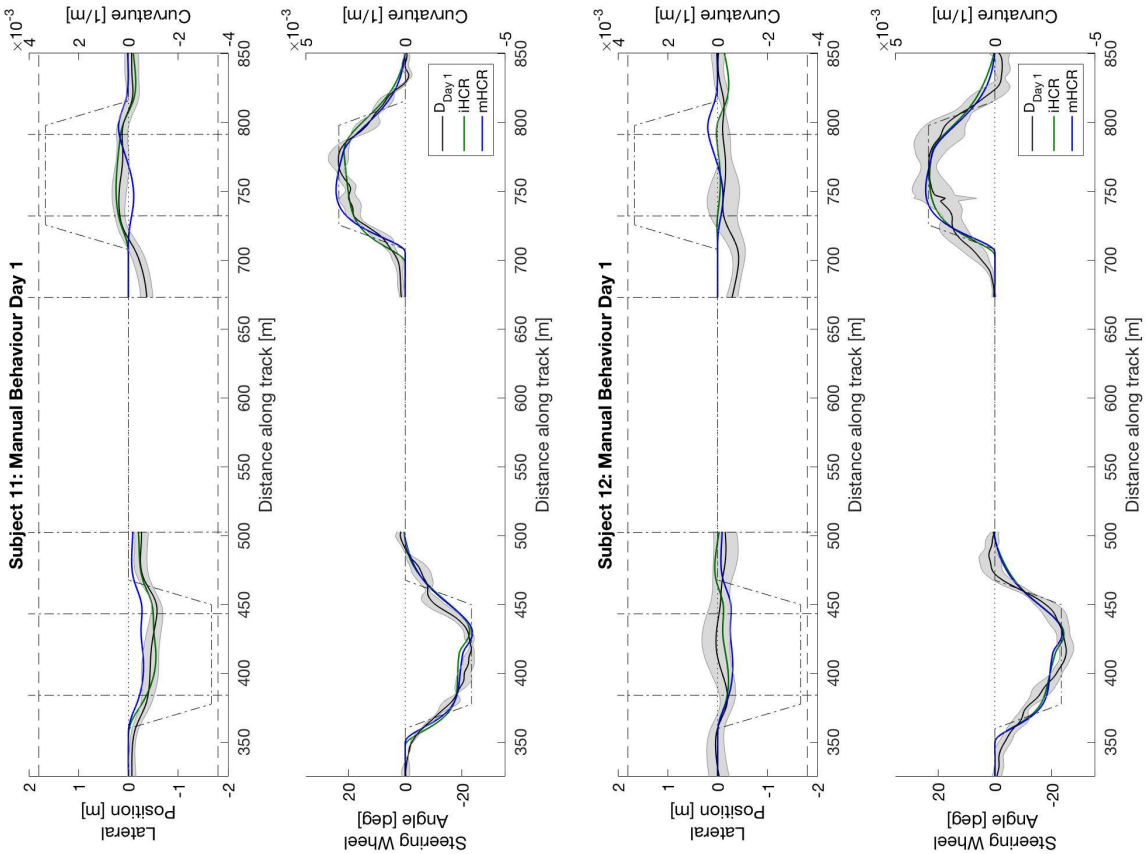
Subject 11: Manual Behaviour Day 1
Subject 12: Manual Behaviour Day 1
Lateral Position [m]
Steering Wheel Angle [deg]
Curvature [1/m]
Distance along track [m]
D_Day 1
iHCR
mHCR

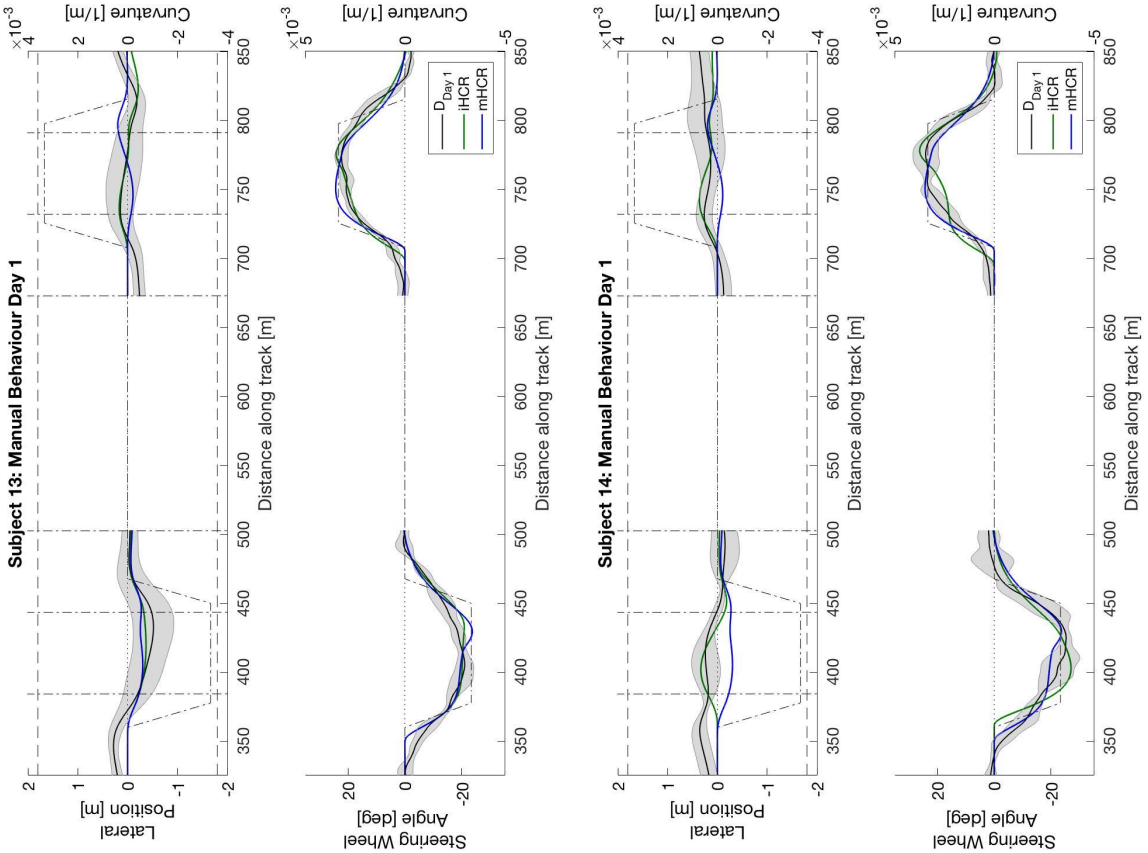
Subject 13: Manual Behaviour Day 1
Subject 14: Manual Behaviour Day 1
Lateral Position [m]
Curvature [1/m]
Steering Wheel Angle [deg]
Distance along track [m]
D Day 1
iHCR
mHCR

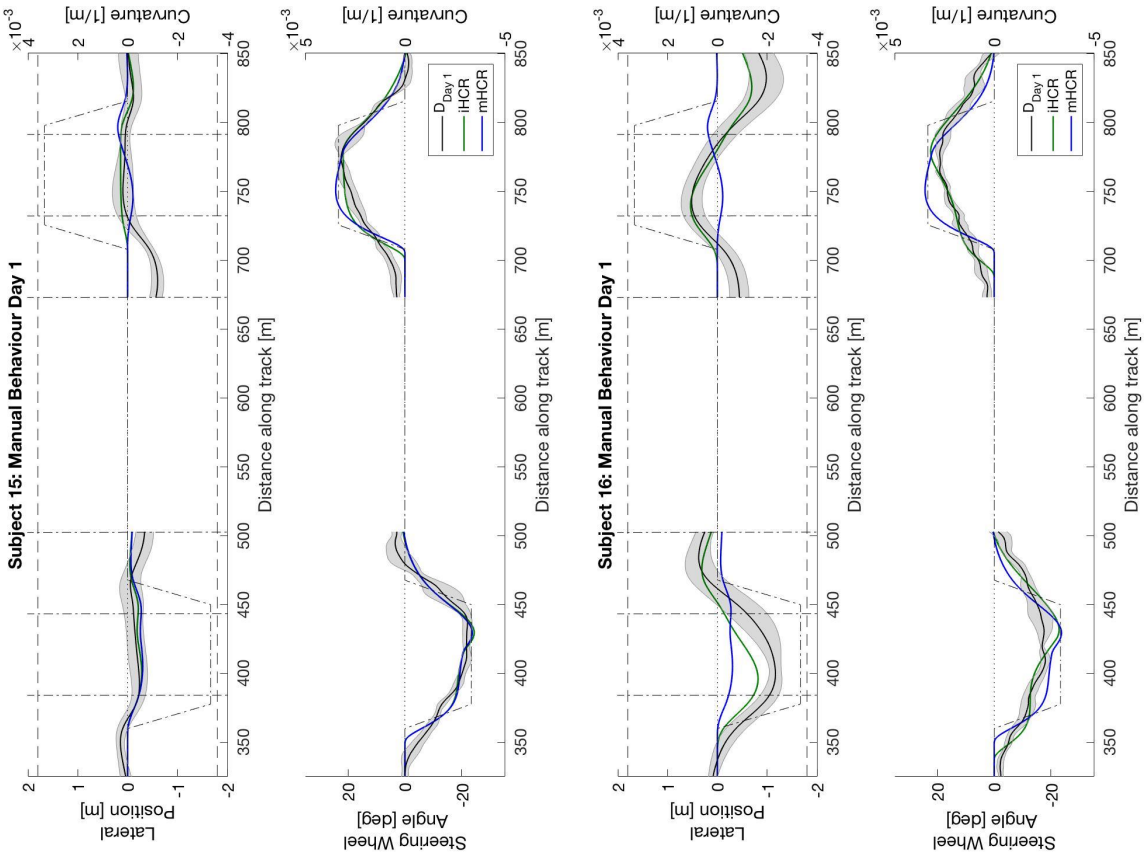
Subject 15: Manual Behaviour Day 1
Subject 16: Manual Behaviour Day 1
Lateral Position [m]
Curvature [1/m]
Steering Wheel Angle [deg]
Distance along track [m]
D Day 1
iHCR
mHCR

C.4. Model Fit Evaluation

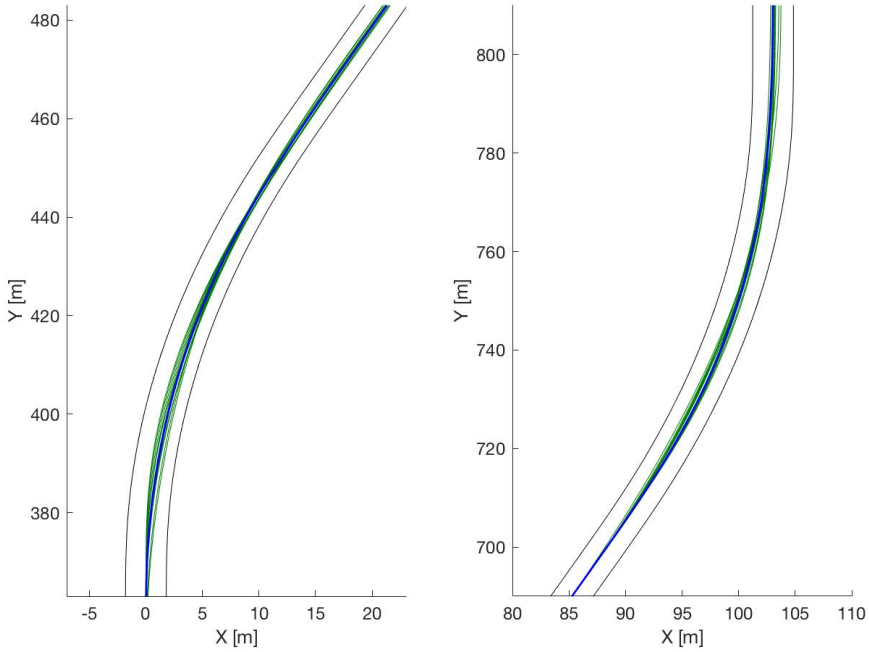

Figure C.7: All 16 individual fitted references (iHCR's, green lines) and the single one-size-fits-all reference (mHCR, blue line) tuned on the average driver behaviour.

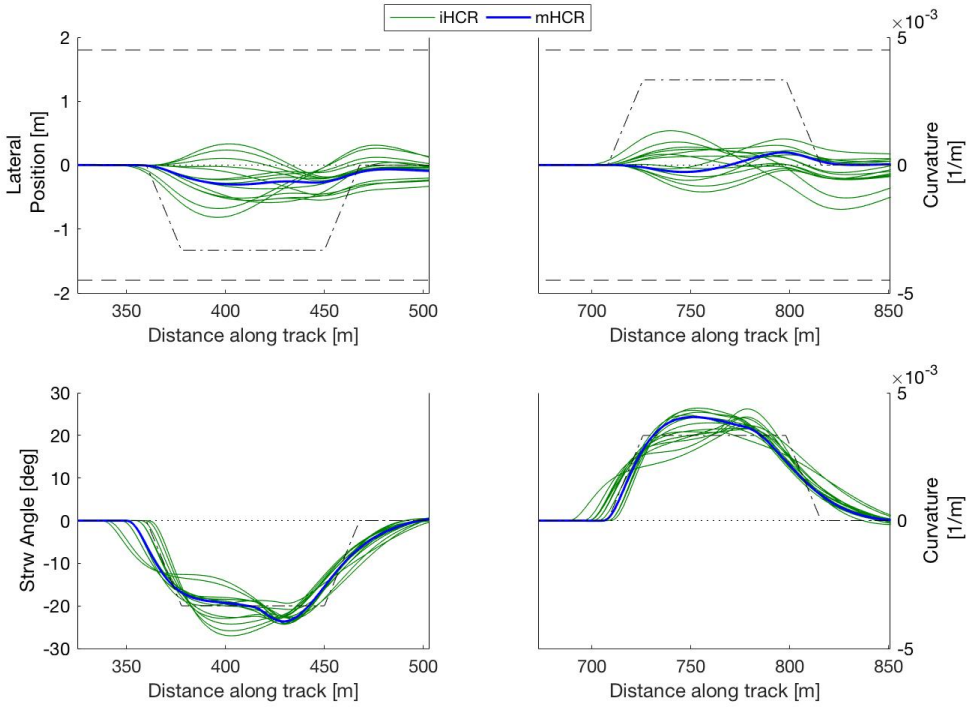

Figure C.8: Results for all 16 individual fitted references (iHCR's, green lines) and the single one-size-fits-all reference (mHCR, blue line) tuned on the average driver behaviour. The spread in the individual references indicate that drivers showed different behaviour when driving with manual control. The mHCR cuts the curve more in the right curves compared to the left curves.

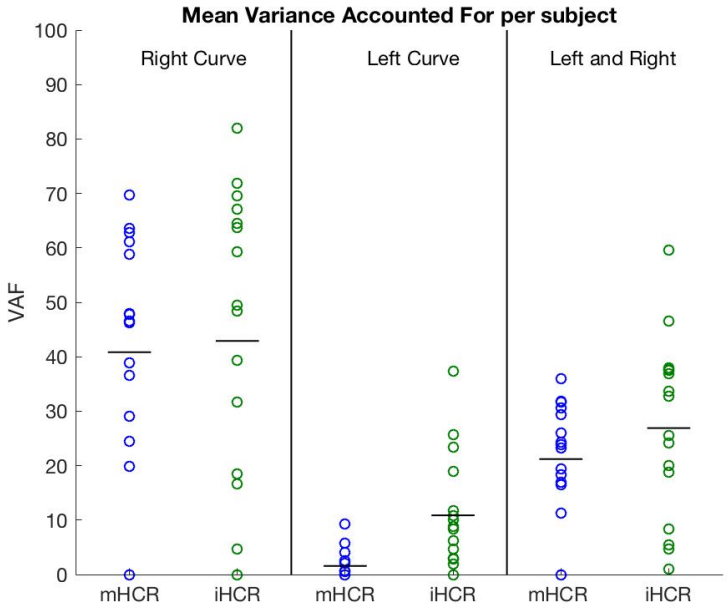

Figure C.9: Results for the mean VAF values over the five curve repetitions for right curves and left curves, visualized for all subjects for mHCR (blue) and individual HCR (green). The horizontal black lines indicate the mean over the VAF values from the 16 subjects.

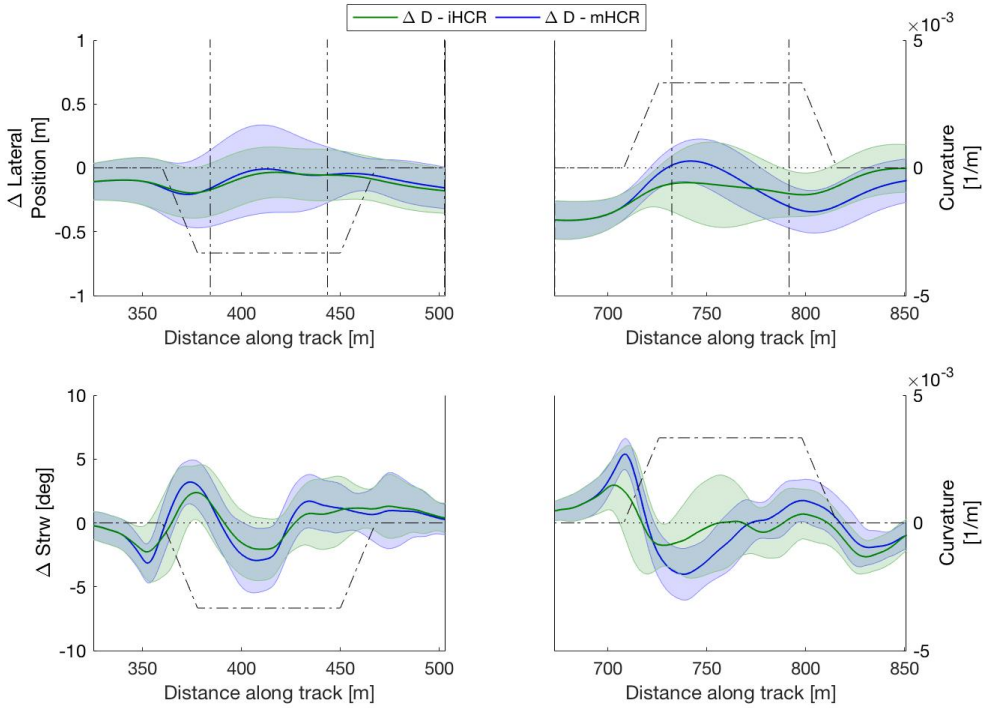

Figure C.10: *Top:* Lateral error between the manual behaviour and the iHCR and mHCR. The error with the mHCR has a larger STD in the right curves. *Bottom:* Error in Steering Wheel Angle between the manual driver behaviour and the iHCR and mHCR. The peaks in the steering wheel angles are higher for the mHCR, indicating that indeed the iHCR is a closer match to the drivers behaviour.

	Right Curve					Left Curve				
Subject nr.	Kp	Kc	BSD	ESD	t_{far}	Kc	Kp	BSD	ESD	t_{far}
1	2.375	4	12.5	55	3.5	2.5	5	12.5	55	3.5
2	2.75	1	12.5	40	2	2.375	0	12.5	55	2
3	2.625	0	15	55	3.5	2.25	0	2.5	55	3.5
4	2.375	2	12.5	50	3.5	2.5	4	1	55	3.5
5	2.625	1	15	55	3.5	2.25	1	5	40	3.5
6	2.375	0	7.5	55	3.5	2.25	0	1	40	3.5
7	2.5	0	22.5	40	2.5	2.5	5	15	55	3.5
8	2.375	5	5	50	3.5	2.375	0	2.5	55	3.5
9	2.375	0	2.5	40	3.5	2.25	0	1	40	3.5
10	2.5	0	7.5	55	3.5	2.5	0	5	45	3.5
11	2.625	0	15	55	3	2.375	0	12.5	45	3.5
12	2.5	4	12.5	55	3.5	2.25	2	7.5	40	3.5
13	2.375	0	12.5	40	3.5	2.25	3	12.5	55	3.5
14	2.5	0	1	45	3.5	2.5	5	15	55	3.5
15	2.625	5	12.5	55	3.5	2.375	3	10	40	3.5
16	2.375	0	25	45	2	2.25	0	22.5	50	2.5
OSFA	2.5	4	12.5	55	3.5	2.375	0	5	40	3.5

Table C.1: Identified Parameters for the five parameters in the driver-model for all 16 subjects and the OSFA trajectory

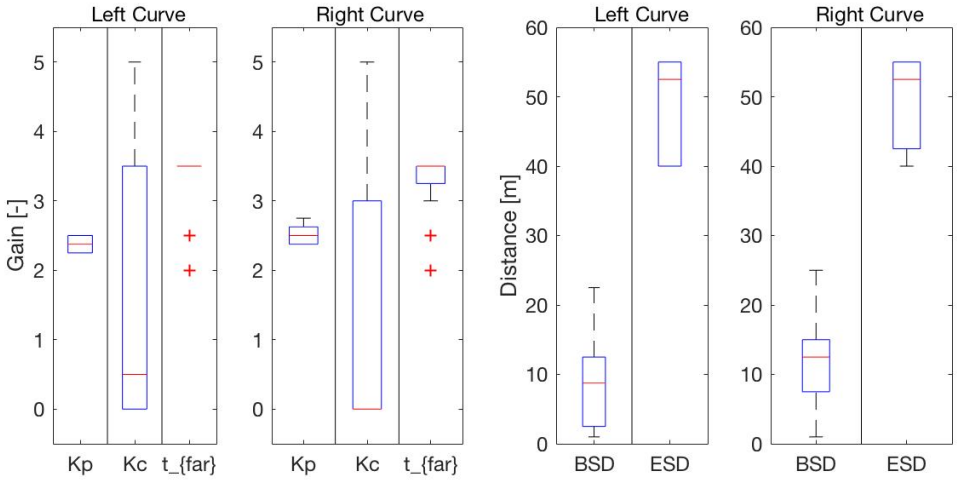

Figure C.11: Identified Parameters for the five parameters in the driver-model for all 16 subjects.

C.5. Performance

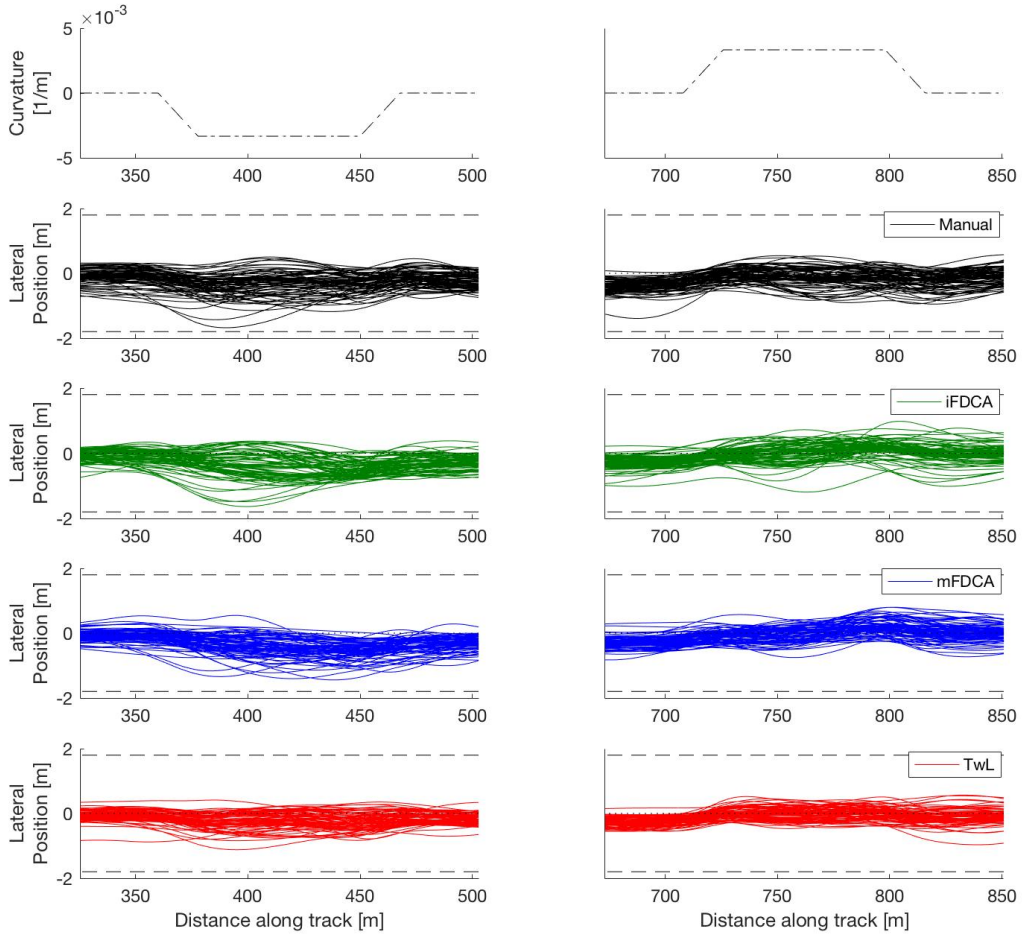

Figure C.12: Drivers lateral positions in the curves for the five curve repetitions of the 16 subjects, resulting in 80 trajectories per curve. The results are visualized separately for the four different conditions.

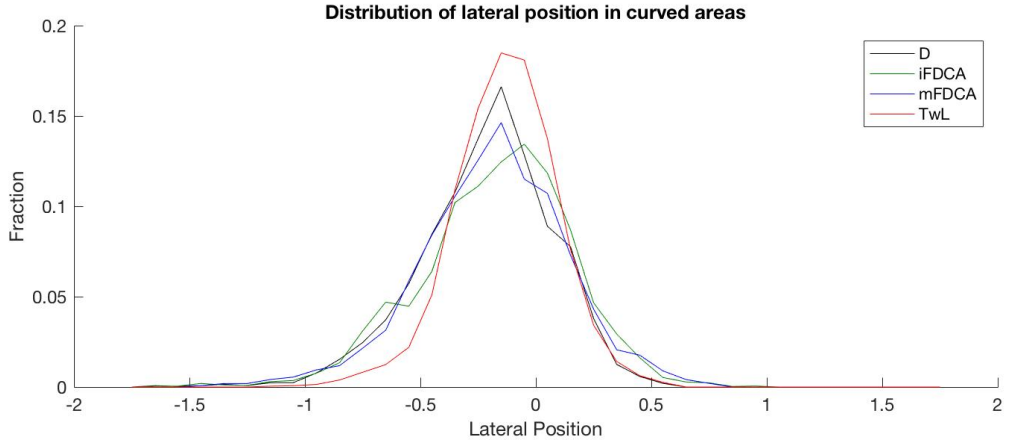

Figure C.13: Distribution of lateral position in the curved sections for the four conditions, averaged over all subjects. With TwL drivers stayed closer to the lane center compared with the other conditions.

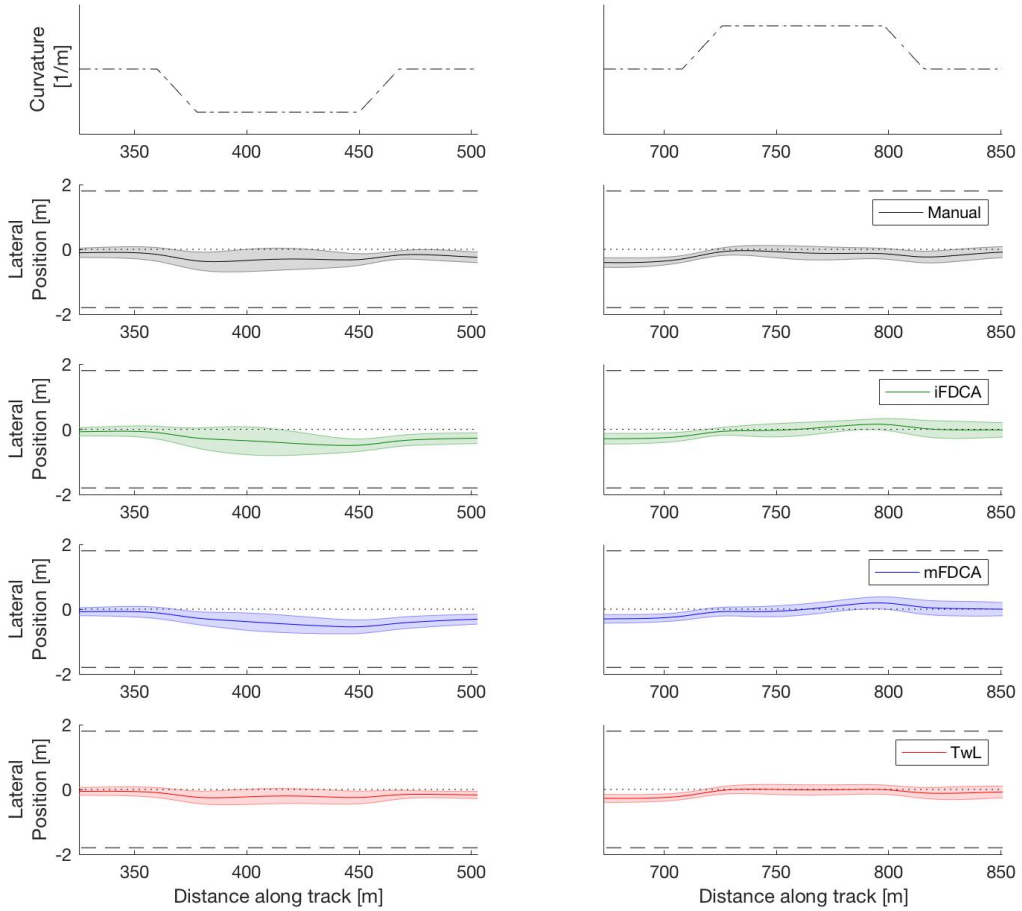

Figure C.14: Drivers lateral positions in the curves (mean and STD between subjects). The results are visualized separately for the four different conditions.

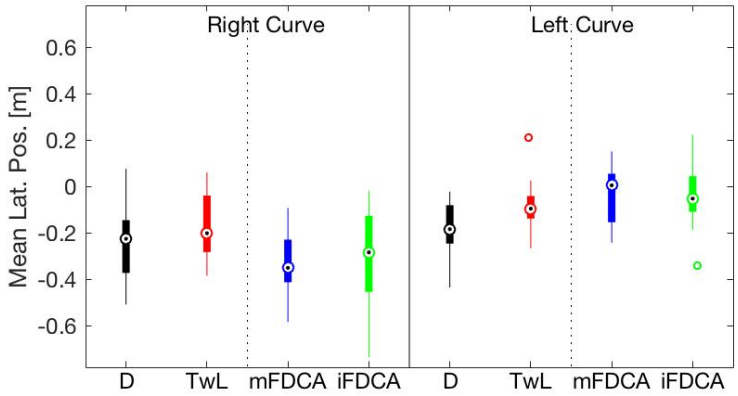

Figure C.15: Mean absolute lateral position over the distance from 35 meter to 35 meter after the curve. The results for left and right curves are visualized for the four conditions. With TwL (red), the drivers drove closer to the center-line.

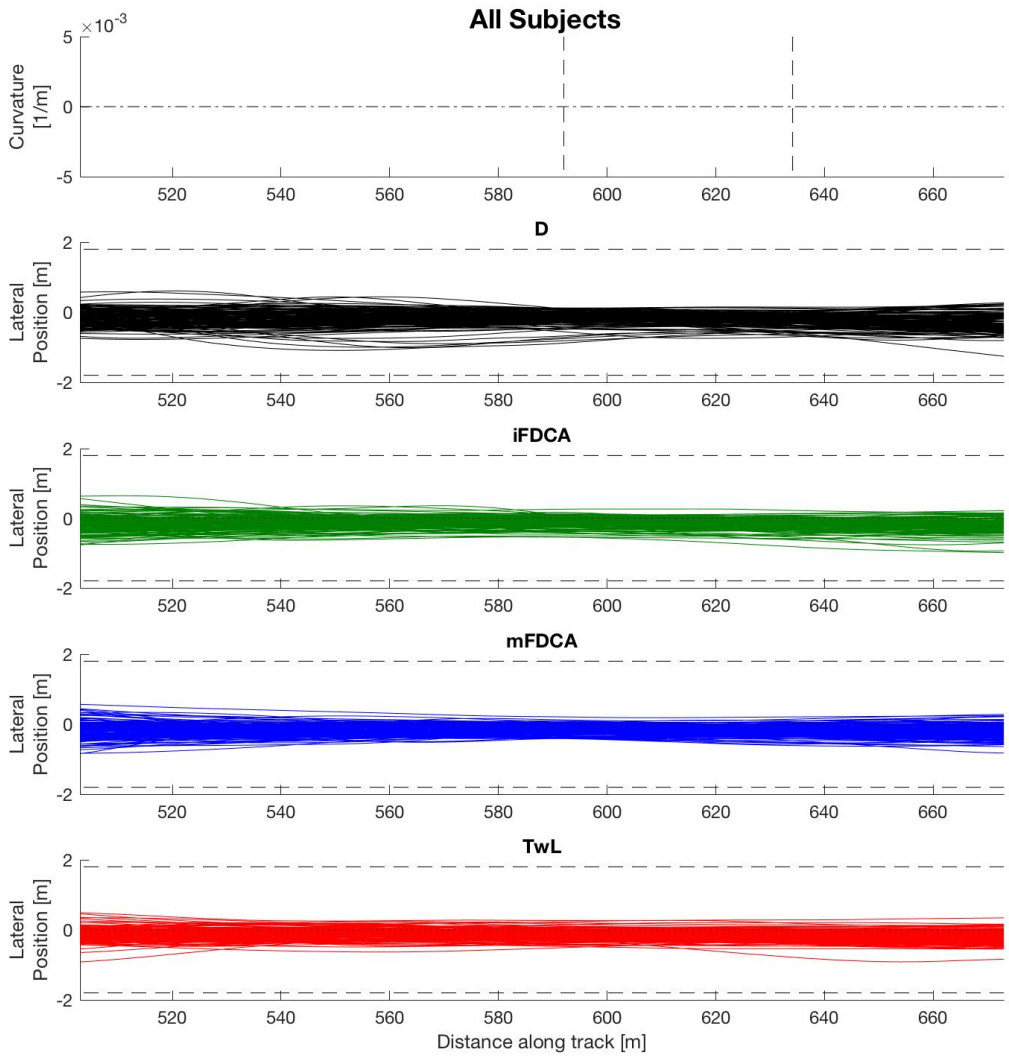

Figure C.16: Drivers lateral positions in the straight sections, visualized separately for the four conditions. Each driver drove every straight section nine times in every condition, resulting in 144 trajectories per condition.

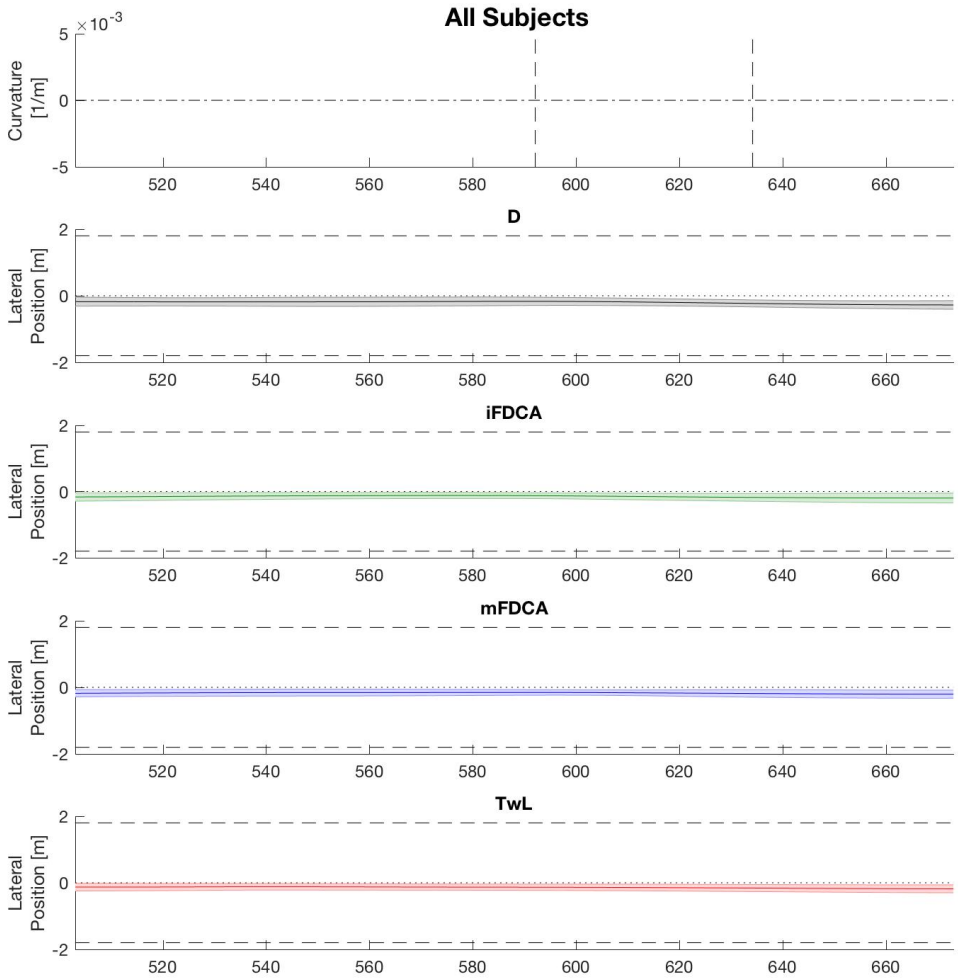

Figure C.17: Drivers lateral positions in the straight sections (mean and STD between subjects), visualized separately for the four conditions. In the top plot the location of the cones are indicated with the vertical dashed black lines.

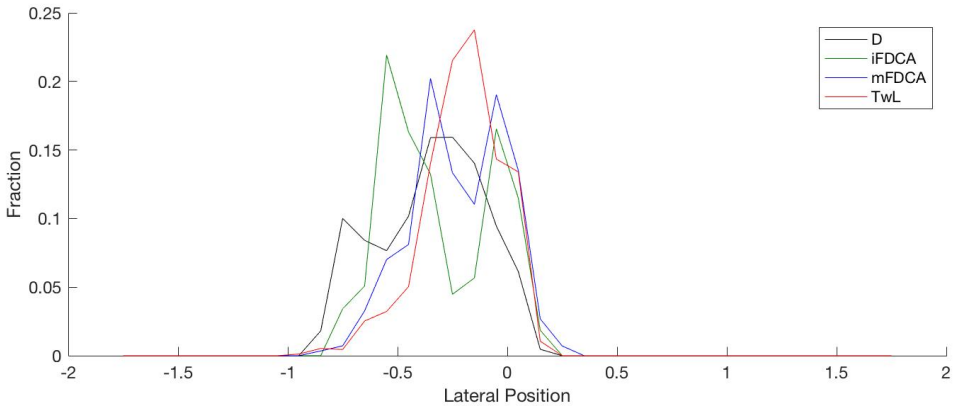

Figure C.18: Distribution of lateral position in the straight sections for the four conditions, averaged over all subjects. In the TwL condition drivers stayed closer to the lane center compared with the other conditions.

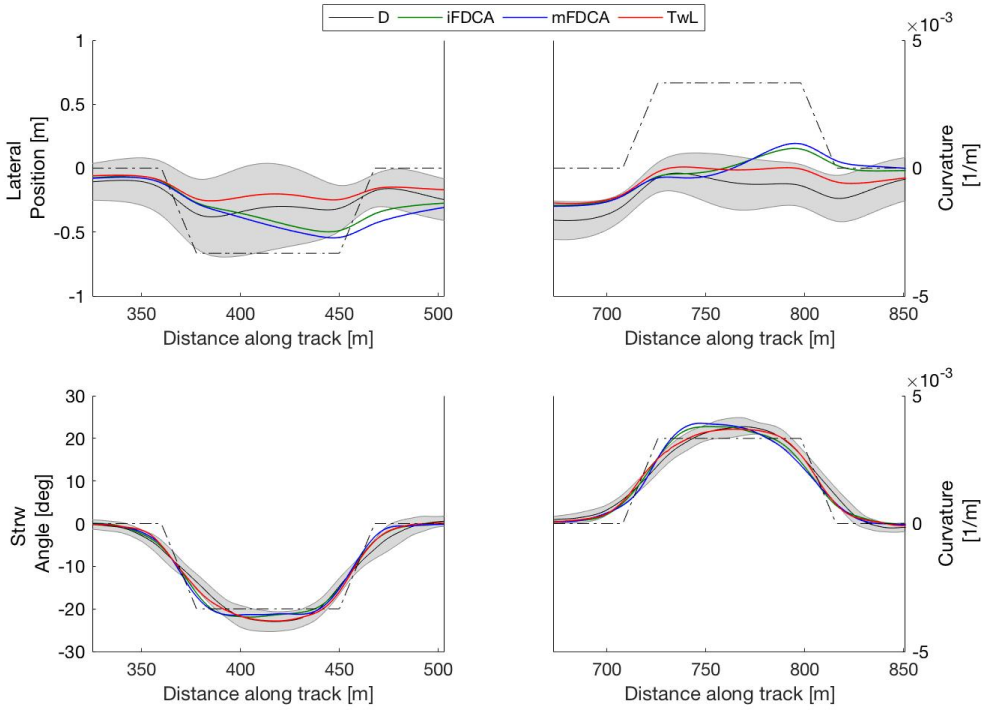

Figure C.19: *Top:* Drivers mean lateral positions in left curves (right column) and right curves (left column). *Bottom:* Mean steering wheel angles for left curves (right column) and right curves (left column). Both the mean lateral positions and mean steering wheel angles are visualized for the thee conditions with controllers; the iFDCA (green), the mFDCA (blue), and TwL (red). The grey area represent the variability of the drivers with manual control. With the FDCA controllers the behaviour is outside of the own variability of the drivers.

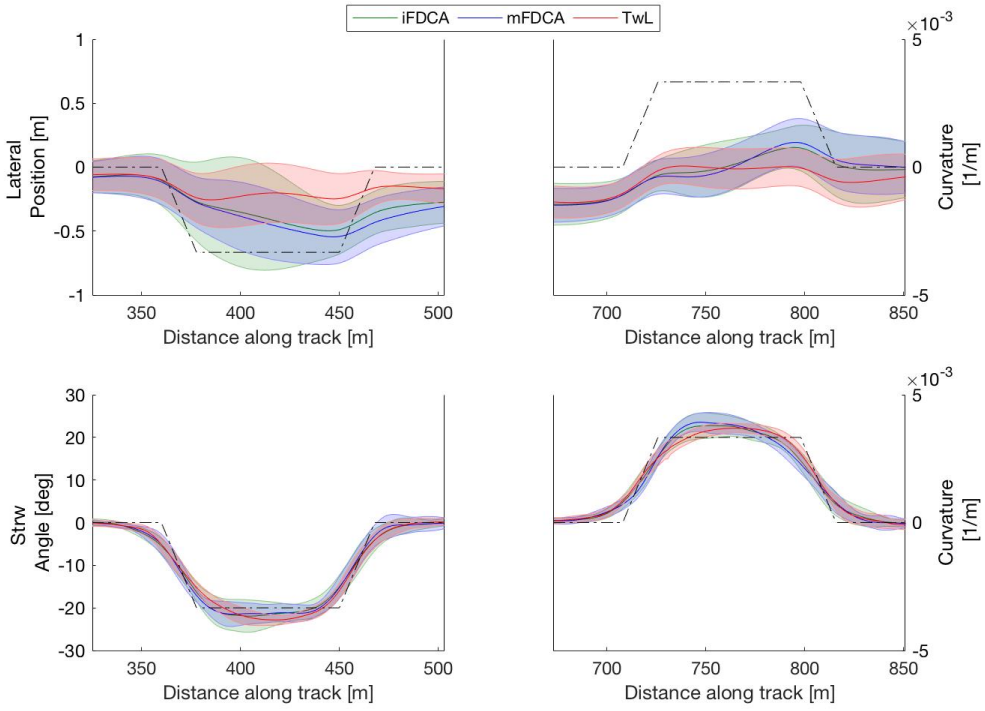

Figure C.20: *Top:* Drivers lateral positions (mean and STD between subjects) for left curves (right column) and right curves (left column). *Bottom:* Steering wheel angles (Mean and STD between subjects) for left curves (right column) and right curves (left column). Both the positions and steering wheel angles are visualized for the conditions with the three controllers; the iFDCA (green), the mFDCA (blue), and TwL (red).

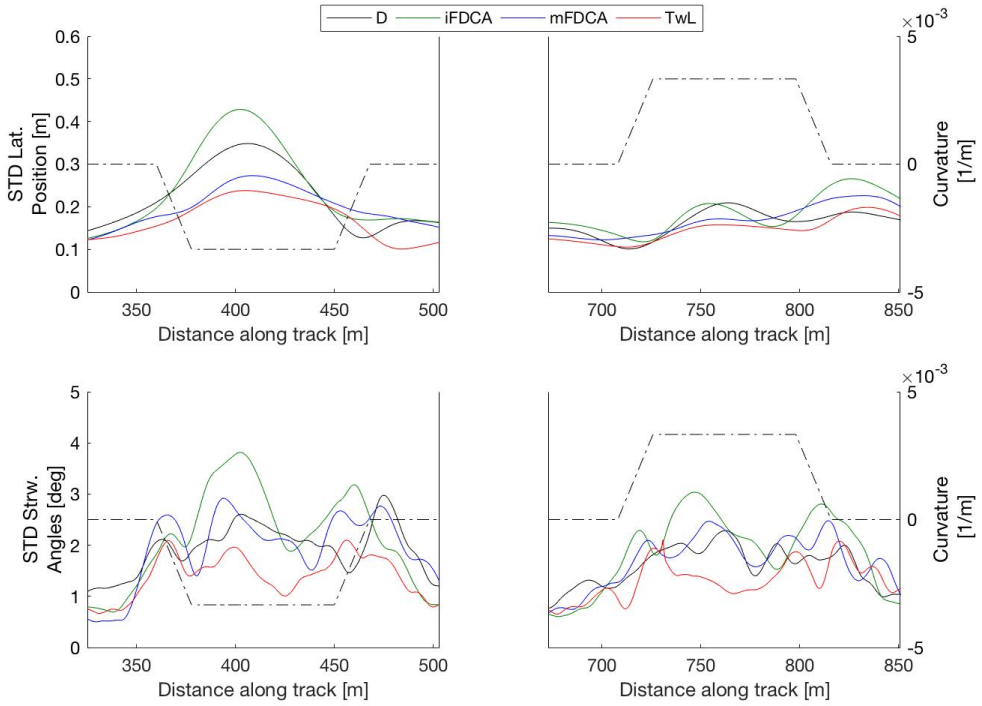

Figure C.21: *Top:* STD of the lateral positions between subjects for left curves (right column) and right curves (left column). *Bottom:* STD of steering wheel angles between subjects. For both the positions and angles the STD for the iFDCA condition is bigger than the mFDCA and TwL conditions, indicating that drivers drover more different with iFDCA, where the behaviour was more alike for the average tuned controllers (mFDCA and TwL).

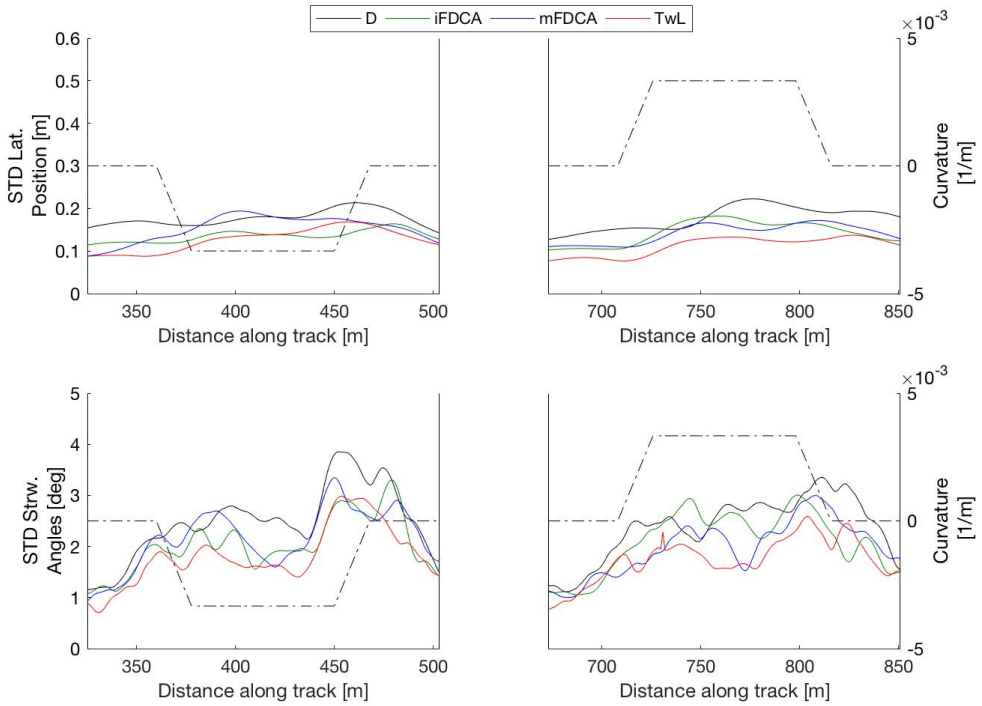

Figure C.22: *Top:* STD within subjects for the lateral position for left curves (right column) and right curves (left column). *Bottom:* STD within subjects for the steering wheel angles. The STD within subjects indicate the variability of drivers within their own driving behaviour.

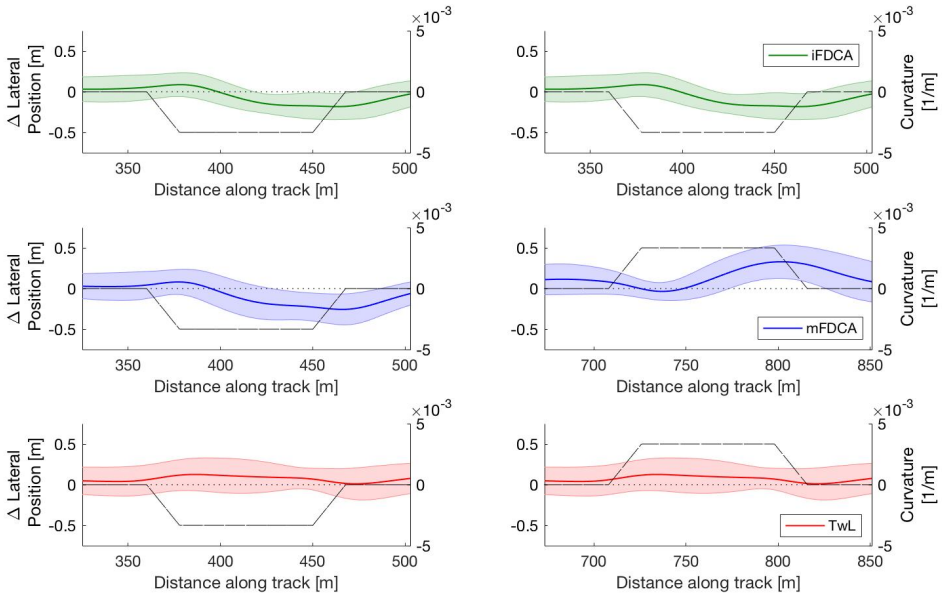

Figure C.23: Lateral Distance (mean and STD between subjects) between the trajectory driven with manual control and the trajectories driven when guided with the three HSC systems. For the TwL condition the error is positive, indicating that the drivers was located more to the center when they were guided. The plots for the FDCA conditions show that the error is negative, thus drivers cut the curve more, particularly at the end of the curve. Also the error in the initial position is positive, since drivers approach the curve more from the center-line when they were guided with the controllers.

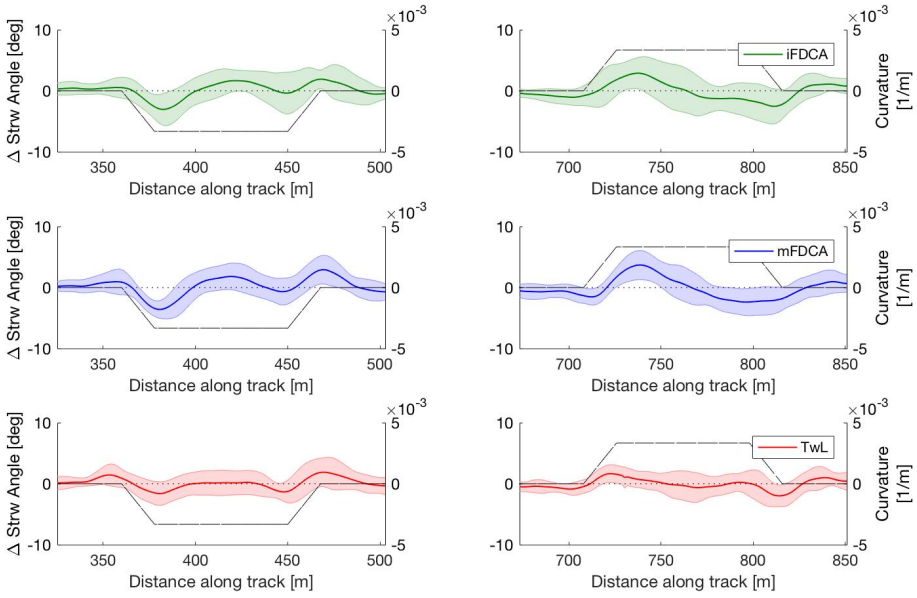

Figure C.24: Error in steering wheel angles (mean and STD between subjects) between the manual trajectory and the trajectories with the three guidance systems. A negative error in the right curves means a larger steering wheel angle in the guided condition. A negative error in the left curves means a smaller steering wheel angle in the guided condition. The plots for the FDCA conditions show slightly larger errors for the mFDCA condition. For the TwL condition the error in steering wheel angle is the lowest, however comparing with the conflict plots indicate that the drivers had to apply a high torques to make sure that these angles were reached.

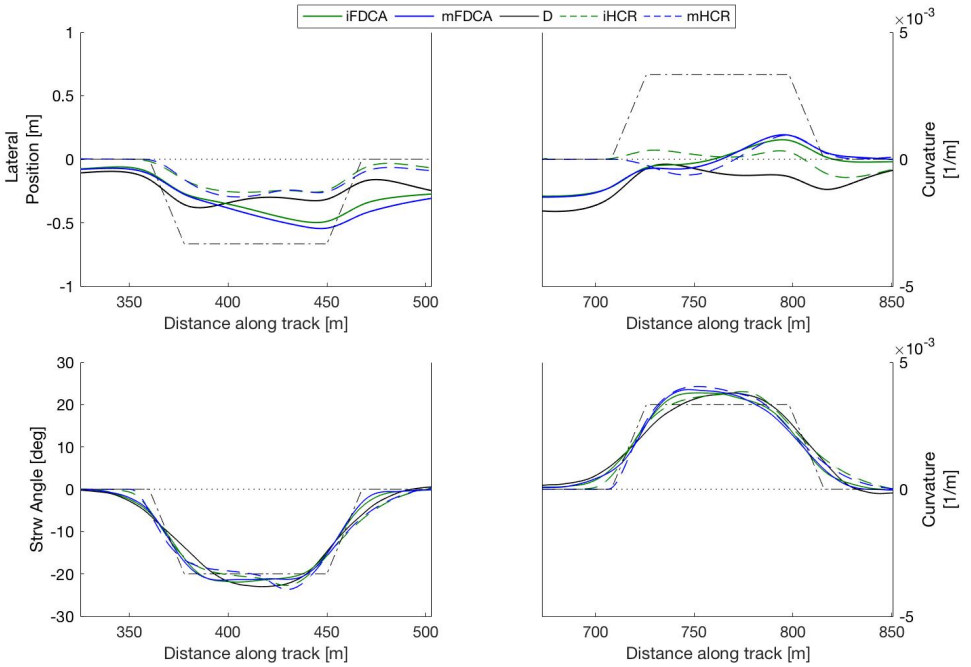

Figure C.25: Results for the individual HCR (dashed green line), mHCR (dashed blue line), the drivers behaviour when supported with iFDCA (green line), and supported with mFDCA (blue line), and with manual control (black line). The top plots show the lateral positions and the bottoms plots the steering wheel angles. Drivers did cut the curve a lot more than the HCR's for both FDCA conditions. The manual behaviour in the left curves does not match the HCR anymore, indicating that drivers changed their manual behaviour between the first and second experiment day. Both HCR's start steering later than the drivers, resulting in a discrepancy in steering wheel angles later in the curve.

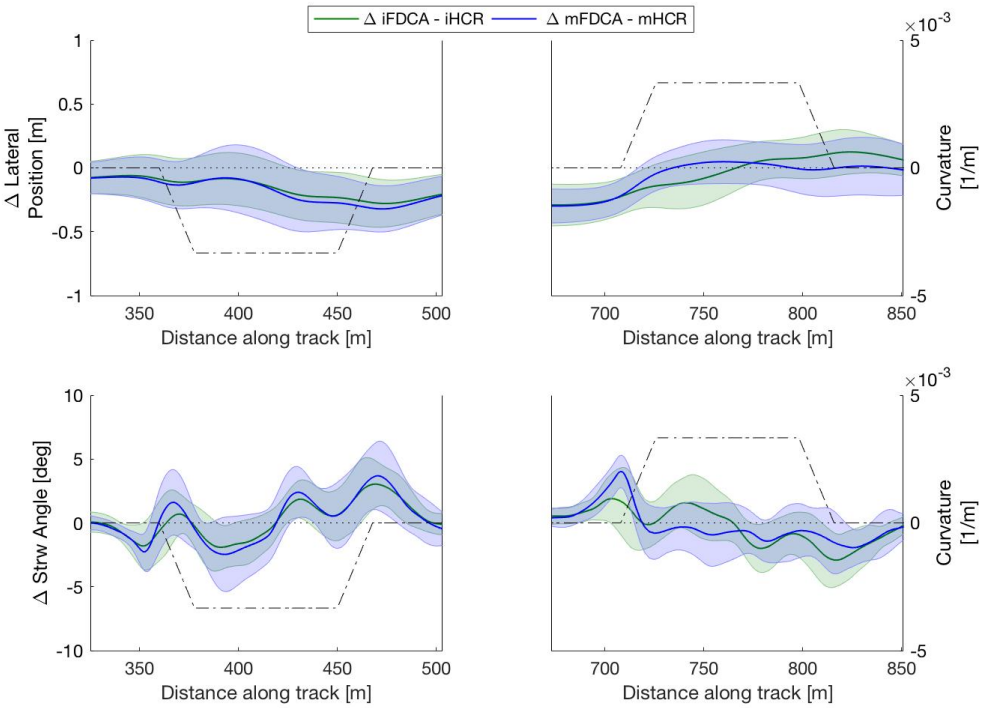

Figure C.26: Error in behaviour (mean and STD between subjects) between iHCR (green) and mHCR (blue) and the drivers behaviour when supported with corresponding FDCA system. The top plots show the lateral positions and the bottoms plots the steering wheel angles. The errors in the behaviour give an indication how close the drivers followed the intentions of the model. On average drivers followed the intention of both systems, although the peaks in the right curve seem higher for the steering wheel error. In the left curves the same peak in the beginning of the curve is seen as in the plot for the HCR match (figure C.10).

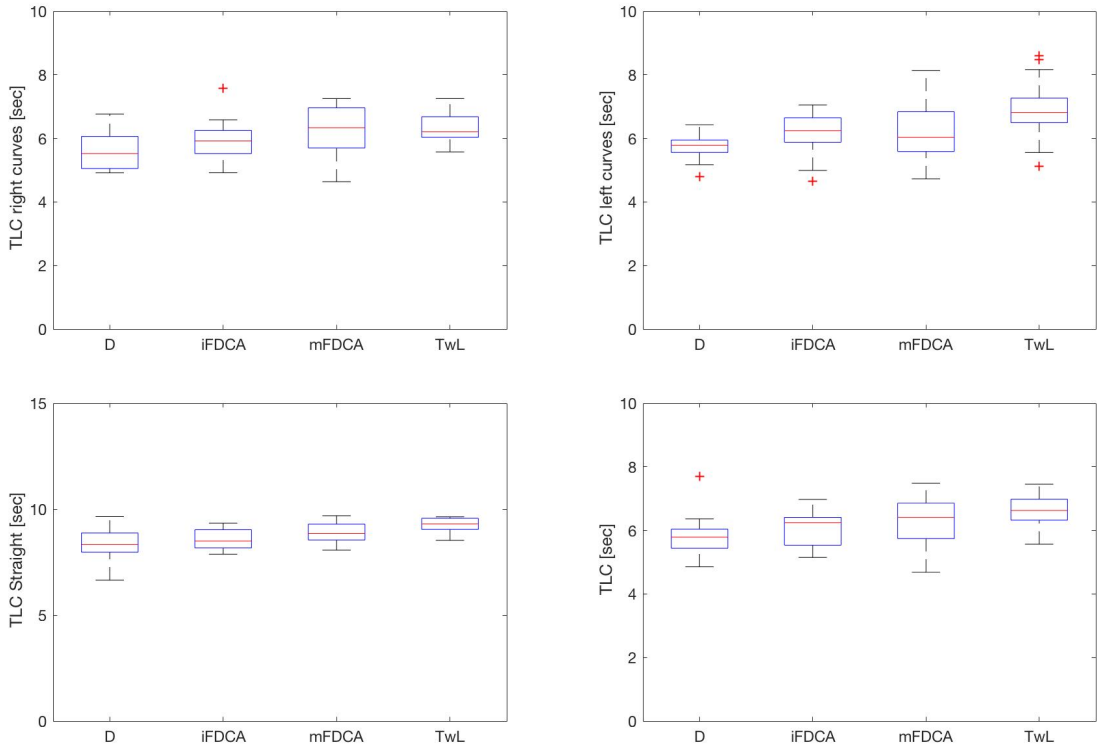

Figure C.27: *Top Left:* TLC over the in the right curves. *Top Right:* TLC in the left curves. *Bottom Left:* TLC in the straight parts. *Bottom Right:* TLC over the whole road. *All:* The ANOVA showed that the mean TLC in the curves is significantly different between the conditions. It does slightly increase for all guided conditions compared to manual (D) control, the pairwise comparison showed that it is significant between the D and TwL condition ($p = 0.014$) and between the iFDCA and TwL condition ($p = 0.019$).

C.6. Acceptance

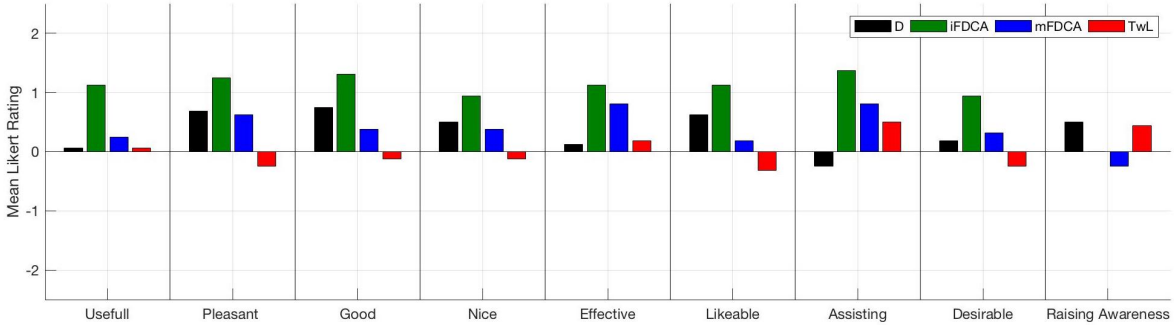

Figure C.28: The results of all nine questions in the questionnaire from Van Der Laan, averaged over all 16 participants. The rating for the iFDCA system is higher for all questions except for raising awareness. The rating for the TwL system is lowest for all questions except for raising awareness. Clear differences are also seen between the iFDCA and the mFDCA.

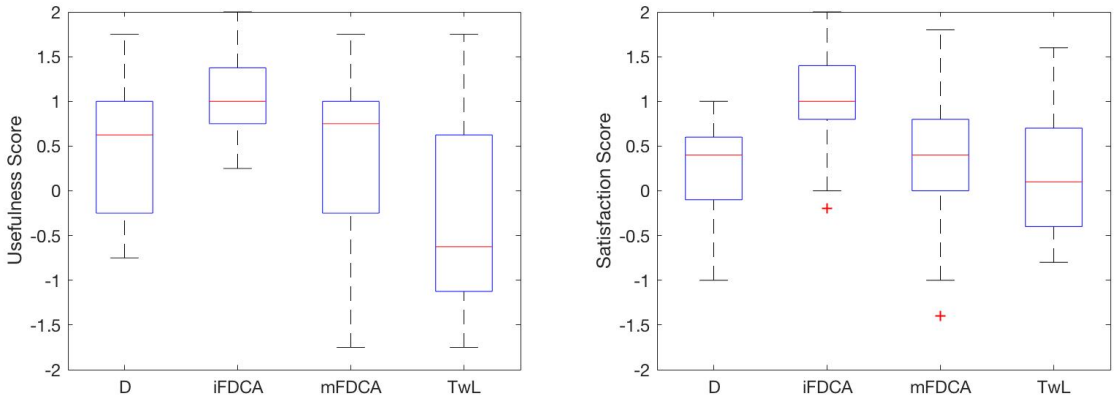

Figure C.29: *Left:* The pairwise comparison for the Usefulness Score showed that iFDCA is significantly higher compared to TwL ($p = 0.01$) and manual ($p = 0.018$), but only slightly higher compared to mFDCA ($p = 0.12$) *Right:* The pairwise comparison for the Satisfaction Score showed that the results for iFDCA are significantly higher than D and TwL ($p < 0.01, p = 0.03$), but not significantly higher than mFDCA ($p = 0.3$).

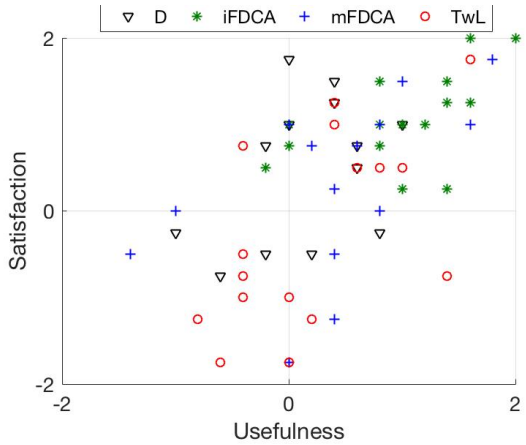

Figure C.30: Usefulness Score and Satisfaction Score for all 16 subjects. The iFDCA rates (green) are mainly in the upper right corner, where the TwL (red) are more located in the bottom left corner. One participant had high scores for the TwL condition, the participant mentioned that he liked that the steering wheel felt stiffer and thereby more like his own car.

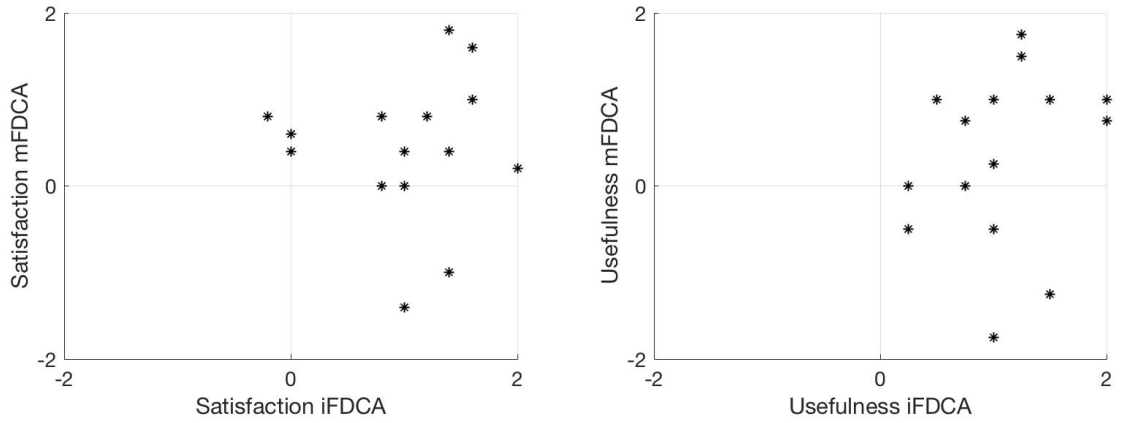

Figure C.31: *Left:* The usefulness for the iFDCA and mFDCA separately for each subject. *Right:* The satisfaction for the iFDCA and mFDCA separately for each subject.

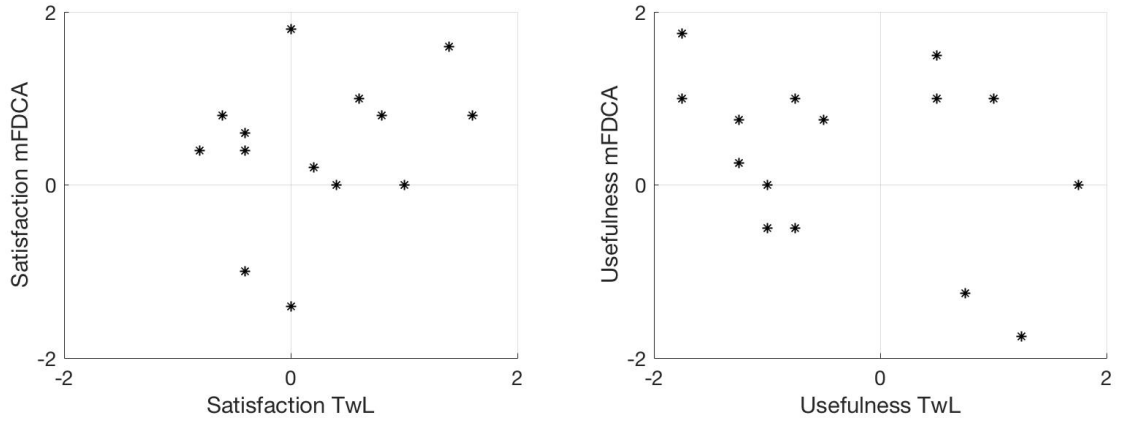

Figure C.32: *Left:* The usefulness for the TwL and mFDCA separately for each subject. *Right:* The satisfaction for the TwL and mFDCA separately for each subject.

C.7. Workload

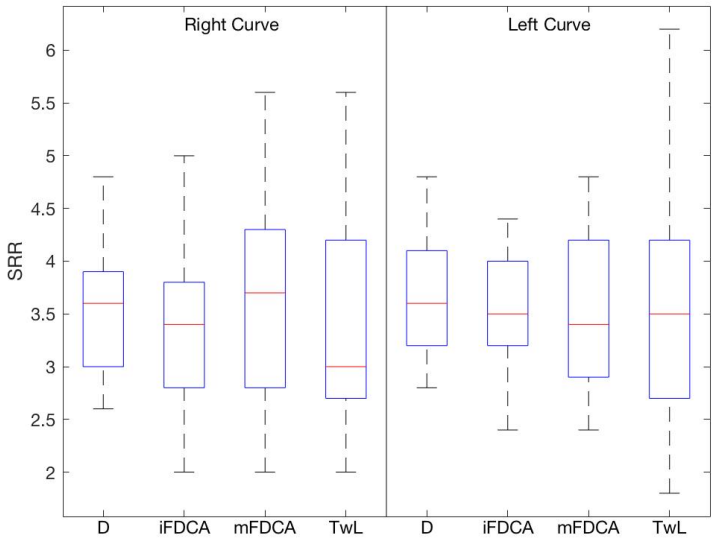

Figure C.33: Average Steering Reversal Rate (SRR) for the right and left curves. The SRR over the whole trajectory showed a slight decrease for the iFDCA and TwL controllers compared with the manual condition. The mFDCA controller shows a minimal increase, but none of these differences were significant. Also between left and right curves no significant differences were found.

C.8. Torques

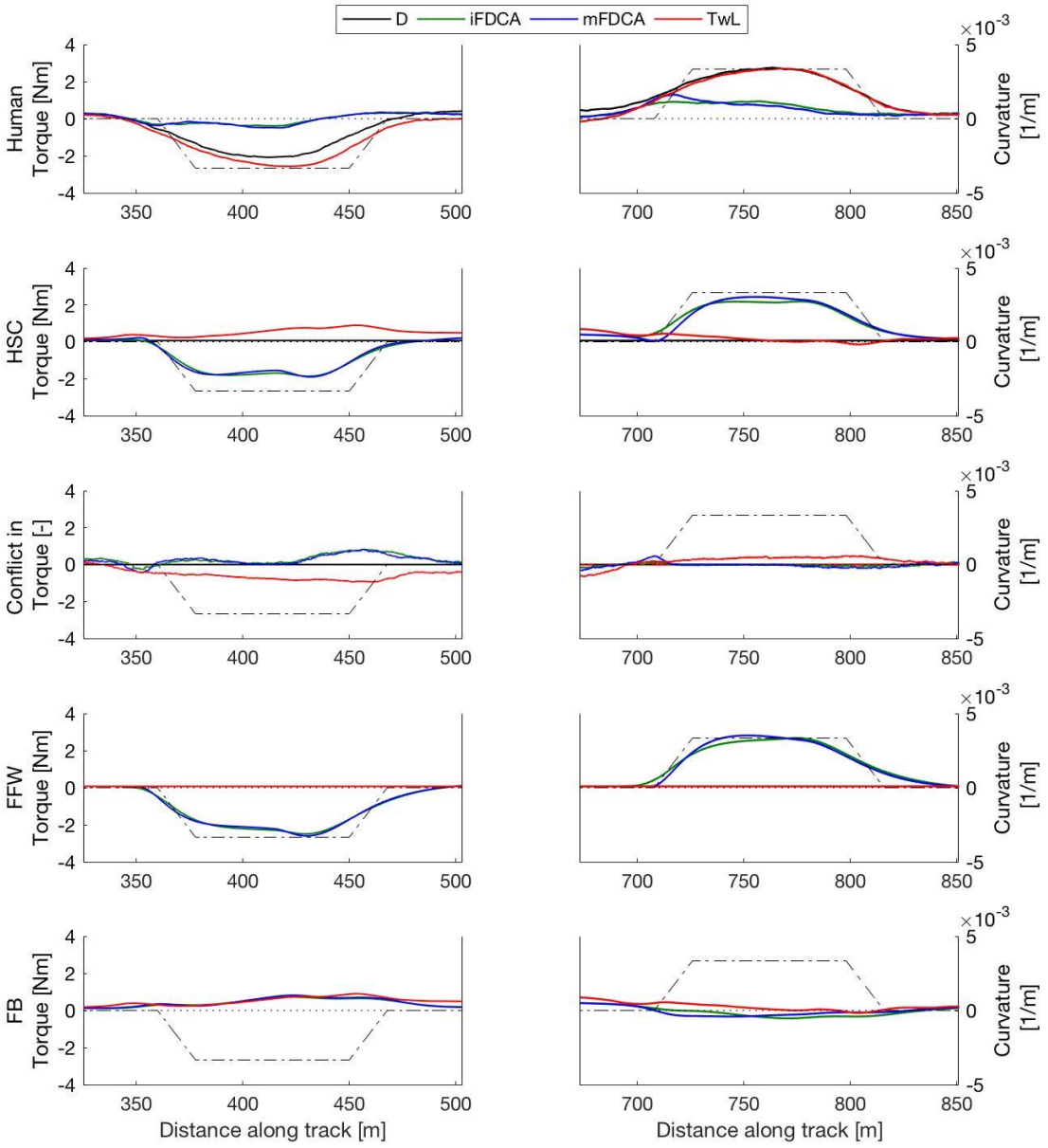

Figure C.34: Torques (mean over all 16 subjects) applied by the driver (first row) and HSC system (second row) on the steering wheel over the length of the curves for manual (black), iFDCA (green), mFDCA (blue) and TwL (red). The third row shows the conflicts occurrence between the HSC torque and driver torque. The fourth and fifth row show the HSC torque separated in the feed-forward and feedback component respectively. All results are visualized for right curves (left columns) and left curves (right columns).

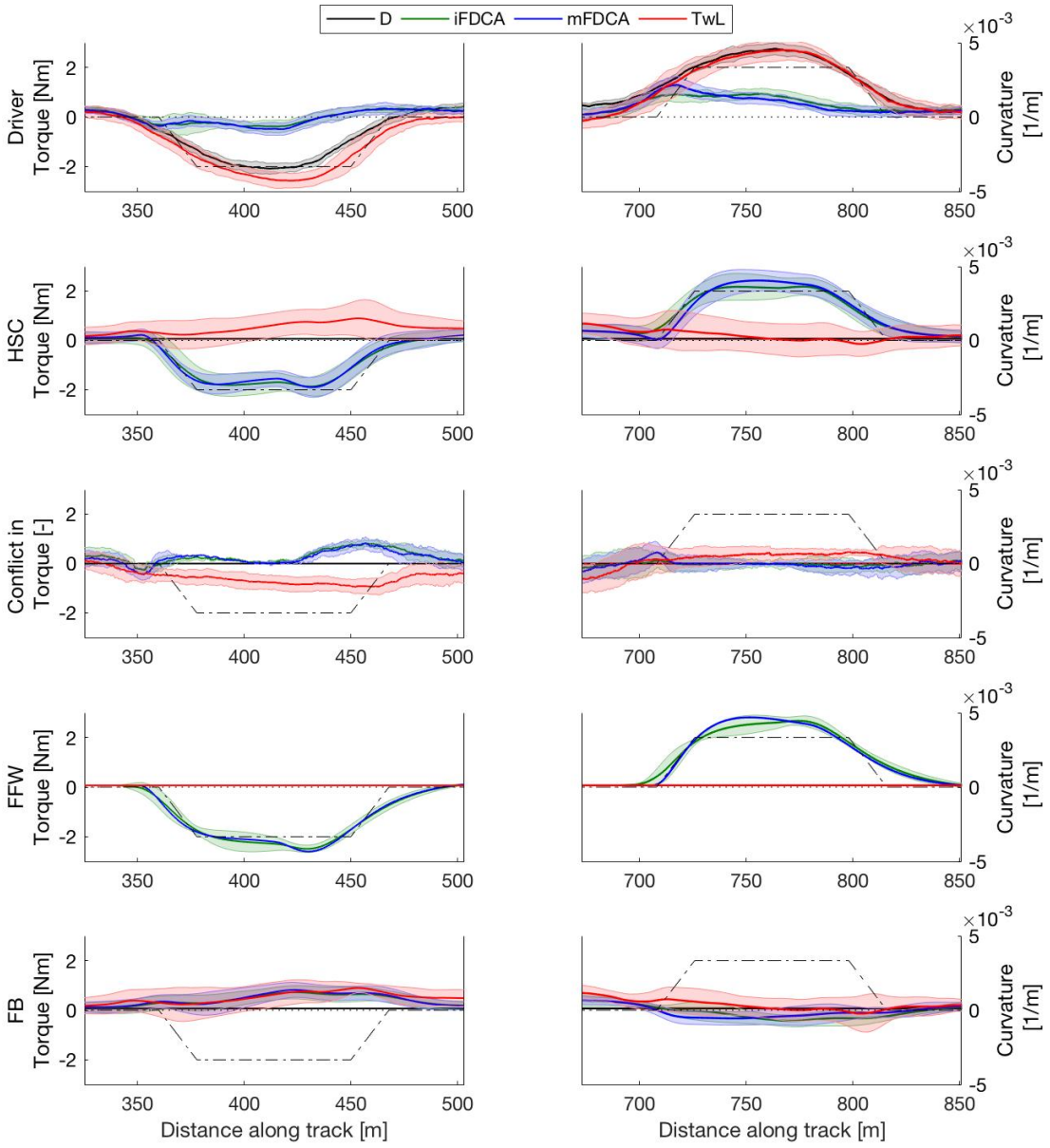

Figure C.35: Torques (mean and STD between 16 subjects) applied by the driver (first row) and HSC system (second row) on the steering wheel over the length of the curves for manual (black), iFDCA (green), mFDCA (blue) and TwL (red). The third row shows the conflicts occurrence between the HSC torque and driver torque. The fourth and fifth row show the HSC torque separated in the feed-forward and feedback component respectively. All results are visualized for right curves (left columns) and left curves (right columns).

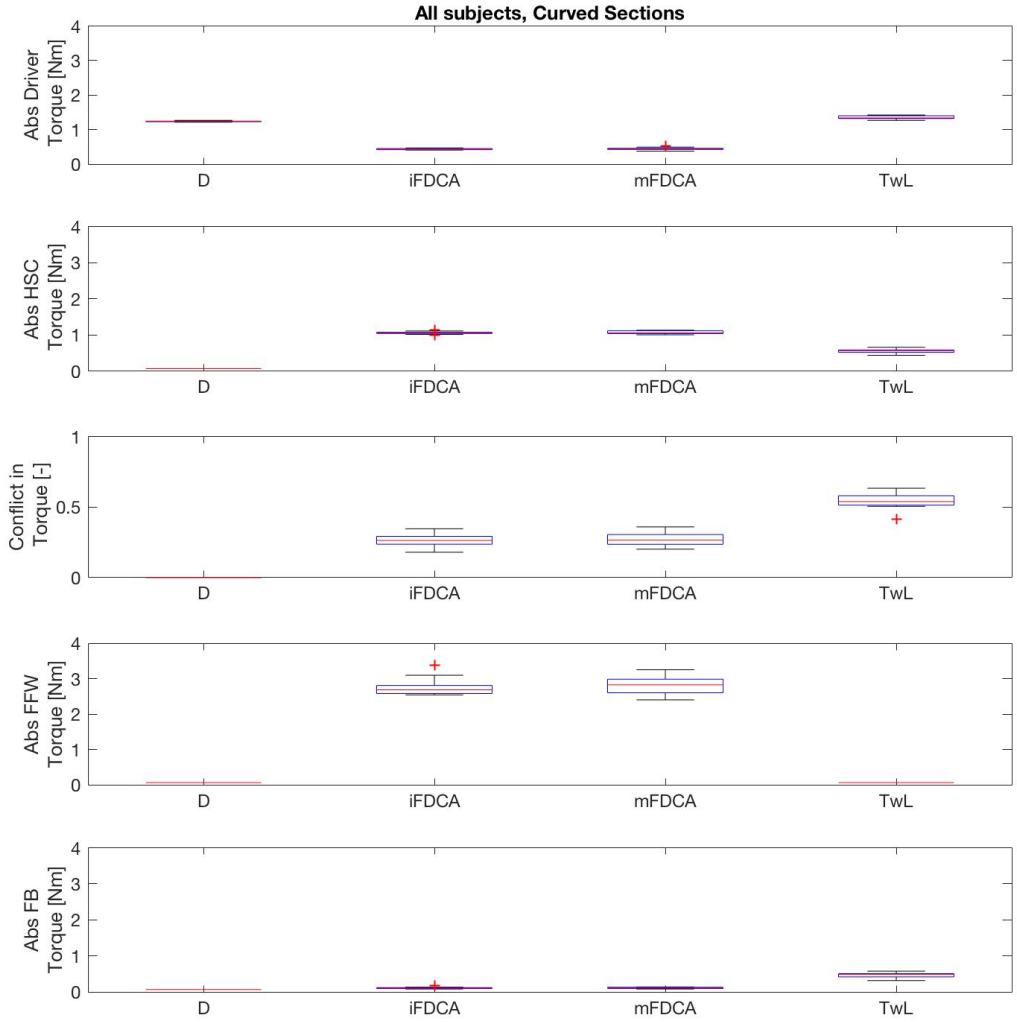

Figure C.36: Boxplot of the torques applied by the driver (first row) and HSC system (second row) on the steering wheel for the four conditions. The third row shows the conflicts occurrence between the HSC torques and driver torque. The fourth and fifth row show the HSC torque separated in the feed-forward and feedback component respectively.

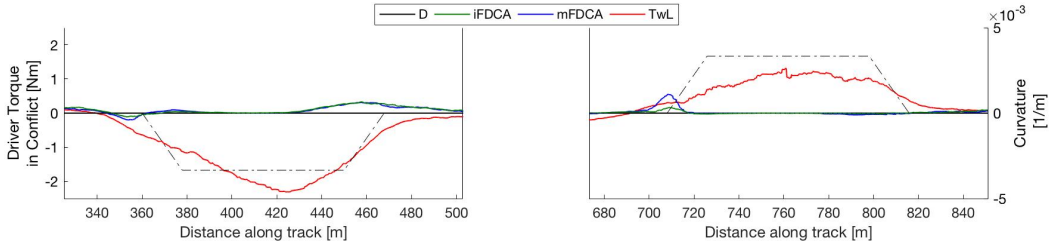

Figure C.37: The driver torque when the driver is opposing the HSC torque (mean and STD between subjects). For TwL (red) the torques are a lot higher, since TwL does not provide support forces.

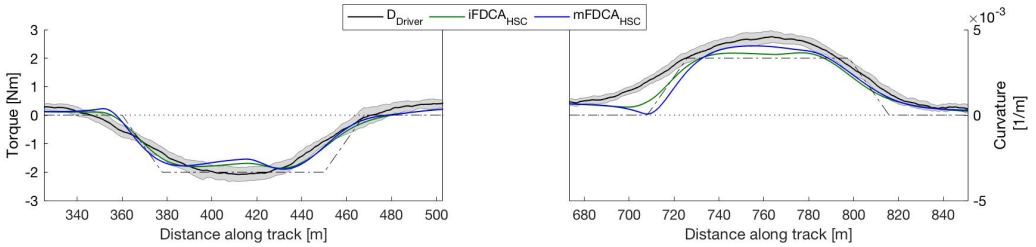

Figure C.38: The results for the mean HSC torque over all subjects in the iFDCA (green) and mFDCA (blue) condition and the driver torque in the manual condition (black). In the right curves (left column) the HSC torque exceeds the driver torque in the beginning of the curve.

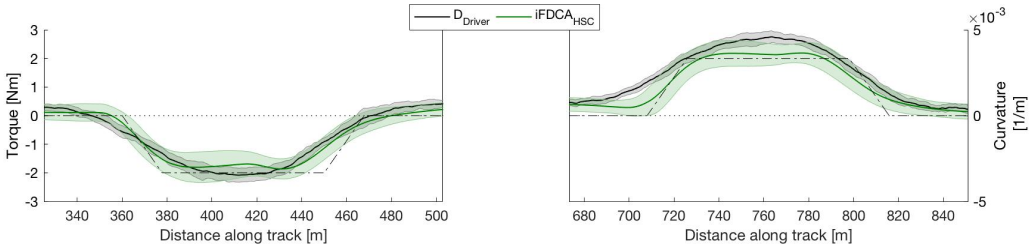

Figure C.39: The results for the HSC torque over all subjects in the iFDCA condition (mean and STD in green) and the driver torque in the manual condition (black).

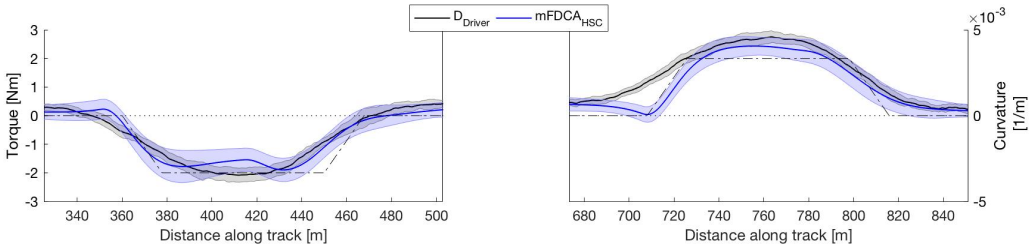

Figure C.40: The results for the HSC torque over all subjects in the mFDCA condition (mean and STD in blue) and the driver torque in the manual condition (black).

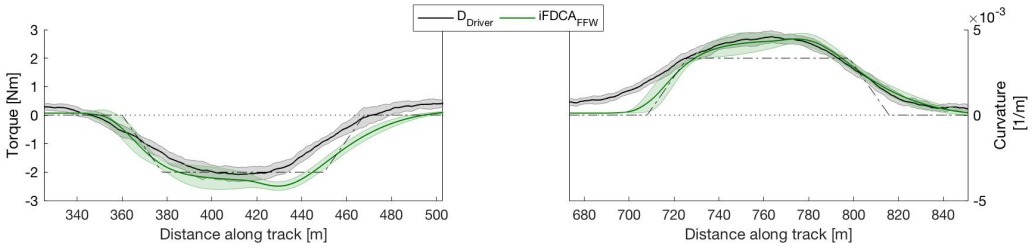

Figure C.41: The results for the feed-forward component of the HSC torque over all subjects in the iFDCA condition (green) and the driver torque in the manual condition (black).

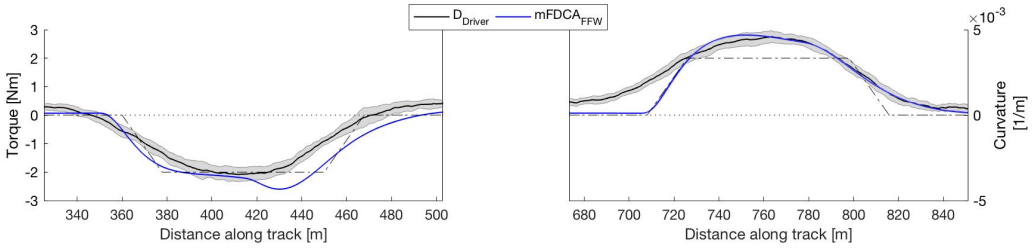

Figure C.42: The results for the feed-forward component of the HSC torque over all subjects in the mFDCA condition (blue) and the driver torque in the manual condition (black).

C.9. Additional Analyses: Subjective vs. Objective measures

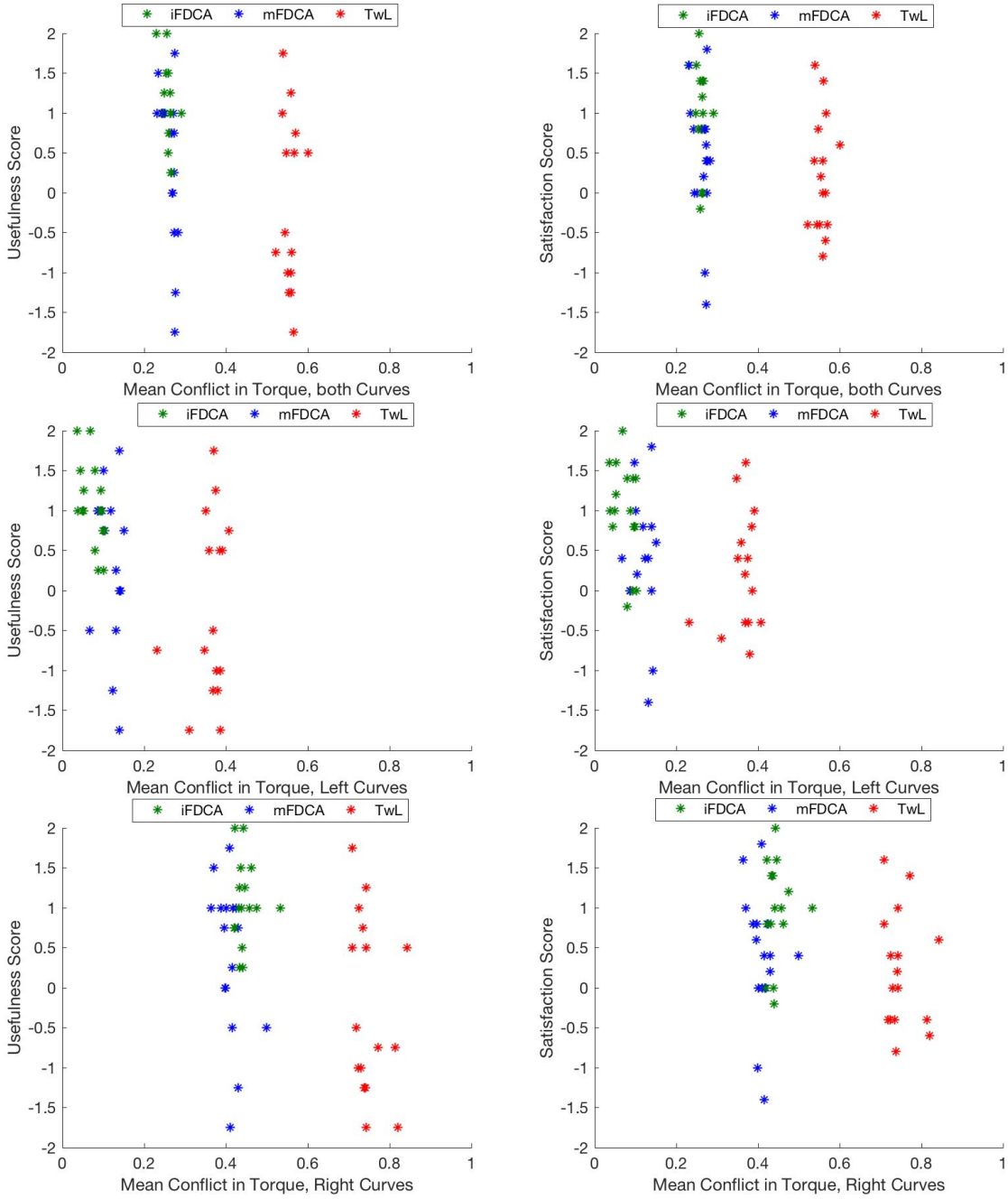

Figure C.43: The mean occurrence of conflicts with the iFDCA(green), mFDCA (blue) and TwL (red) vs. the usefulness score (left) and the satisfaction score (right) per subject.

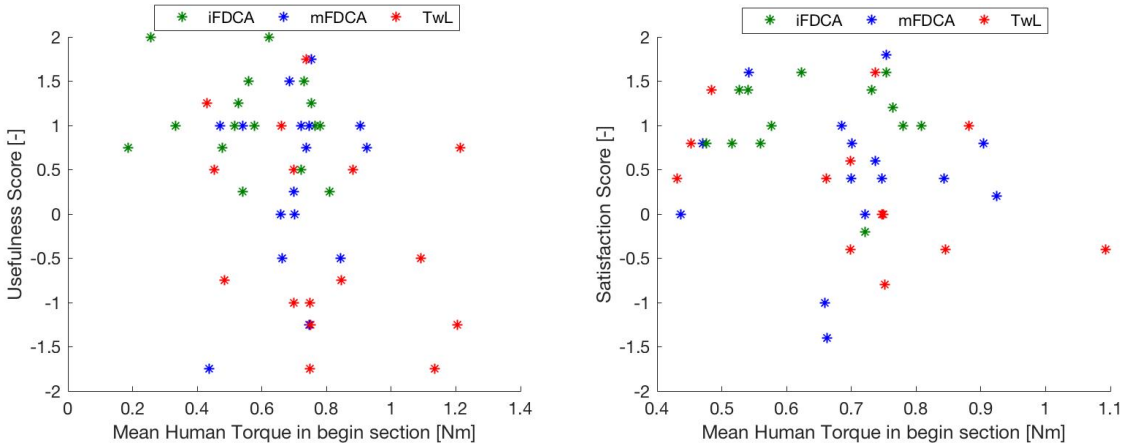

Figure C.44: The mean human torque in the first section per subject when supported with the iFDCA(green), mFDCA (blue) and TwL (red) vs. the usefulness score (left) and the satisfaction score (right) of that subject with the systems.

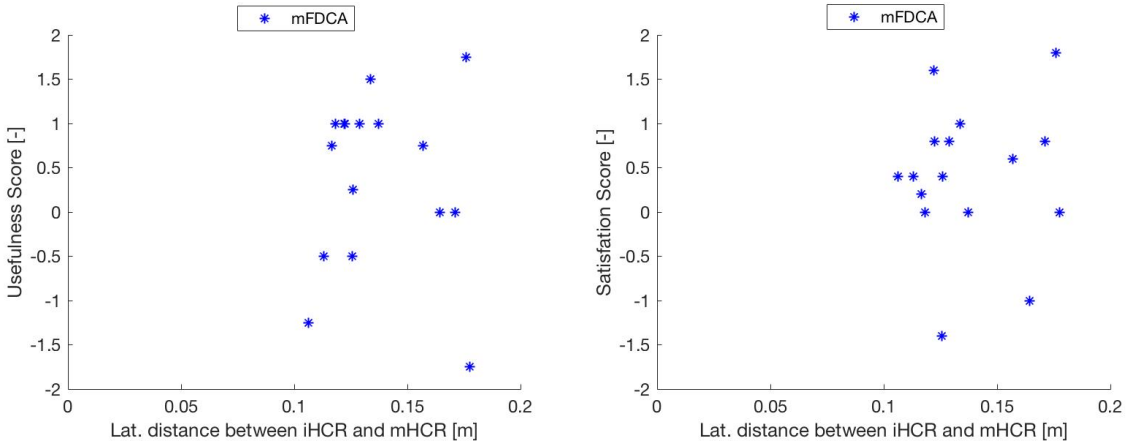

Figure C.45: The lateral distance between the iHCR and mHCR indicate how close both HCR were to each other. The plot does not indicate that drivers liked the system more when the error was small, which is contradicting the expectations.

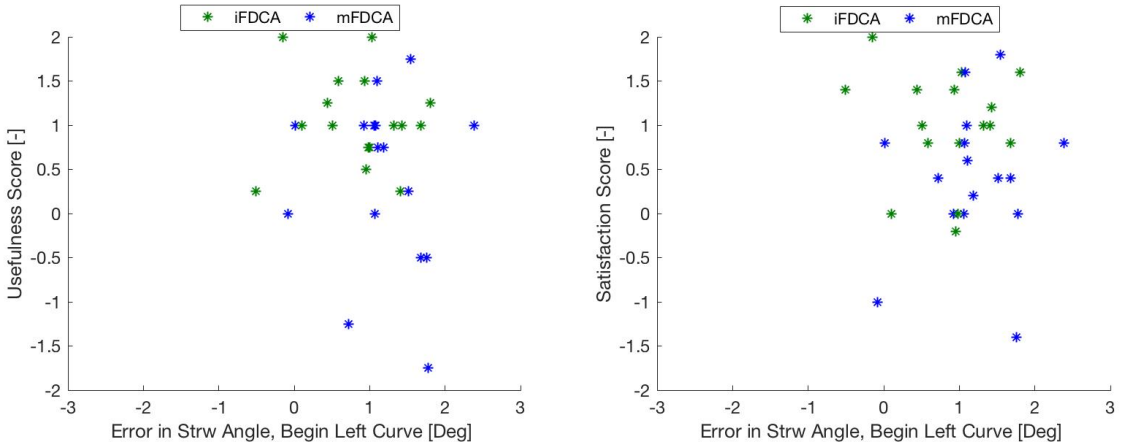

Figure C.46: Error in steering wheel angle in the beginning of the left curves versus the Satisfaction and usefulness score. The error is averaged over the lateral positions between 673.2 meter and 732.2 meter along the road. It was hypothesized that a higher error would result in lower usefulness and satisfaction.

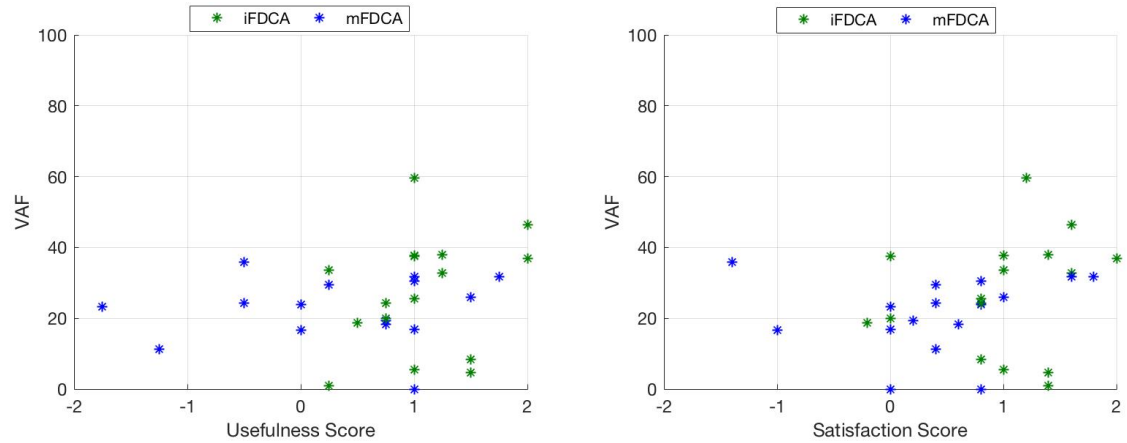

Figure C.47: The VAF for each subject for the iHCR and mHCR and the corresponding Usefulness Score and Satisfaction Score when supported with the corresponding systems. It was expected that a higher VAF would lead to higher ratings, this is not clearly visible in the results.

C.10. Individual Results

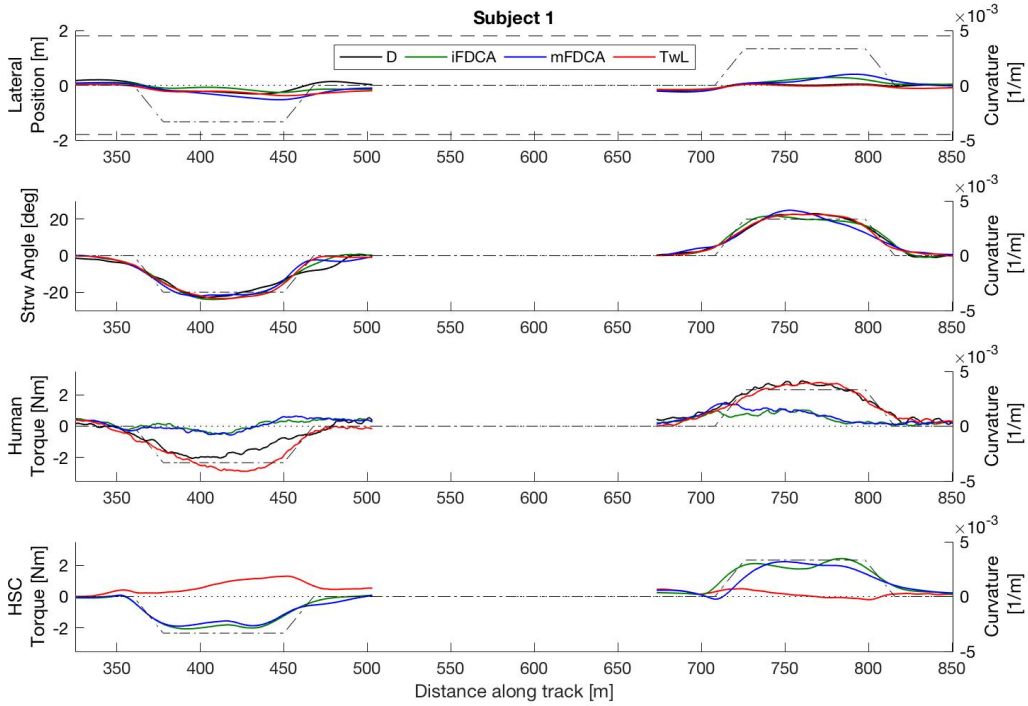

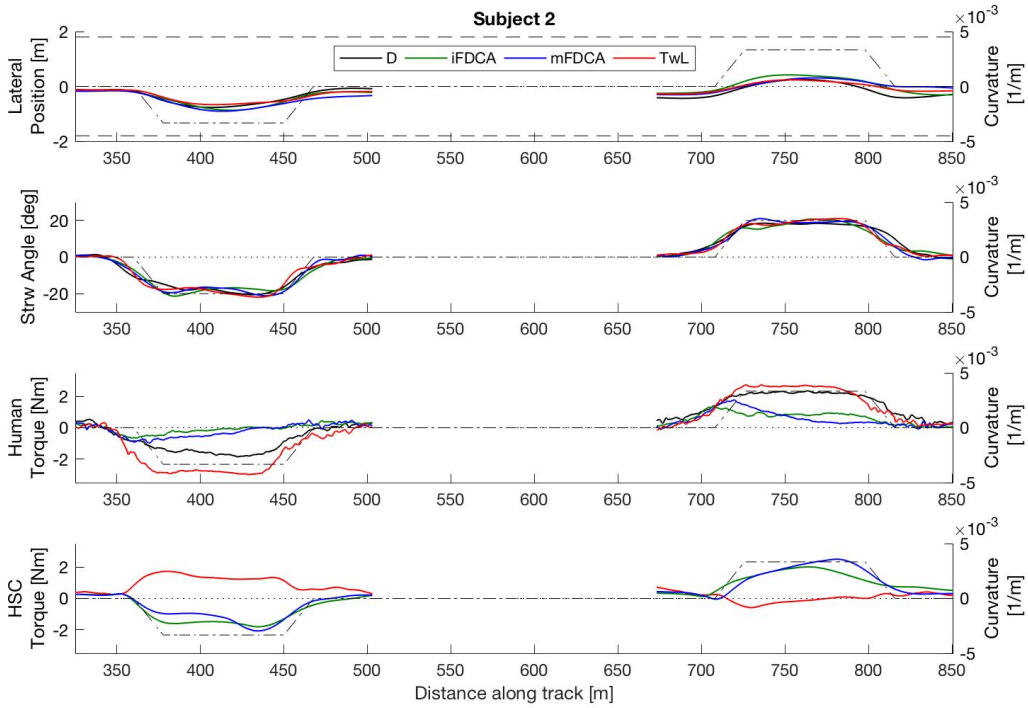

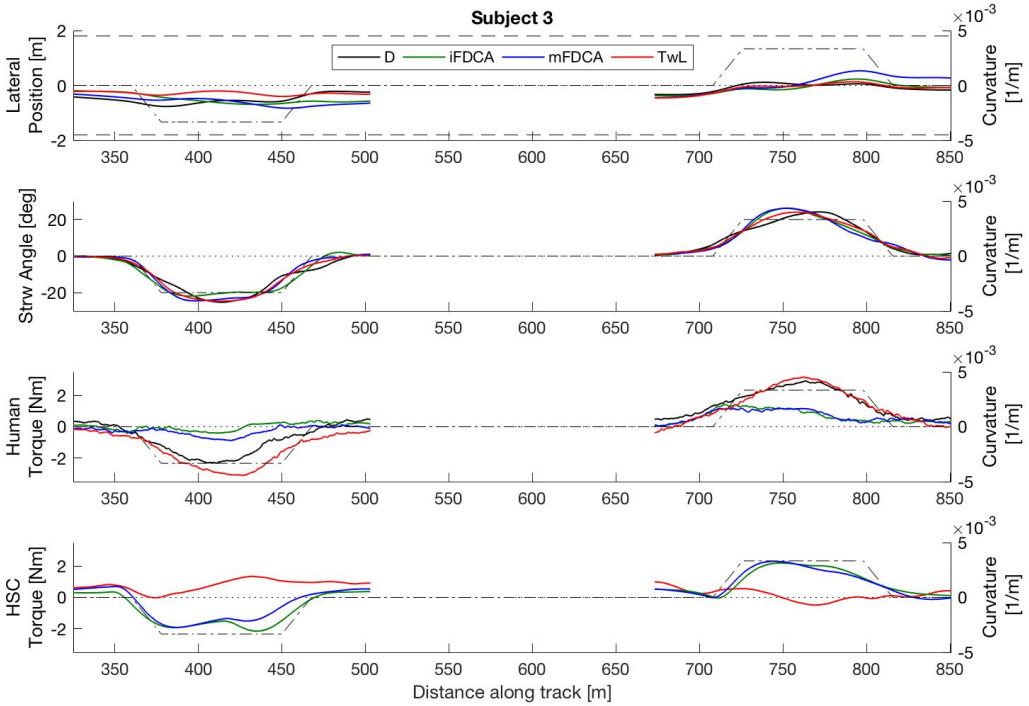
Subject 3
D
iFDCA
mFDCA
TwL
Lateral Position [m]
Strw Angle [deg]
Human Torque [Nm]
HSC Torque [Nm]
Curvature [1/m]
×10^-3
Distance along track [m]

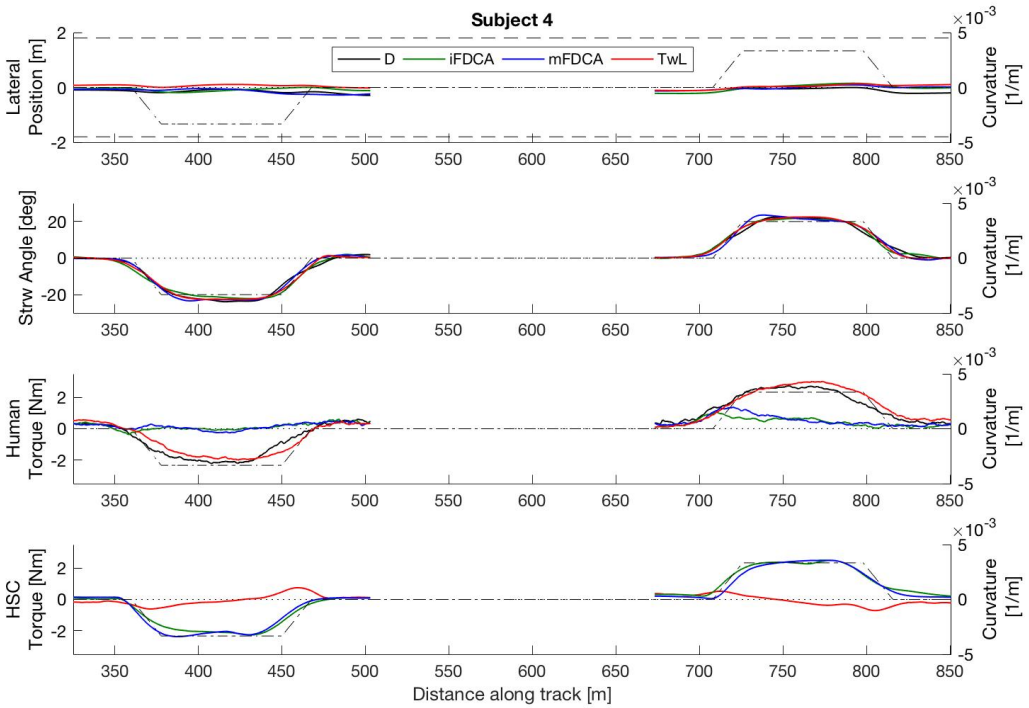
Subject 4
D
iFDCA
mFDCA
TwL
Lateral Position [m]
Strw Angle [deg]
Human Torque [Nm]
HSC Torque [Nm]
Curvature [1/m]
×10^-3
Distance along track [m]

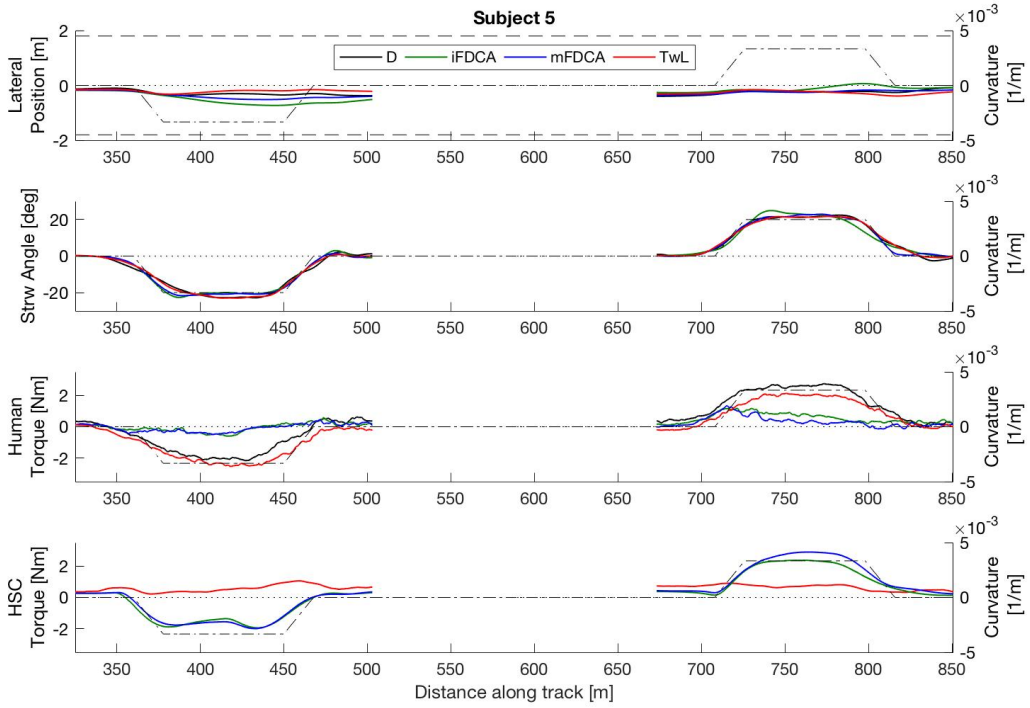
Subject 5
D
iFDCA
mFDCA
TwL
Lateral Position [m]
Strw Angle [deg]
Human Torque [Nm]
HSC Torque [Nm]
Curvature [1/m]
×10^-3
Distance along track [m]

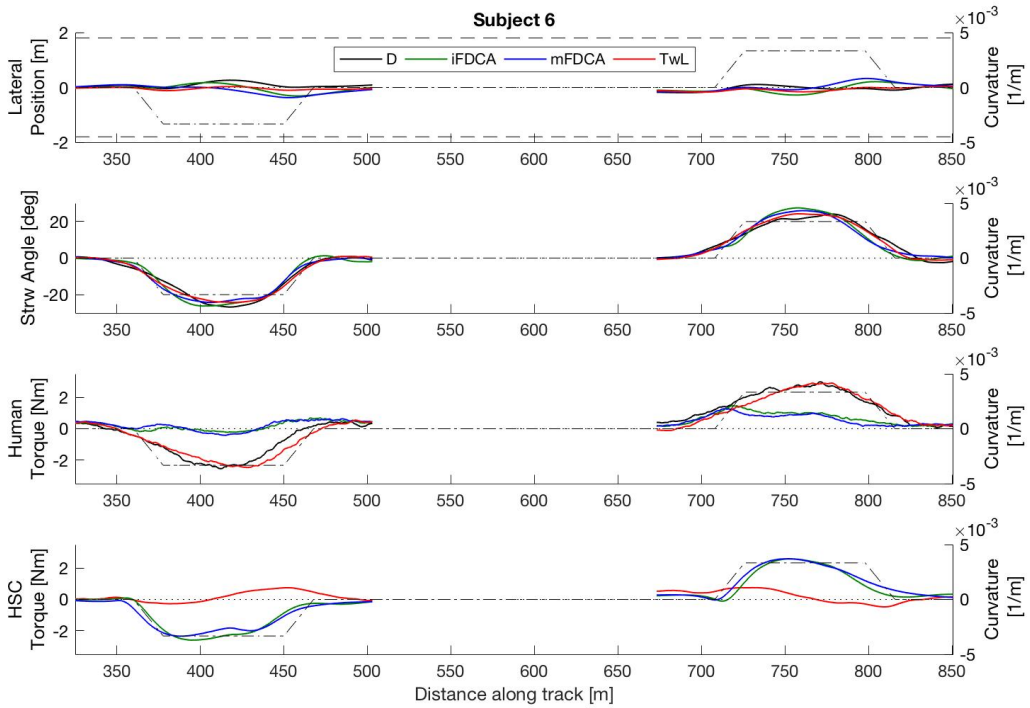
Subject 6
D
iFDCA
mFDCA
TwL
Lateral Position [m]
Strw Angle [deg]
Human Torque [Nm]
HSC Torque [Nm]
Curvature [1/m]
×10^-3
Distance along track [m]

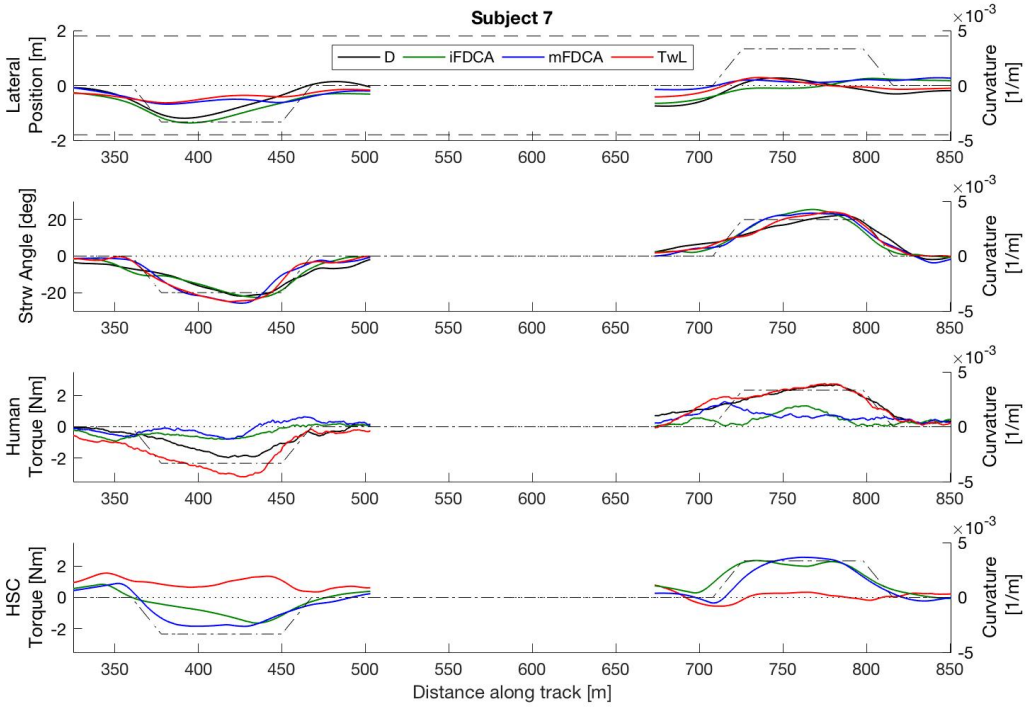
Subject 7
D
iFDCA
mFDCA
TwL
Lateral Position [m]
Strw Angle [deg]
Human Torque [Nm]
HSC Torque [Nm]
Curvature [1/m]
Distance along track [m]

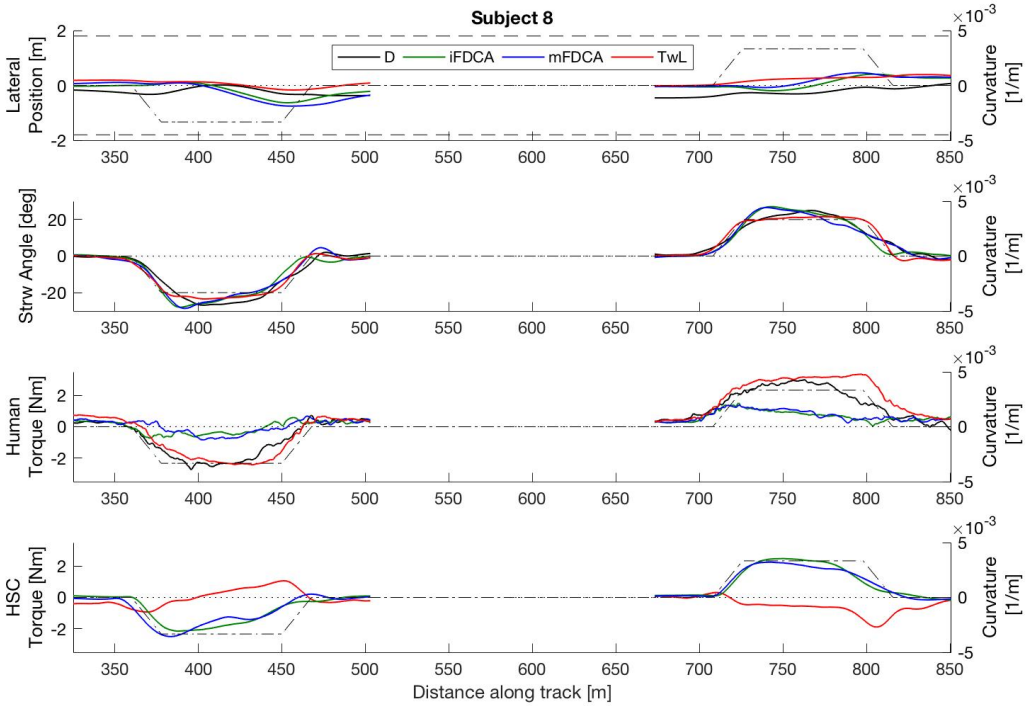
Subject 8
D
iFDCA
mFDCA
TwL
Lateral Position [m]
Strw Angle [deg]
Human Torque [Nm]
HSC Torque [Nm]
Curvature [1/m]
Distance along track [m]

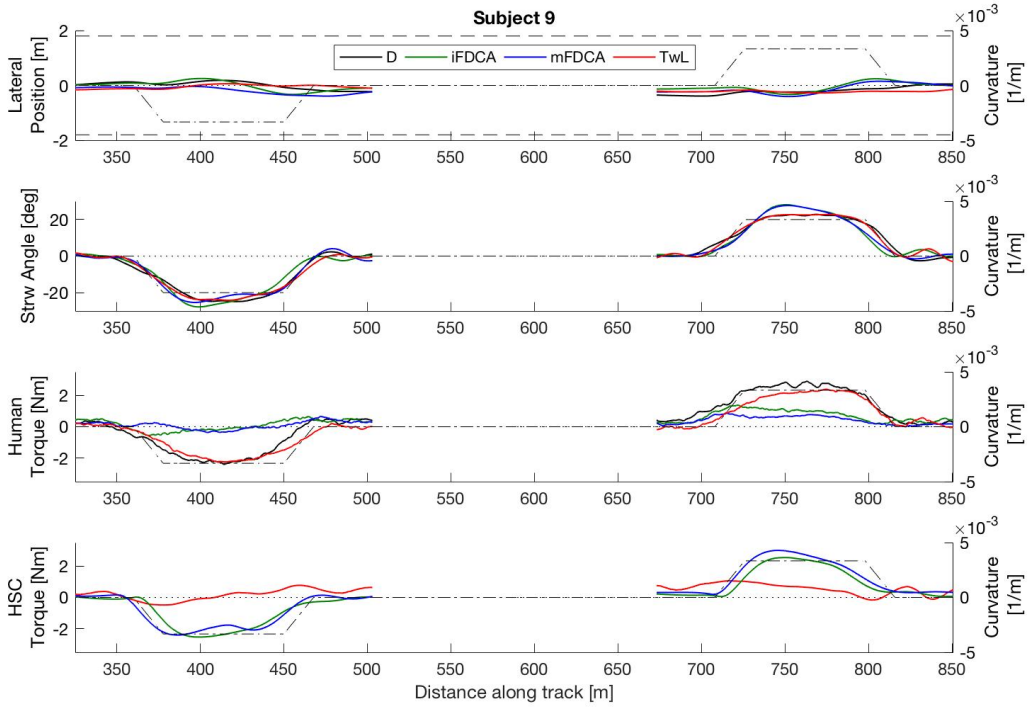
Subject 9
D
iFDCA
mFDCA
TwL
Lateral Position [m]
Strw Angle [deg]
Human Torque [Nm]
HSC Torque [Nm]
Curvature [1/m]
Distance along track [m]

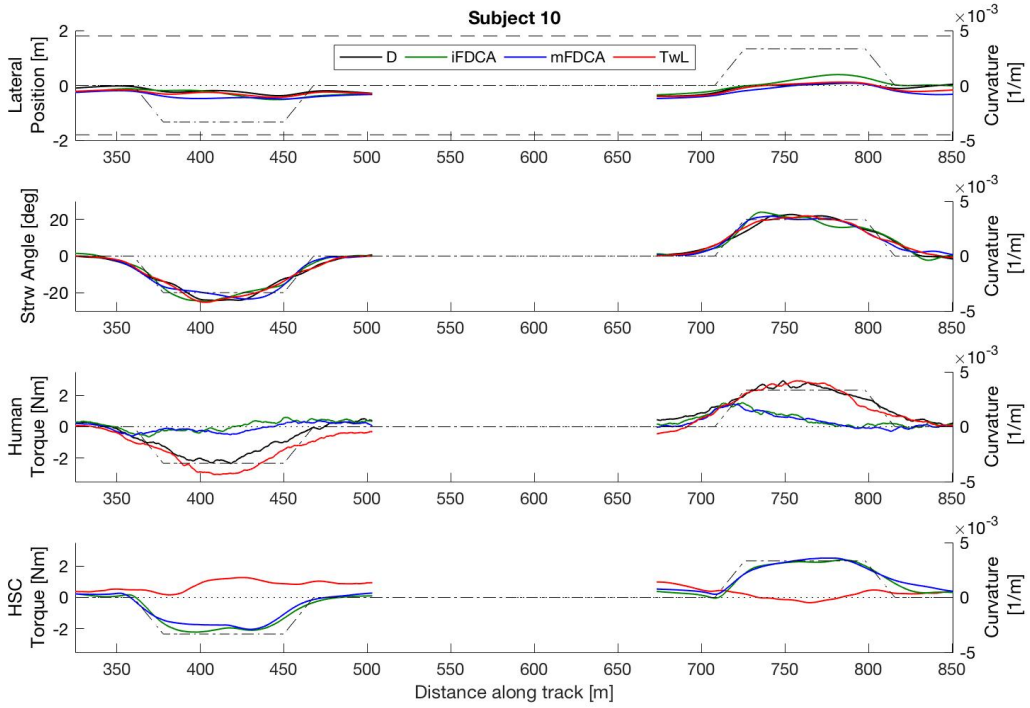
Subject 10
D
iFDCA
mFDCA
TwL
Lateral Position [m]
Strw Angle [deg]
Human Torque [Nm]
HSC Torque [Nm]
Curvature [1/m]
Distance along track [m]

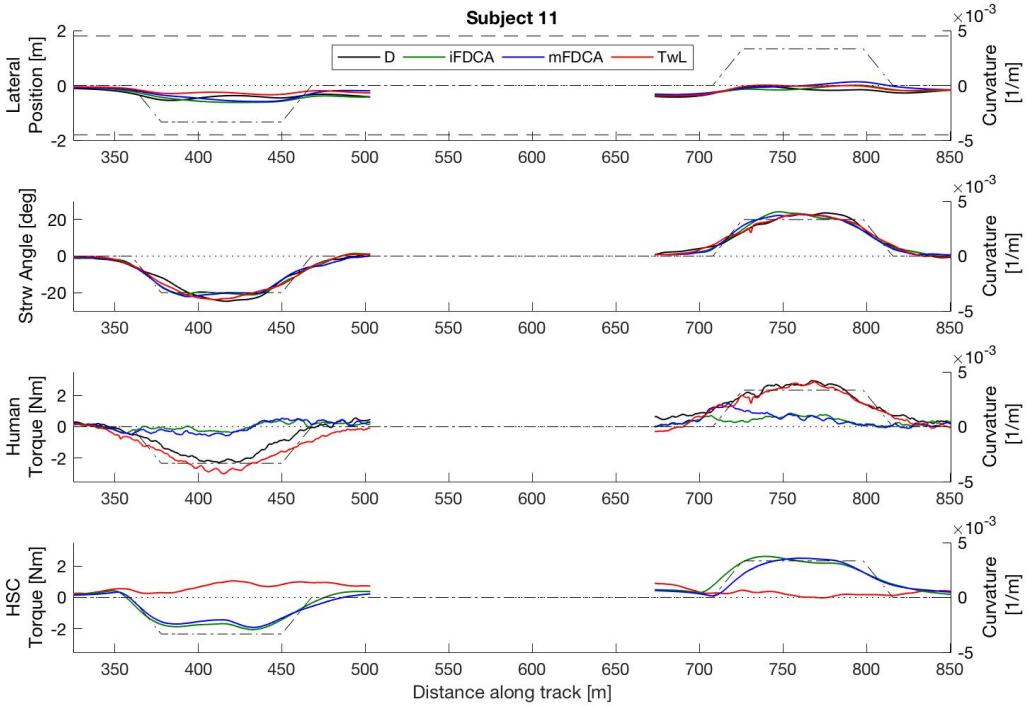
Subject 11
D
iFDCA
mFDCA
TwL
Lateral Position [m]
Strw Angle [deg]
Human Torque [Nm]
HSC Torque [Nm]
Curvature [1/m]
×10^-3
Distance along track [m]

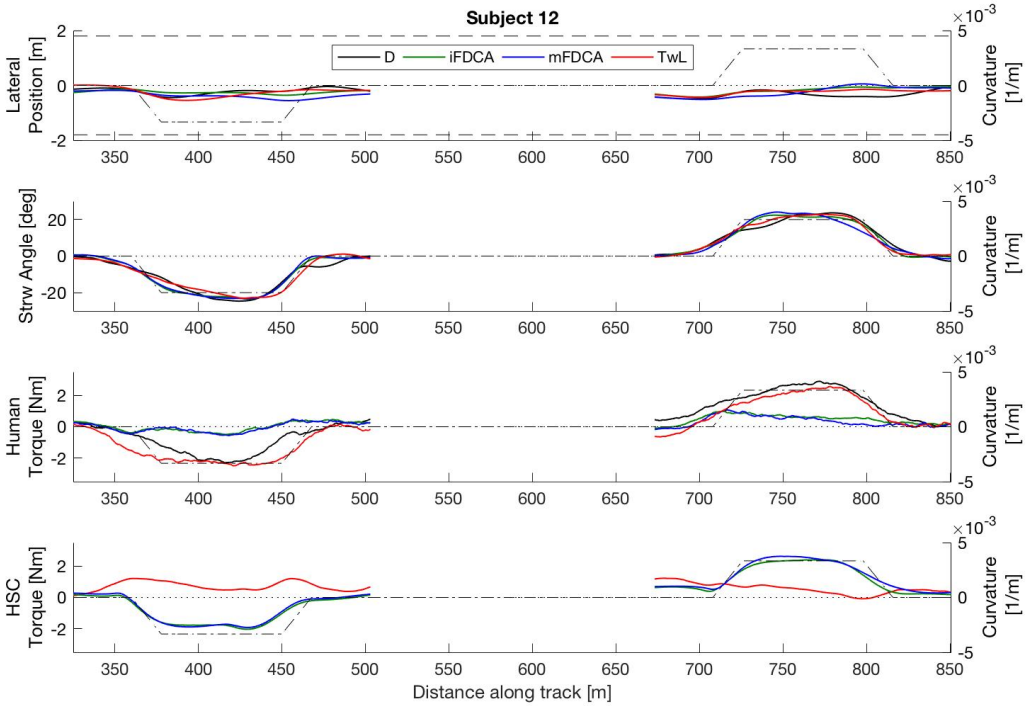
Subject 12
D
iFDCA
mFDCA
TwL
Lateral Position [m]
Strw Angle [deg]
Human Torque [Nm]
HSC Torque [Nm]
Curvature [1/m]
×10^-3
Distance along track [m]

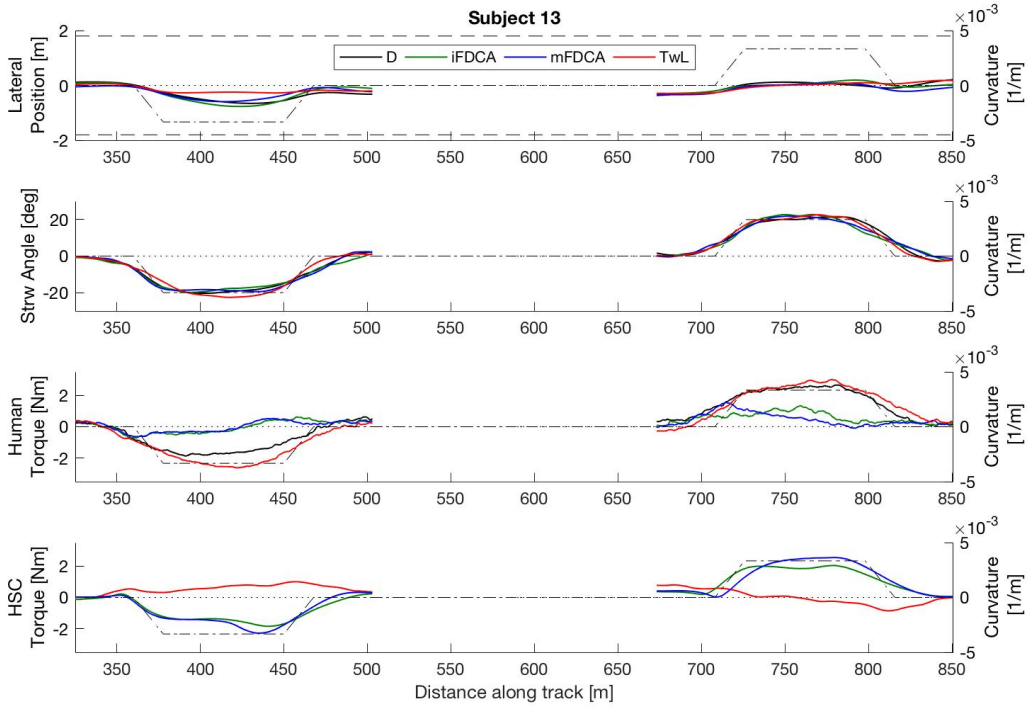
Subject 13
D
iFDCA
mFDCA
TwL
Lateral Position [m]
Strw Angle [deg]
Human Torque [Nm]
HSC Torque [Nm]
Curvature [1/m]
Distance along track [m]

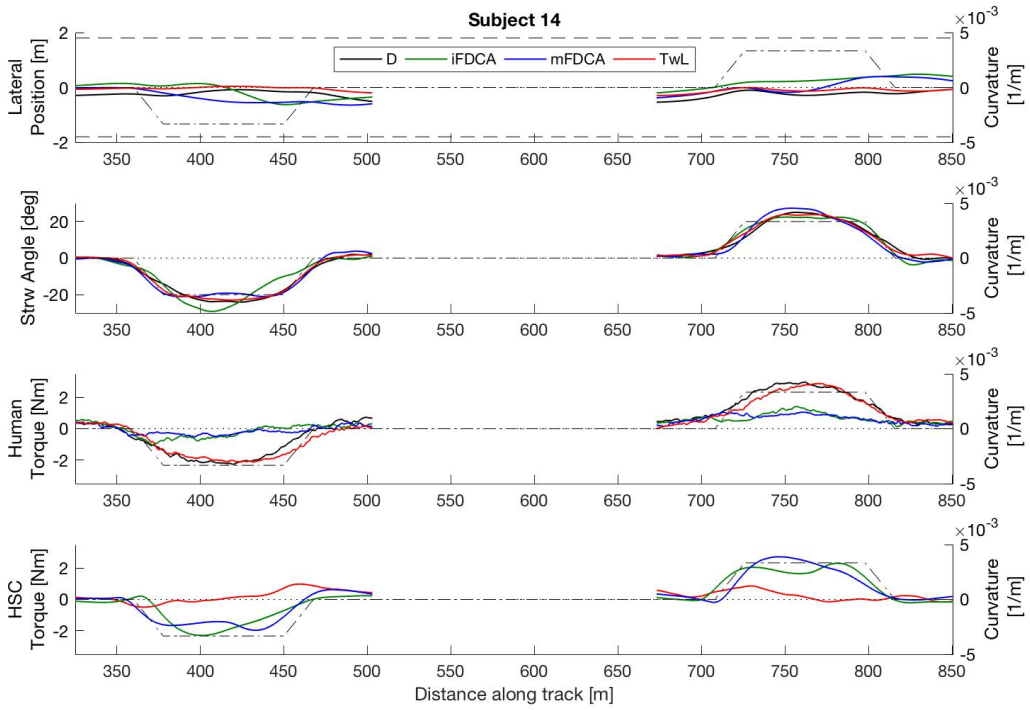
Subject 14
D
iFDCA
mFDCA
TwL
Lateral Position [m]
Strw Angle [deg]
Human Torque [Nm]
HSC Torque [Nm]
Curvature [1/m]
Distance along track [m]

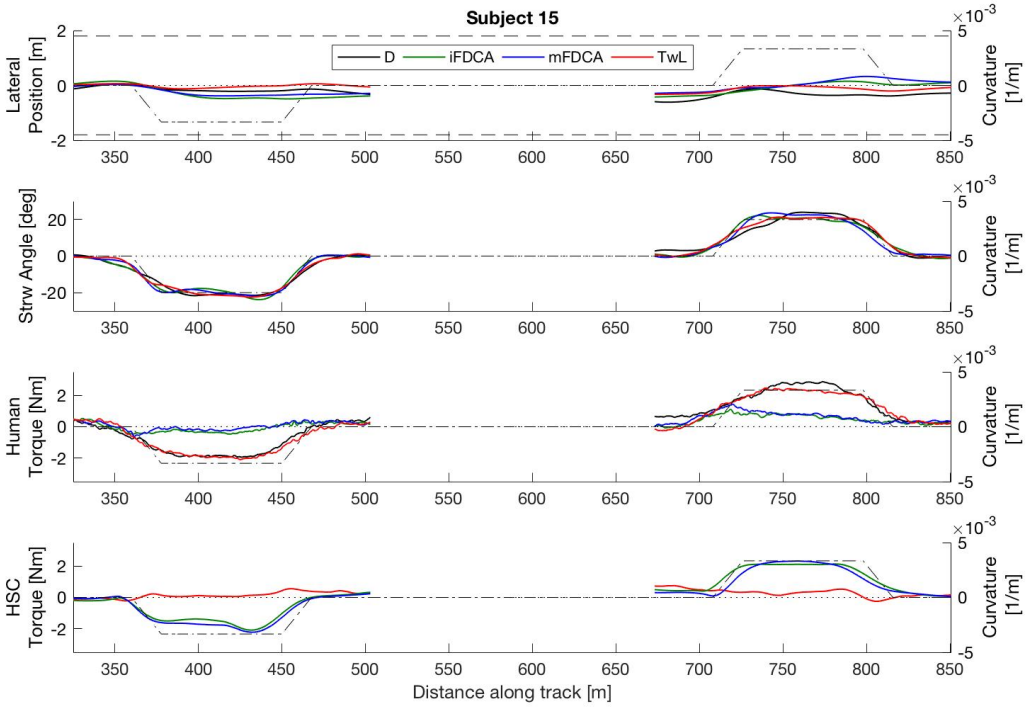

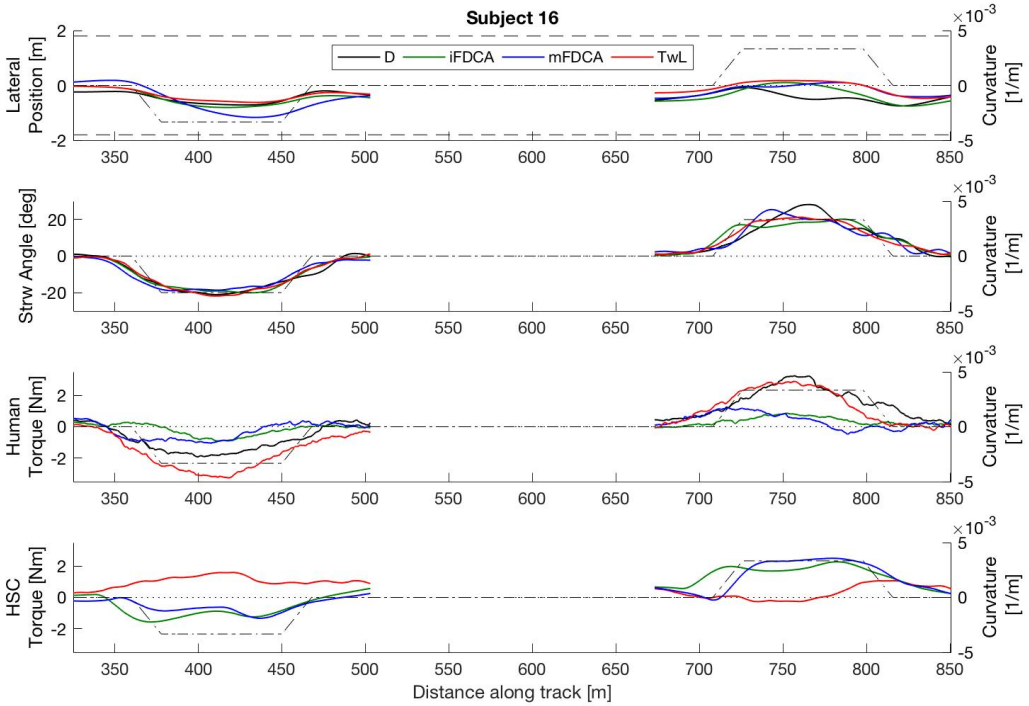

C.11. Statistical Analysis

		iHCR	**mHCR**								
	M (SD)	M (SD)	M (SD)	M (SD)	p-value	1-2	1-3	1-4	2-3	2-4	3-4
Driver-model performance											
Lat. Error to HCR [m]	-	0.25 (0.078)	0.26 (0.083)	-	0.371						
Strw. Error to HCR [m]	-	2.78 (0.49)	2.81 (0.55)	-	0.885						
VAF [-]	-	26.89 (16.49)	21.21 (10.61)		0.0634						
	D	**iFDCA**	**mFDCA**	**TwL**							
	M (SD)	M (SD)	M (SD)	M (SD)	p-value	1-2	1-3	1-4	2-3	2-4	3-4
Acceptance											
Usefulness Score [-]	0.41 (0.75)	1.11 (0.52)	0.40 (0.98)	-0.18 (1.12)	< 0.01	x				x	
Satisfaction Score [-]	0.23 (0.54)	1.00 (0.62)	0.43 (0.82)	0.20 (0.72)	<0.01	xx				x	
Conflict in Torques [-]	0 (0)	0.26 (0.05)	0.27 (0.06)	0.54 (0.11)	<0.01	xx	xx	xx		xx	xx
Performance											
Mean Lat. Error to HCR [m]	-	0.22 (0.10)	0.23 (0.08)	-	0.52						
Mean Lat. Position [m]	0.28 (0.10)	0.28 (0.12)	0.29 (0.10)	0.20 (0.07)	<0.01			xx		xx	x
TLC [-]	5.81 (0.64)	6.03 (0.53)	6.57 (1.46)	6.62 (0.55)	0.017			x		x	
Workload											
SRR	3.31 (0.50)	3.26 (0.67)	3.34 (0.77)	3.15 (1.03)	0.688						
Abs Driver Torque	1.24 (0.04)	0.44 (0.07)	0.45 (0.08)	1.35 (0.15)	<0.01	xx	xx			xx	xx

Table C.2: Results of the pairwise comparisons between the four conditions for the two-way ANOVA. x = $p < 0.05$, xx = $p < 0.01$.

	Left	**Right**		
	M	M	p-value	
	(SD)	(SD)		1-2
Driver-model performance				
Mean Lat. Error to HCR	0.28	0.23	0.044	x
	(0.08)	(0.10)		
Mean Strw. Error to HCR	2.85	2.74	0.597	
	(0.54)	(0.52)		
VAF [-]	6.22	41.8	<0.01	xx
	(4.81)	(23.75)		
Acceptance				
Conflict in Torques [-]	0.16	0.38	<0.01	xx
	0.06	0.05		
Performance				
Mean Lat. Error to HCR [m]	0.21	0.23	0.17	
	(0.06)	(0.10)		
Mean Lat. Position [m]	0.22	0.30	0.002	xx
	(0.06)	(0.13)		
TLC [-]	6.48	6.04	0.057	
	(0.02)	(0.02)		
Workload				
SRR	3.21	3.32	0.139	
	(0.65)	(0.66)		
Abs Driver Torque	1.00	0.74	<0.01	xx
	(0.08)	(0.07)		

Table C.3: Results for pairwise comparisons between the curve-directions for the two-way ANOVA. x = $p < 0.05$, xx = $p < 0.01$

	D		iFDCA		mFDCA		TwL											
Metric	Left	Right	Left	Right	Left	Right	Left	Right	1-3	1-5	1-7	2-4	2-6	2-8	1-2	3-4	5-6	7-8
Acceptance																		
% Time Conflict in Torque	0 (0)	0 (0)	0.10 (0.07)	0.42 (0.10)	0.15 (0.08)	0.40 (0.11)	0.37 (0.13)	0.72 (0.17)	xx	xx	xx	xx	xx	xx		xx	xx	xx
Performance																		
Mean lat. error to HCR [m]	-	-	0.22 (0.08)	0.22 (0.12)	0.21 (0.06)	0.25 (0.12)	-	-	-	-	-	-	-	-	-			-
Abs Mean Lat. Position [m]	0.26 (0.09)	0.30 (0.14)	0.22 (0.09)	0.34 (0.17)	0.22 (0.06)	0.36 (0.14)	0.18 (0.06)	0.22 (0.11)			x			x		x	xx	
TLC [sec]	6.01 (1.25)	5.61 (0.56)	6.12 (0.69)	5.93 (0.65)	6.84 (2.86)	6.3 (0.77)	6.92 (0.93)	6.31 (0.49)			x							
Workload																		
SRR [-]	3.28 (0.58)	3.35 (0.62)	3.23 (0.82)	3.29 (0.67)	3.29 (0.97)	3.4 (0.80)	3.05 (1.02)	3.25 (1.17)										
Abs Driver Torque [-]	1.49 (0.01)	1.00 (0.07)	0.56 (0.1)	0.32 (0.07)	0.55 (0.11)	0.34 (0.09)	1.41 (0.2)	1.30 (0.2)	xx	xx		xx	xx	x	xx	xx	xx	

Metric	3-5	3-7	5-7	4-6	4-8	6-8
Acceptance						
Conflict in Torque [-]	xx	xx	xx		xx	xx
Performance						
Mean lat. error to HCR [m]		-	-		-	-
Abs Mean Lat. Position [m]					x	xx
TLC [sec]						
Workload						
SRR [-]						
Abs Driver Torque [-]		xx	xx		xx	xx

Table C.4: Results of the pairwise comparisons of the one-way repeated measures ANOVA for dependent variables over the four conditions and two curve directions. x = $p < 0.05$, xx = $p < 0.01$

	iFDCA		**mFDCA**					
Metric	Left	Right	Left	Right	1-2	3-4	1-3	2-4
Driver-model performance								
Lat. Error to HCR [m]	0.28	0.21	0.27	0.24				
	(0.08)	(0.09)	(0.09)	(0.10)				
Strw Angle Error to HCR [m]	2.80	2.75	2.89	2.74				
	(0.59)	(0.48)	(0.63)	(0.59)				
VAF [-]	10.87	42.91	1.57	40.84	xx	xx	x	
	(10.51)	(27.65)	(2.70)	(21.51)				

Table C.5: Results of the pairwise comparisons of the one-way repeated measure ANOVA for dependent variables over the two FDCA conditions and two curve directions. x = $p < 0.05$, xx = $p < 0.01$

D

Appendix D: Informed Consent

Informed Consent Form

Researchers: Wietske Scholtens - Student Email: w.m.scholtens@student.tudelft.nl Tel: +31652659026 Dr. ir. D.A. Abbink – Supervisor Email: d.a.abbink@tudelft.nl	**Location** TU Delft, Faculty of Aerospace Engineering Department of Control and Operations – Control and Simulation HMI-Lab, room 0.38 Kluyverweg 1 2628 HS Delft

Before agreeing to participate in this study it is important that the information in this document is carefully read and understood. This document will describe the purpose, procedures, risks and possible discomforts of this experiment.

Purpose of the research
The purpose of this research is to investigate the effect of individualising a haptic shared control system on the comfort, workload, behaviour and performance of drivers. A haptic shared control system uses torques on the steering wheel to guide the driver. The intentions from the control system can be determined in different ways. This study investigates the effect of a general and individualised tuning of the control system. The results will be statistically analysed and published in a master thesis, as well as a possible publication.

Procedure
This study will be performed on two separate days. On both days you will be requested to drive in a fixed base driving simulator and will be instructed how to operate it. The simulator will drive with a fixed speed and has a automatic shifting gearbox, so you do not have to control the gas pedal and the shifting gear. Furthermore you are requested to keep your **both hands on the steering wheel in a ten-to-two position.**

On the first day no torques are applied on the steering wheel and you will be asked to drive as you normally would over a rural road track. If you exceed the lane boundaries the experiment needs to restart. At some points in the track you will see a narrowing of the road, indicated with cones. Try not to hit the cones. Before the actual experiment starts you will drive one training trial to familiarize with the system. After the training round you will again drive on a rural road track, both trials will take about 3 minutes.

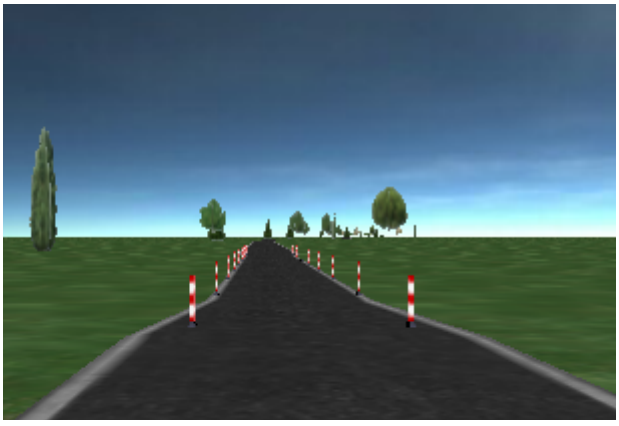

The experiment on the second day will consist of 4 different conditions (no controller, controller 1, controller 2 and controller 3). Again you are asked to drive as you normally would and to stay within the lane boundaries. Before each condition you can again drive one training trial to familiarize with the system. Each trial will take about 3 minutes.

Task instructions:
During the entire track you are asked to drive as you normally would, staying within the lanes and avoid hitting the cones.

Duration:
Day 1: the first part of the experiment will take about 20 minutes, this includes filling out the questionnaires and driving both training trial and real trial.

Day 2: the second part of the experiment will take about 30 minutes. This includes filling out the questionnaires and driving the training trials and real trials for all conditions.

Risks and discomforts:
During the experiment some people (<5% of the population) can feel different kind of sicknesses such as: visuomotor dysfunctions (eyestrain, blurred vision, difficulty focussing), nausea, drowsiness, fatigue or headache. If you feel uncomfortable in any way you are advised to rest for a couple of minutes or to stop the experiment.

Confidential:
All data recorded in the experiment will be kept confidential and will only be used for research purposes only. You will only be identified with a subject number.

Rights
You are allowed to withdraw from the experiment at any time, without mentioning any reason or consequences.

Questions
If anything is unclear or you have any other questions regarding the experiment or research, please contact W. Scholtens.

I have read and understood the information provided above and give permission to process the data for the purpose of the study as described above. I agree to voluntarily participate in this study and know my rights to withdraw.

Name:

Signature: **Date:**

E

Appendix E: Van Der Laan Questionnaire

Van Der Laan Questionnaire

To be filled in by researcher:

Participant nr:	Control type:	Date:

I find the system (please tick a box on every line):

1 Useful	|__|__|__|__|__|	Useless
2 Pleasant	|__|__|__|__|__|	Unpleasant
3 Bad	|__|__|__|__|__|	Good
4 Nice	|__|__|__|__|__|	Annoying
5 Effective	|__|__|__|__|__|	Superfluous
6 Irritating	|__|__|__|__|__|	Likeable
7 Assisting	|__|__|__|__|__|	Worthless
8 Undesirable	|__|__|__|__|__|	Desirable
9 Raising Alertness	|__|__|__|__|__|	Sleep-inducing

Comments on the experiment and system:

……
……
……
……
……
……
……

Appendix F: Introductory Analysis

This appendix will discuss the investigations in the introductory phase for the HCR generation and the control structure.

F.1. HCR Generation

In the introductory phase the driver-model is evaluated to check whether the model is able to capture human driver behaviour. This is done by comparing the model outputs with data from driving simulator tests performed in the same group. Note that the driver-model is extended after this evaluation, so that also different steering out behaviour can be captured. This extension was not included when the results in this section were generated, therefore the only 3 parameters that were varied are K_p, K_c and BSD. Furthermore t_{far} was set to a constant value and the clothoidal section was excluded from the BSD.

F.1.1. Parameter Sensitivity Introductory Model

To check the effect of changing the parameters, each parameters is varied separately while the others were kept constant.

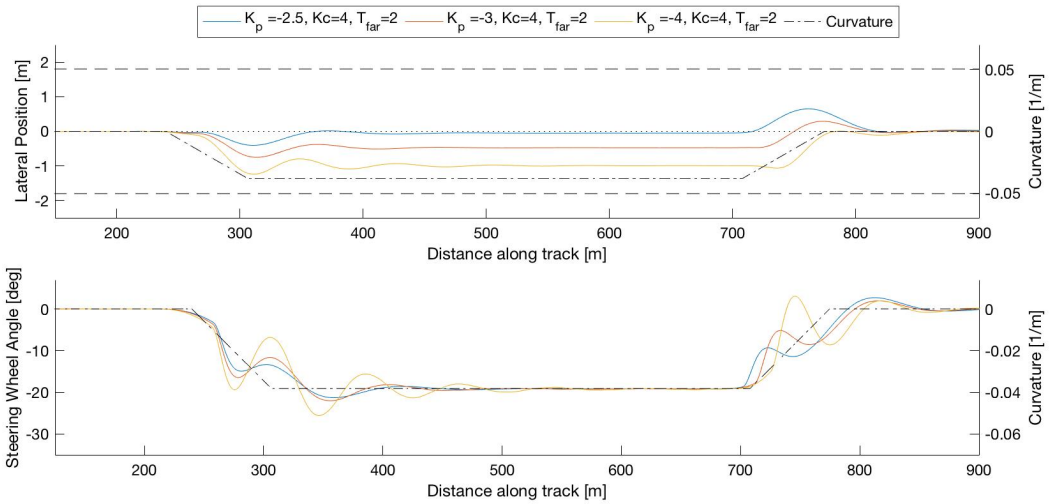

Figure F.1: Effect of changing K_p on the lateral positions (top) and steering wheel angles (bottom). The dashed horizontal lines in the top plot indicate the lane boundaries.

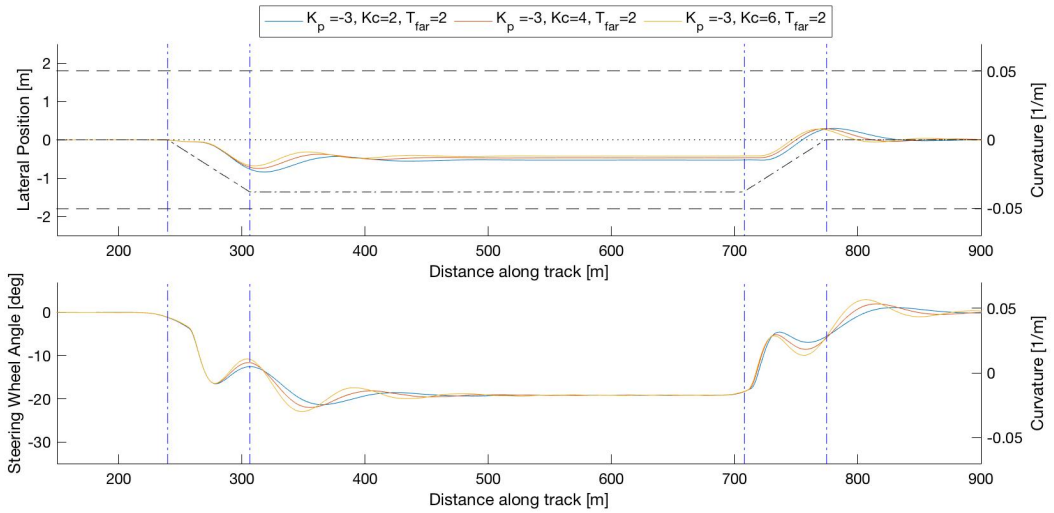

Figure F.2: Effect of changing K_c on the lateral positions (top) and steering wheel angles (bottom). The dashed horizontal lines in the top plot indicate the lane boundaries.

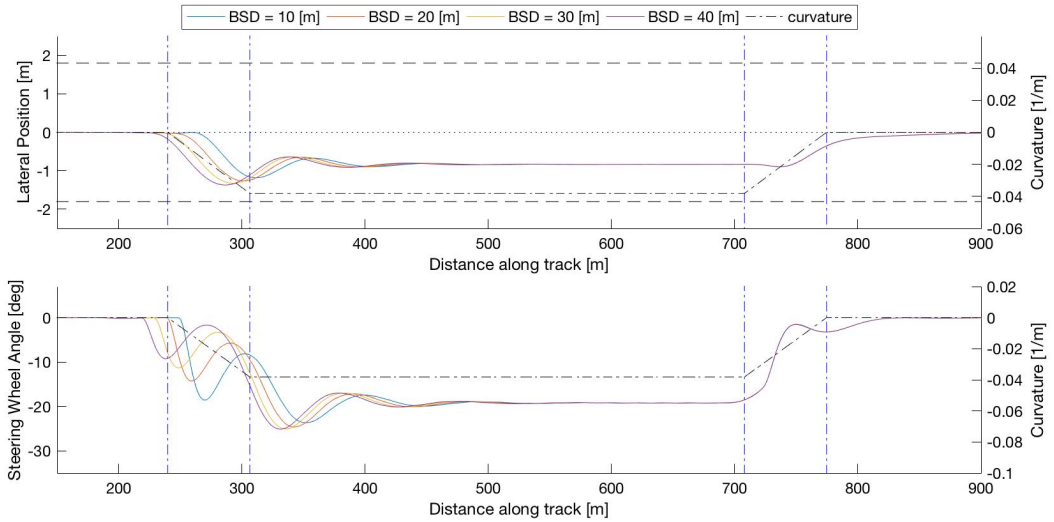

Figure F.3: Effect of changing the point where the driver starts steering into the curve on the lateral positions (top) and steering wheel angles (bottom). Note that the BSD is a lot higher than in the final driver-model because the clothoidal section was here also incorporated in the distance. The dashed horizontal lines in the top plot indicate the lane boundaries. t_{far} = 3, K_p = 4, K_c 2

F.1.2. Descriptiveness & Realism

For the comparison with real human behaviour, data from an earlier experiment is used. This road had a road-width of 3.6 meters and the drivers drove with constant velocity of 20 m/s. Based on the range indicated by Saleh [8] the values for K_p are varied from [2:0.25:5] and K_c from [0:2:24]. The initial steering distance before the curve (BSD) is varied between 10, 15, 20, 25 and 30 meters and $t_{far]}$ was set to a constant of 3 seconds. These times are chosen based on the recorded data and on Boer [3] who found that drivers start steering into the curve between 20 and 30 meters before the start of the curve.

The descriptiveness is determined, where only trajectories with a lateral position that does not exceed an absolute value of 1.5 meters are used. Only trajectories that were produces with less than six steering reversals per curve are used. The green areas in figure F.4 and figure F.5 represent the capabilities of the introductory model, the pink area represents the driver behaviour. The versatility is thereafter calculated as a percentage of the grey area that is covered by the green area. In this case the versatility is 47.6% and 49.1% for respectively the first and second curve.

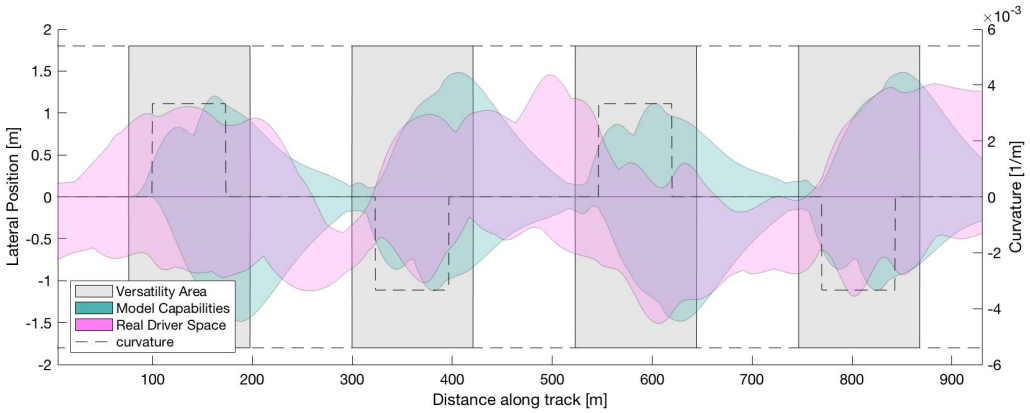

Figure F.4: Results for the descriptiveness area, generated with steering reversals < 6 per curve. The purple area visualizes the lateral positions driven by all drivers, where the green area visualizes the model capabilities. The gray area represents all possible lateral positions in the curve that the driver can drive. The descriptiveness is the percentage of the gray area that is covered by the green area, which is 47.6% and 49.1% for respectively the first and second curve.

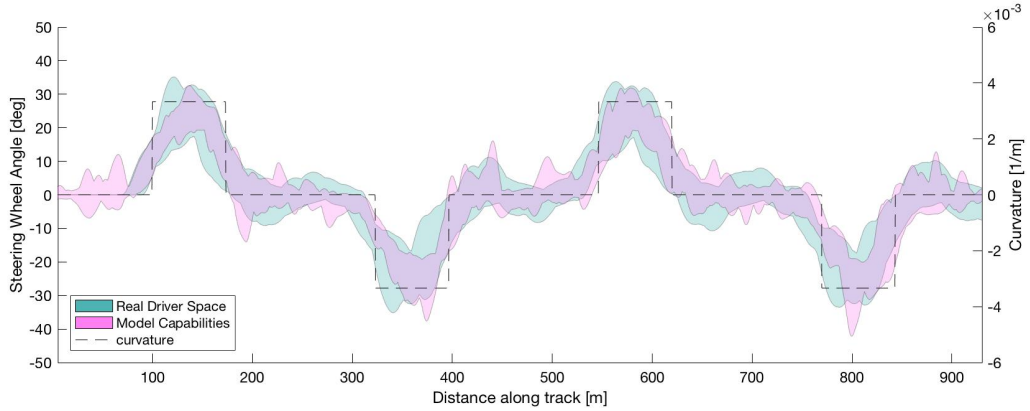

Figure F.5: Results for the measured steering angles during the experiment and the generated steering angles from the model, filtered for SRR < 6 per curve

F.1.3. Conflicts with current controller

To obtain the optimal model fit it is investigated in which regions drivers are more likely to perceive the guidance forces as conflicting. In some regions drivers might use more satisfying control and they care less about the trajectory, probably resulting in higher acceptance and lower conflicts. Looking at experimental data should provide more insight in the occurrence of conflicts, with the goal to determine optimizing criteria to find the most optimal trajectory. Here most optimal is defined as the trajectory which causes the fewest conflicts.

Until now no metric is found that can properly evaluate the acceptance or drivers likeliness of the guiding forces. Most researches [5] [1] [7] [6] use the conflicting forces to determine if a conflict occurs. However, in my literature research I found that this is not always a good indication of a conflict. Looking at the questionnaires can give further insight in the occurrence of conflicts. To evaluate the acceptance the results from the NASA TLX questionnaire as well as the forces on the steering wheel are used. The Physical Demand values from the questionnaires were divided in groups with values lower than 10 and values higher than 40, representing a group who liked the guidance forces and a group who did not like the guidance forces.

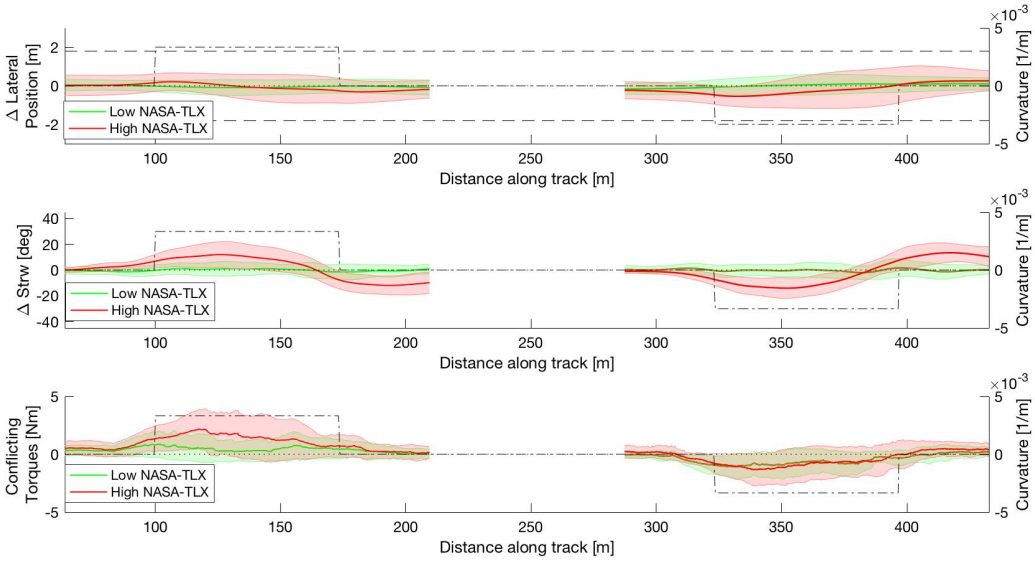

Figure F.6: *Top*: Differences in lateral position between manual control and lateral position with HSC. A positive value means that the HSC position was higher than the manual value. *Middle*: Differences in steering wheel angles with manual control and steering wheel angles with HSC. *Bottom*: Mean conflicting torques. All plots show results for the subjects with low NASA-TLX values (green) and High NASA-TLX values (red).

Here it can be seen that the mean conflicting force is lower for participants who liked the guiding forces. Furthermore, it seems that the error between the trajectories with manual and HSC is higher for the group with high NASA-TLX values (the group who did not appreciate the guiding forces). In the beginning of the left curve the value is higher, meaning that the HSC trajectory is closer to the left lane-boundary. At the end of the curve the opposite is visible, meaning that the trajectory with HSC is closer to the right boundary. For the group who liked the guiding forces the error is close to zero, meaning that the trajectories with manual control and HSC are similar.

This might be a result of that people who did not cut the curves did like the controller, since the controller lets you steer to the center of the road. Where people who did cut the curves had to adjust their trajectory to the middle of the curve, leading to frustration.

It seems that the conflicting torques are higher in the beginning than in the end of the curve for drivers with low NASA-TLX values. For both groups the forces already start building up before the beginning of the curve, therefore the point where the controller starts steering in and out of the curve might be important to increase acceptance. The last notable thing is the differences in left and right turns. This might be a result of the positioning of the driver in the car. The driver is located on the left side of the car, which increases the driver's capability to anticipate the distance to the left side of the road. Therefore more curve-cutting behaviour can be expected when taking left curves, leading to higher conflicts when steering to the left.

F.1.4. Fitting method

The descriptiveness already gives an idea how well the model can capture different driver styles. To check whether the model is able to reproduce human like trajectories the output can be compared with real driver data. To find the parameters which produce the best match with the driver both the lateral error and the steering angle are evaluated. To find the trajectory closest to that of the driver, the error between the lateral position of the model trajectory and the real driver trajectory is optimized using:

$$f_{Lateral\_Error} = \sum |(Driver\_lateral\_Error - Model\_lateral\_Error)^2| \tag{F.1}$$

(F.2)

And in similar way for the steering angles:

$$f_{SWAngle} = \sum |(Driver\_SW\_Angle - Model\_SW\_Angle)^2| \tag{F.3}$$

(F.4)

The curve is separated in different parts to assign different weights to different locations in the curve. The error values are multiplied with the weighing values to determine the total error value:

$$f_{tot} = g_1 * f_{Lat.ErrorIn} + g_2 * f_{Lat.ErrorMid} + g_3 * f_{Lat.ErrorOut} + h_1 * f_{SWAngleIn} + h_2 * f_{SWAngleMid} + h_3 * f_{SWAngleOut} \tag{F.5}$$

	Begin [m]	End [m]
In Part	64.1	124.1
Mid Part	124.1	160.3
Out Part	160.3	196.5
Curve	100	173.1

Table F.1: Definition of different sections of the curve based on lateral position on the road

F.1.5. Model fit on manual trajectories

To evaluate if the model is able to reproduce realistic driver behaviour it is fit on manual trajectories. Only trajectories with less than 6 steering reversals per curve are included in the search for the closest trajectory fit. An example of a fitted trajectory is shown for subject 3 in figure F.7. Here the model is fitted on the left curves only.

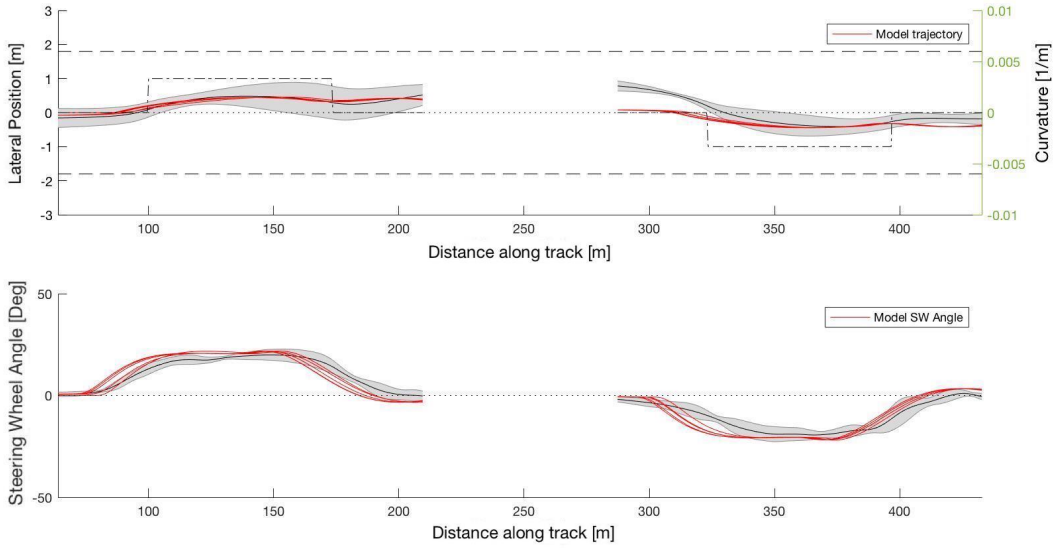

Figure F.7: Example of an the drivers variability (grey) and the identified model (red) for subject 3.

To used weighting factors to fit the model on the drivers behaviour are listed in table F.2. Due to a different initial lateral position on the road fitting on the steering wheel angles led to very different lateral positions. Therefore only the lateral position is now used to fit the trajectory.

	g_1	g_2	g_3	h_1	h_2	h_3
Weighing	2	1.5	2	0	0	0

Table F.2: Weighing factors for different sections of the curve for the model fit in figure F.7

One of the limitations of this model is that is can not replicate biases in straight roads sections, which is clearly visible in figure F.7. Especially for the right turns it shows that the model starts from the center of the road, where the driver always initiates the curve from the left side of the road.

F.2. Control Structure

The HCR is used in a shared controller, such that both the controller and the human deliver torques on the steering wheel. The shared control architecture is based on van Paassen's work [11], who argues that a good haptic shared control system requires proper tuning of four design choices:

- An human compatible reference trajectory (HCR)
- An feed-forward torque (LoHS)
- An feed-back correction torque (SoHF)
- An Haptic Controller (LoHA)

These four components are shown in figure F.8. The control torques are based on a Human-Compatible-Reference (HCR), which can be interpreted as a virtual car driving on the same road. The virtual car behaviour will be fitted to match the driving style of the current driver, as discussed in the previous chapter.

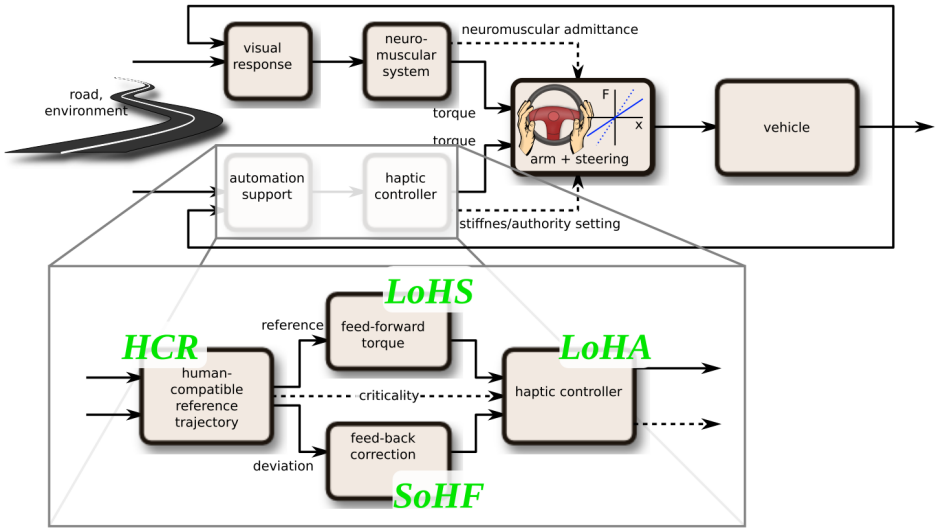

Figure F.8: Control Scheme replicated from van Paassen [11], where in this study the LoHA is not implemented.

F.2.1. Control Structure in Matlab Simulation

The used control structure is based on van Paassen's work [11], who proposed to separate the controller in two components: a support torque and a feedback torque.

Level of Haptic Support

The first component of the controller is the Level of Haptic Support (LoHS), which behaves like a feed-forward (FFW) controller. The LoHS delivers torques on the steering wheel based on the steering wheel angles from the virtual car that drives on the HCR. A K_{LoHS} of 1 would drive the car autonomously without additional needed torques from the driver, however if the car somehow deviates from the reference trajectory this error is not corrected, as displayed in figure F.9. Choosing lower values for K_{LoHS} requires human torques to stay on the HCR, which will be discussed later. The steering wheel is modelled as a gain, this approximated is made since the frequencies of the change in steering wheel angles are low. The LoHS torques are calculated using equation F.6. Here K_{SW} is the steering wheel stiffness and $\Theta_{SW,HCR}$ is the steering wheel angle of the virtual car.

$$\Gamma_{LoHS} = K_{LoHS} \cdot \Gamma_{HCR} = K_{LoHS} \cdot K_{SW} \cdot \Theta_{SW,HCR} \tag{F.6}$$

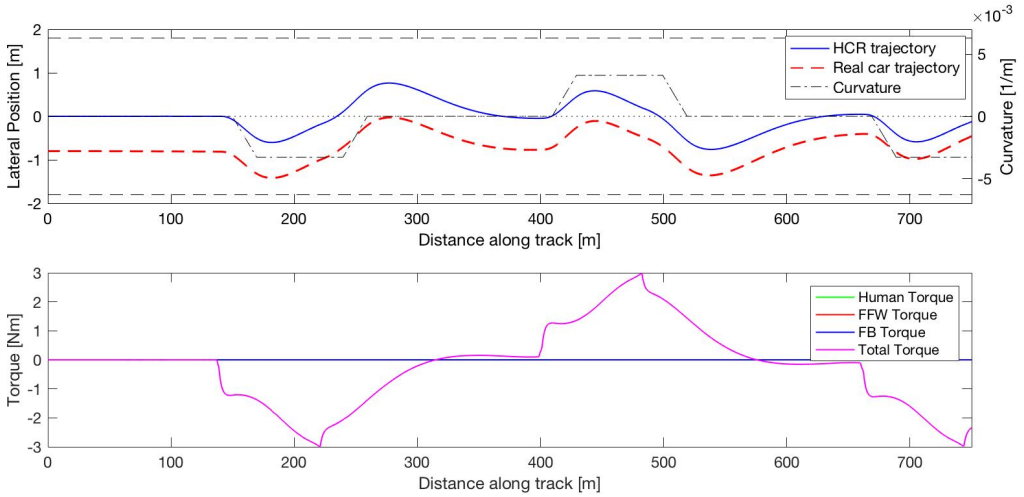

Figure F.9: Results for lateral position (top) and torques (bottom) when no driver torque is applied on the steering wheel, only the FFW component is active and the car starts with an initial error to the reference. The results show that the car is guided to drive the same curvature as the HCR, but does not approach the HCR. $K_{LoHS} = 1$, LoHA = 2

Strength of Haptic Feedback

The second component of the controller is the Strength of Haptic Feedback, which acts like a feedback (FB) controller for the position and the heading. Since the FB controller only acts if there is a difference in heading or position with the virtual car, the car first needs to deviate from the HCR before torques are presented on the steering wheel. This is clearly visible in the curved sections in figure F.10.

The FB torque is composed of two parts, a position and heading component. The $\Delta\psi$ is the difference between heading of the car and the heading of the virtual car. Δy is the lateral distance between the car position and the nearest HCR position. Both are multiplied with a gain as in equation F.7.

$$\Gamma_{SoHF} = K_{\psi} \cdot \Delta\psi + K_{y} \cdot \Delta y \tag{F.7}$$

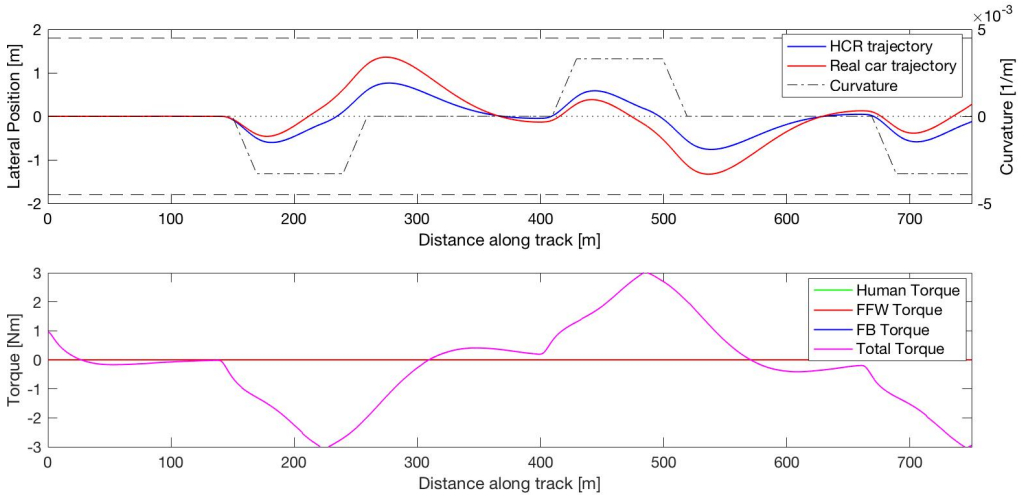

Figure F.10: Results for lateral position (top) and torques (bottom) when no driver torque is applied on the steering wheel and only the FB component is active. The controller only provides torques when an error with the reference occurs, thereby resulting in overshoot behaviour in the curves. $K_{\psi} = 50$, $K_{y} = 1.3$, LoHA = 2

Combined LoHS and SoHF

When both components are combined the car is able to stay close to the HCR and also approaches the center line if the initial condition is located next to the road.

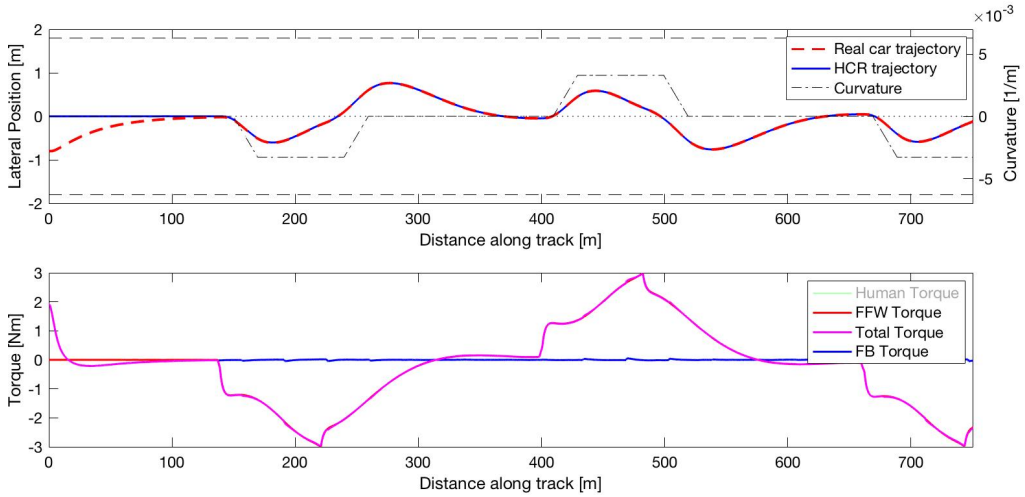

Figure F.11: Results for lateral position (top) and torques (bottom) when no driver torque is applied on the steering wheel and both FB and FFW components are active. $K_\psi = 50$, $K_y = 1.5$, $K_{LoHS} = 1$, LoHA = 2

Level of Haptic Authority

The Level of Haptic Authority (LoHA) determines how the driver and machine contributions are balanced and thereby who has the highest authority over the car. In the final experiment the LoHA is not implemented. To investigate the effects of changing the LoHA it was implemented in the simulation in MATLAB.

In this simulation the LoHA is implemented by changing the steering wheel stiffness (K_s). The FB and FFW torques scale with the same stiffness. A high stiffness is therefore harder to override by the human, leading to a higher authority of the control system. Figure F.12 shows that setting the LoHA to 0.5 and 2 does change the applied torques on the steering wheel. However, since the LoHA effects both the steering wheel stiffness and the control torques the trajectory is the same.

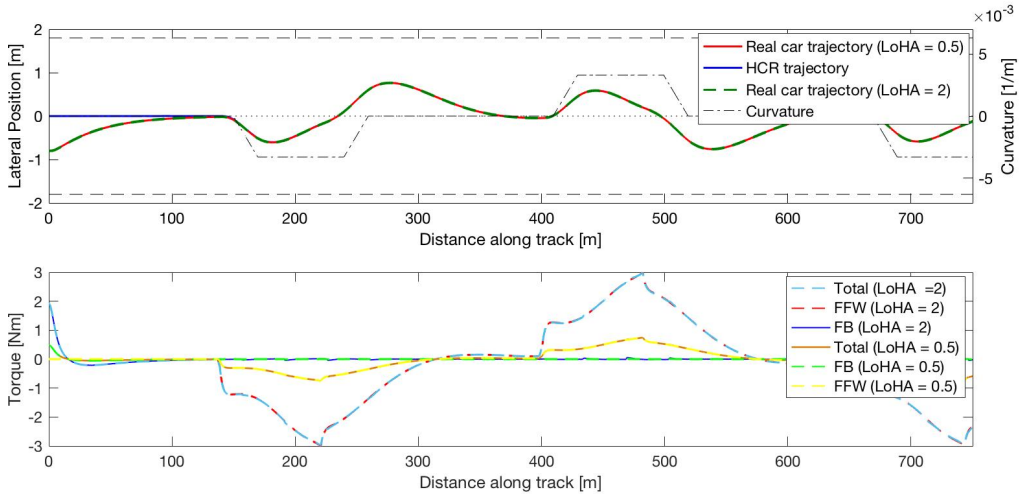

Figure F.12: Results for lateral position (top) and torques (bottom) when no driver torque is applied on the steering wheel and both FB and FFW components are active, for two different settings of the LoHA (2 and 0.5). The results lead to the same lateral positions, but different torques on the steering wheel. $K_\psi = 50$, $K_y = 1.5$, $K_{LoHS} = 1$.

F.2.2. Sharing Control with the driver

In the previous examples only the contribution of the controller is taken into account and the driver does not exert torques on the steering wheel. The car was tuned such that it can drive autonomously without requiring the torque from the human, which is not the idea of shared control. When both the controller and the driver are simulated, both apply torques on the steering wheel. This leads to too large steering wheel angles, K_τ and the human torque therefore need to be scaled. This determines the contribution of both the FFW controller

and the human. When K_{LoHS} is set to 0.5 the FFW torques deliver 50 % of the required torques to reach the HCR steering wheel angle. The other half needs to be exerted by the human, therefore the human torque is also scaled, such that the total of the added torques from human and system add up to 1. Note that this is a very simplified simulation of a Human, where the driver does not change their own stiffness and their desired trajectory is not influenced by the control torques. Figure F.13 shows the situation where the human and system have the same reference and both deliver 50% of the torques required to reach their desired steering wheel angles. The human torque and FFW torque are almost identical, and the FB torque is close to zero because there is no deviation in position or heading.

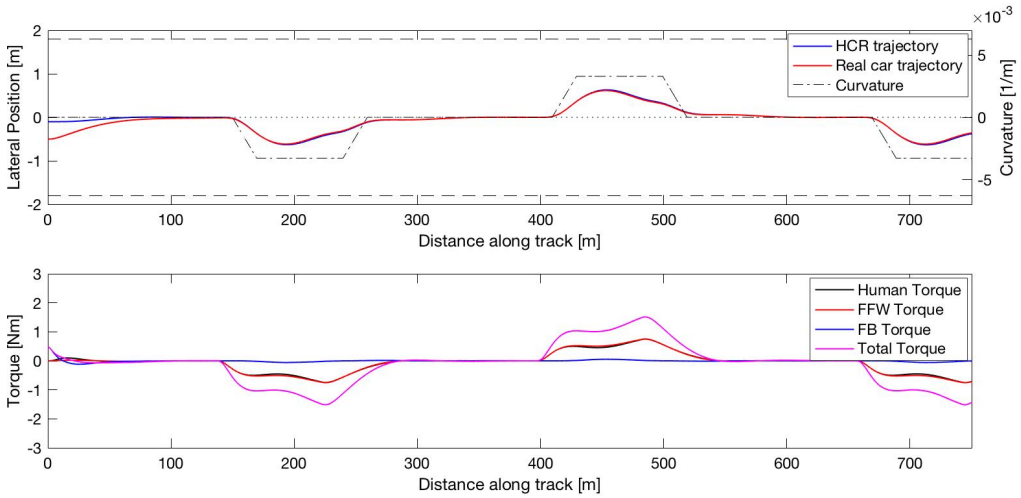

Figure F.13: Results for lateral position (top) and torques (bottom) when both FB and FFW components are active and the simulated driver and the controller desire the same trajectory. $K_{\psi} = 50$, $K_y = 1.5$, $K_{LoHS} = 0.5$. LoHA = 1. The weighing factor of both the driver and controller is set to 50%.

If the HCR does not match the drivers intentions deviations from the HCR can occur, which can result in FB torques that counteract the FFW torques. The sum of the control torques is smaller, requiring more torques from the human, as in figure F.14.

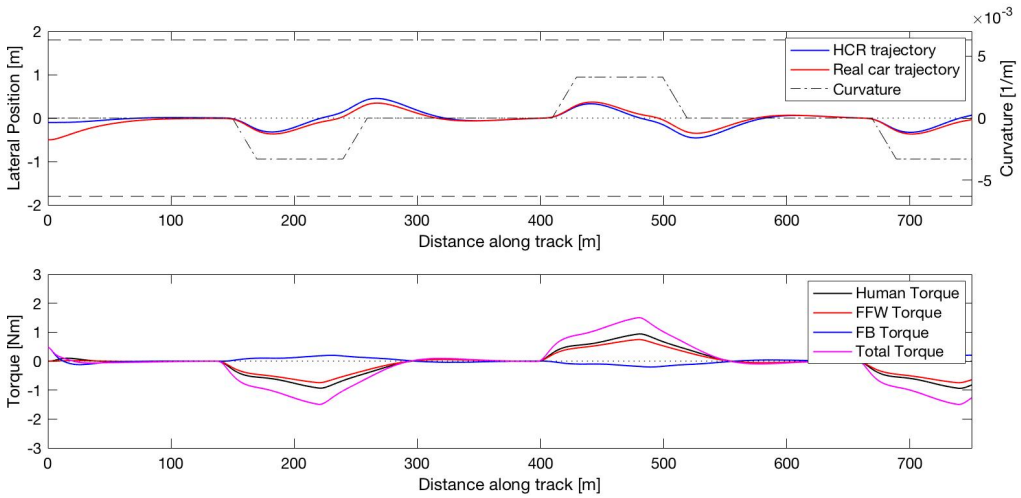

Figure F.14: Results for lateral position (top) and torques (bottom) when both FB and FFW components are active and the simulated driver and controller have different desired trajectories. This results in FB torques and a difference between the FFW torque and human torque. $K_{\psi} = 50$, $K_y = 1.5$, $K_{LoHS} = 0.5$. LoHA = 1. The weighing factor of both the driver and controller is set to 50%.

If the deviation increases the FB torque can become higher than the FFW torque, such that the sum of the torques counteract the human torque. If the driver insists on staying on his own desired trajectory this requires higher torques than without the shared controller, as seen in figure F.15.

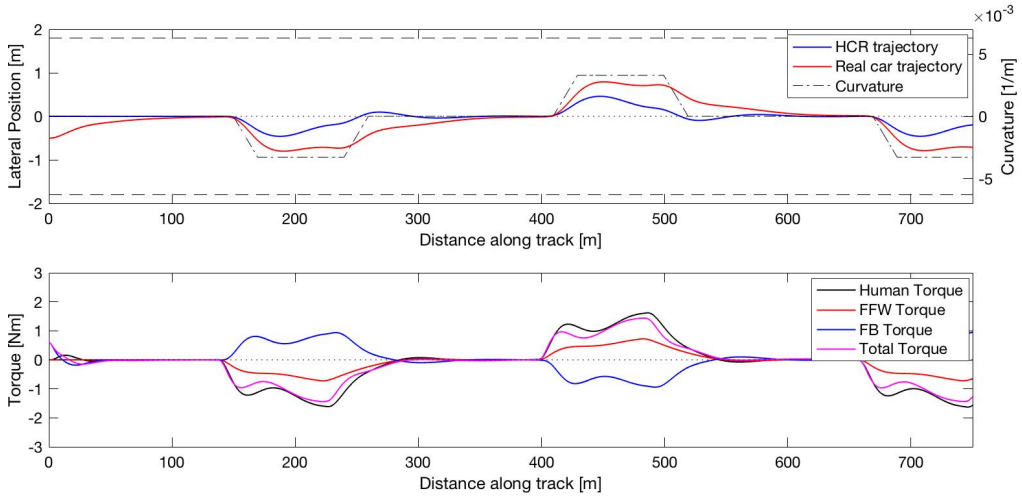

Figure F.15: Results for lateral position (top) and torques (bottom) when both FB and FFW components are active. K_ψ = 50, K_y = 1.5, K_{LoHS} = 0.5. LoHA = 1. The driver and the controller do have different desired trajectories, leading to FB torques higher than the FFW torques, causing the sum of the control torques in a different direction than the drivers' torques.

F.2.3. Controller implementation

Offline vs. Online HCR

Initially the HCR was simulated simultaneously with the real car as in figure F.16. However, when the HCR does not match the real car trajectory this leads to differences in longitudinal distance of the virtual and real car, resulting in FFW torques that do not match with the current position of the car.

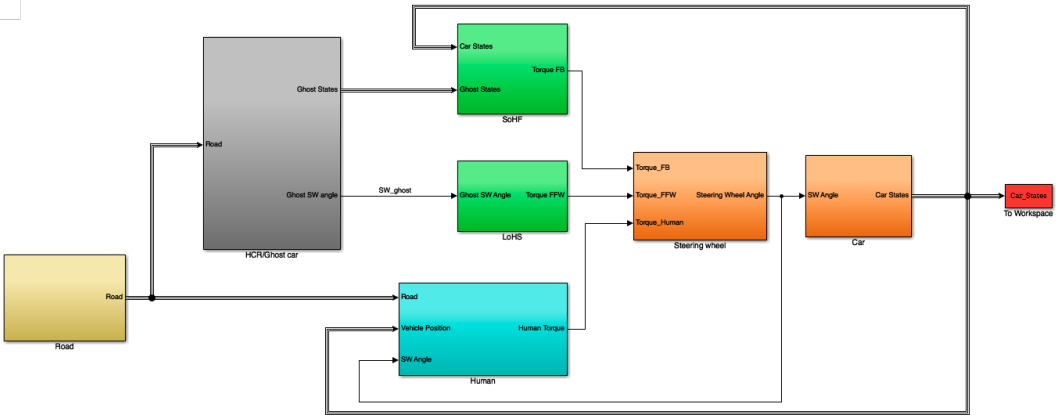

Figure F.16: Schematic representation of human and controller both exerting torques on the steering wheel, with online calculation of the HCR

Therefore the HCR is pre-generated and loaded as a matrix, containing four columns with the global positions, heading and steering wheel angles. The index of the nearest HCR point (NGP) is determined using the global positions. Using the index number the FB and FFW torques are determined relative to the HCR at the same longitudinal position on the road as the real car. A schematic representation is shown in figure F.16.

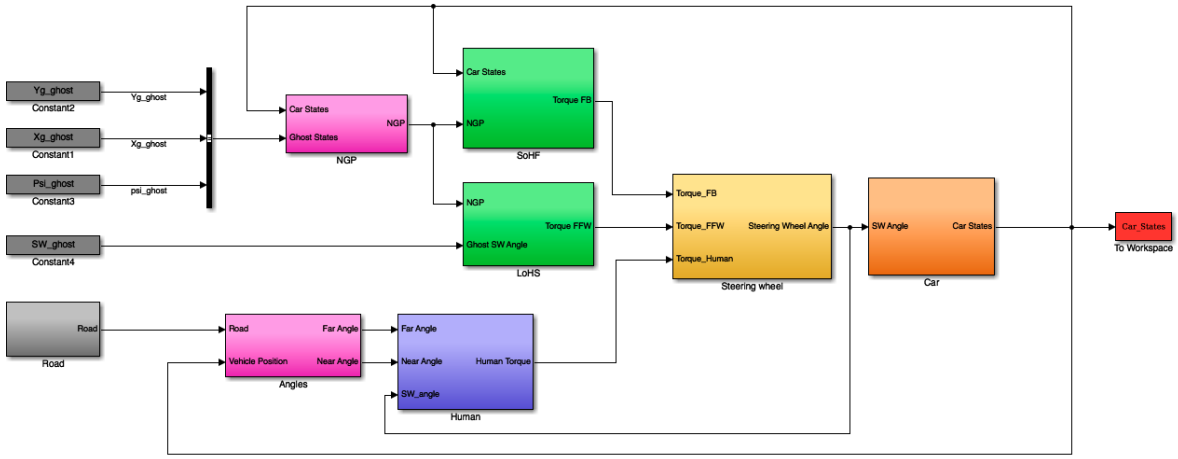

Figure F.17: Schematic representation of human and controller both exerting torques on the steering wheel with offline determination of the HCR.

F.2.4. Steering Wheel Dynamics

In the MATLAB simulation the steering wheel angles from the HCR are used to determine the FFW torques. The torque that is required to get the same steering wheel angle as the HCR can be determined by using the inverse of the steering wheel dynamics. Since the original steering wheel consisted of a second order mass-spring damper system, taking the inverse will not give accurate torques. The frequencies of the change in steering wheel angle is relatively low, therefore the second order system is replaced with a steering wheel that is modelled as a gain. The torque is thereby easily calculated by taking the inverse of the gain.

In DUECA the same approach is followed to determine the FFW torques. The gain that is multiplied with the steering wheel angles is manually tuned to find the parameters which will lead the car to drive over the road autonomously with only FFW torques. However, this might have resulted in output steering wheel angles which did not match the input steering wheel angles from the HCR matrix.

Bibliography

[1] David A. Abbink, Diane Cleij, Mark Mulder, and Marinus M. Van Paassen. The importance of including knowledge of neuromuscular behaviour in haptic shared control. In *Conference Proceedings - IEEE International Conference on Systems, Man and Cybernetics*, pages 3350–3355, 2012.

[2] Sarah Barendswaard, Daan M Pool, and David A Abbink. A Method to Assess Individualized Driver Models: Descriptiveness , Identifiability and Realism. pages 6–8, 2017.

[3] Erwin R Boer. Car following from the driver's perspective. *Transportation Research Part F: Traffic Psychology and Behaviour*, 2(4):201–206, 1999.

[4] Erwin R Boer and Nissan Cambridge. Tangent Point Oriented Curve Negotiation. In *Proceedings of Conference on Intelligent Vehicles*, number 617, 1996.

[5] Rolf Boink, Marinus M. Van Paassen, Mark Mulder, and David A. Abbink. Understanding and reducing conflicts between driver and haptic shared control. In *Conference Proceedings - IEEE International Conference on Systems, Man and Cybernetics*, volume 2014-Janua, pages 1510–1515, 2014.

[6] Arnold W. De Jonge, Jeroen G W Wildenbeest, Henri Boessenkool, and David A. Abbink. The Effect of Trial-by-Trial Adaptation on Conflicts in Haptic Shared Control for Free-Air Teleoperation Tasks. *IEEE Transactions on Haptics*, 9(1):111–120, 2016.

[7] Mark Mulder, David A. Abbink, and Erwin R. Boer. Sharing Control With Haptics Seamless Driver Support From Manual to Automatic Control. *Human Factors: The Journal of the Human Factors and Ergonomics Society*, 54(5):786–798, 2012.

[8] Louay Saleh, Philippe Chevrel, Fabien Claveau, Jean Francois Lafay, and Franck Mars. Shared steering control between a driver and an automation: Stability in the presence of driver behavior uncertainty. *IEEE Transactions on Intelligent Transportation Systems*, 14(2):974–983, 2013.

[9] Dario D Salvucci and Rob Gray. A two-point visual control model of steering. *Perception*, 33(1978): 1233–1249, 2004.

[10] C. Sentouh, P. Chevrel, F. Mars, and F. Claveau. A sensorimotor driver model for steering control. *Conference Proceedings - IEEE International Conference on Systems, Man and Cybernetics*, (October):2462–2467, 2009.

[11] Marinus. M Van Paassen, Rolf Boink, David A. Abbink, Mark Mulder, and Max Mulder. Four design choices for haptic shared control. *Advances in Aviation Psychology*, (July):237–254, 2017.

[12] P Wyzen. *Separating Haptic Feedback and Support Signals: a Solution for Human-Machine Cooperation?* Master thesis, 2017. URL `http://repository.tudelft.nl/islandora/object/uuid{%}3A94de858f-c76e-4b95-bf13-2eb18fba0eae?collection=education`.